PCT/IL 0 4 / 0 0 0 0 6 7

Rec'd PCT/PTO 2 1 JUL 2005

10/542926

REC'D 2 5 FEB 2004

| WIPO | PCT |

מדינת ישראל
STATE OF ISRAEL

Ministry of Justice
Patent Office

משרד המשפטים
לשכת הפטנטים

This is to certify that annexed hereto is a true copy of the documents as originally deposited with the patent application particulars of which are specified on the first page of the annex.

זאת לתעודה כי
רצופים בזה העתקים
נכונים של המסמכים
שהופקדו לכתחילה
עם הבקשה לפטנט
לפי הפרטים הרשומים
בעמוד הראשון של
הנספח.

PRIORITY DOCUMENT
SUBMITTED OR TRANSMITTED IN
COMPLIANCE WITH
RULE 17.1(a) OR (b)

This 27 -01- 2004 היום

רשם הפטנטים
Commissioner of Patents

נתאשר ד״ר מרגוט גנץ
יועצת בכירה לרשם הפטנטים Certified

חוק הפטנטים, התש**●** 1967-

●TENTS LAW, 5727-1967

מספר: Number	**●** 154101
תאריך: Date הוקדם/נדחה Ante/Post-dated	23 -01- 2003

בקשה לפטנט

Application for Patent

אני, (שם המבקש, מענו – ולגבי גוף מאוגד – מקום התאגדותו)

I (Name and address of applicant, and, in case of a body corporate, place of incorporation)

רמות ליד אוניברסיטת תל אביב בע"מ

רחוב חיים לבנון 32

תל אביב 69 975

‌amot At Tel Aviv University Ltd.

2 Haim Levanon Street

‌9 975 Tel Aviv

המציא/ים: ישראל גנות; אלון גורן; אברהם דיין

‌nventor/s: Israel GANNOT; Alon GOREN; Avraham DAYAN

ששמה הוא_____

‌)wner, by virtue of **by an assignment**

בעל אמצאה מכ‌ח __העברה__

of an invention, the title of which is:

מערכת ניתוחית זעיר פולשנית מבוקרת משוב

(עברית)
(Hebrew)

MINIMALLY INVASIVE CONTROLLED SURGICAL SYSTEM WITH FEEDBACK

(באנגלית)
(English)

‌nereby apply for a patent to be granted to me in respect thereof.

מבקש בזאת כי ינתן לי עליה פטנט.

*בקשת חלוקה- ‌Application for Division	*בקשת פטנט מוסף- Application for Patent of Addition	*דרישת דין קדימה Priority Claim		
מבקשת פטנט from Application ‌No._____ מס' dated_____ מיום	*לבקשה/לפטנט for Patent/Appl. No._____ מס' dated_____ מיום	מספר/סימן Number/Mark	תאריך Date	מדינת האיגוד Convention Country

*ייפוי כח: ~~כללי/ מיוחד-רצוף-בזה~~/ עוד יוגש

P.O.A.: ~~general / specific attached~~/ to be filed later

Has been filed in case _____ הוגש בעניין

Address for Service in Israel   המען למסירת הודעות ומסמכים בישראל

G.E. Ehrlich (1995) Ltd.   ג'י. אי. ארליך (1995) בע"מ

28 Bezalel Street   רחוב בצלאל 28

52 521 Ramat Gan   רמת גן 52 521

חתימת המבקש
Signature of Applicant

היום __23__ בחודש __ינואר__ שנת __2003__

This __23rd__ of __January__ __2003__

For the Applicant
Attorney Docket No.:   25694

מערכת ניתוחית זעיר פולשנית מבוקרת משוב

MINIMALLY INVASIVE CONTROLLED SURGICAL SYSTEM
WITH FEEDBACK

Abstract

Minimally Invasive Surgery (MIS) has revolutionized the practice of many surgical disciplines. In the year 2000, 80% of gallbladders have already been removed, laparoscopically. The shorter hospitalization and faster return to daily activities, the decreased discomfort and postoperative complications are major factors in the acceptance of this method. In therapeutic endoscopy micro-knives, electrical diathermy or laser beam replace the conventional hand-held scalpel. The laser "knife" has substantial capabilities over the rest: it can cut incisions, coagulate hemorrhages and ablate (vaporize) neoplastic tissues, while interaction is contact-less and sterile. The laser energy is delivered transendoscopically through rigid or flexible fiberoptic waveguides. Flexible endoscopes are used to access body curved spaces and cavities, such as the digestive tract.

Among the medical lasers in use, Carbon Dioxide (10.6μm) and Erbium YAG (2.94μm) lasers are the most highly absorbed in water and therefore in soft tissue. Hence, considered best for treating such cases as mucosal gastric cancer and Barrett Esophagus, where ablating superficial tissue layer is needed. These two Mid-Infrared lasers are guided by optical hollow waveguides (developed in our group as well as by others). At the present, neither flexible hollow fibers, nor solid core mid-IR fibers, are used in endoscopical applications. Consequently, the unique benefits of Er: YAG laser and the most commonly used CO_2 laser are not yet applied endoscopically to treat internal tissues of the body cavities.

To make this feasible further development is required, taking into consideration the environmental conditions. Irradiating tissue within a closed space, using wavelengths that are mostly absorbed in water will cause the dispersion of hot steam and thus may thermally damage the surrounding tissue. Exploring this issue, experimentally, is the goal of our study.

We have built an experimental setup, software controlled, to simulate on an optical bench the thermal environment within body cavity during a practical transendoscopic surgery. The setup includes all the necessary components for a fully feedback controlled minimally invasive surgery. The results of these experiments will be presented and discussed.

Table of Content

List of Figures

List of Photos

I

List of Thermal Images

List of Graphs

List of Tables

1 Introduction

1.1 Endoscopy

This section backgrounds our study clinically and technologically. It presents the Minimally Invasive Surgery and the evolution of endoscopical instrumentation. It further refers gastroscpoy, emphasizing laser Gastroenterology. Finally it exhibits two types of cancer, along the digestive tract, to demonstrate the need for transendoscopical ablation of superficial lining within cavity-like organs.

1.1.1 Minimally Invasive Surgery (MIS)

During the last 10 years, MIS has revolutionized the practice of many surgical disciplines, replacing conventional procedures by MIS (demonstrated in table 1-1) [1-3]. MIS focuses on minimizing the invasiveness, utilizing technological innovation in video imaging, optical waveguiding and endoscopical instrumentation. This technique requires very small incisions, if any, thus limits disturbance of healthy tissue, compared to conventional surgery, and minimizes the psychological trauma. The decreased pain, discomfort and blood loss, the shorter postoperative hospitalization and faster return to daily activities and consequently the reduced direct and indirect costs, are major factors in the acceptance of this method.

It is possible for surgeons neither to look directly at nor touch the tissues or organs on which they operate, but through an endoscope. Endoscope is the instrument by which endoscopical MIS is performed. It is a tube-like device, inserted through body natural orifices or 1-2cm punctures, and maneuvered to the region of interest. It then enables the surgeon to screen, diagnose and repair body organs, internally. That includes obtaining biopsies, coagulating incisions, ablating cancerous cells and polyps and cutting tissues such that used during gallbladder resection [4-6].

The subsequent section describes the history of endoscopical instrumentation.

Table 1-1 Surgical Procedures Performed by a Minimally Invasive Approach, 1999. Percentages are rounded (Medtech Insight, Mission Viejo, Calif)

	No. of Procedures	Minimally Invasive, %†
General surgery		
Gallbladder	1 084 882	85
Nissen fundoplication	47 087	95
Adhesiolysis	215 760	72
Appendectomy	334 388	22
Colon resection	380 000	7
Hernia repair	820 191	14
Total	2 882 308	47
Gynecology		
Hysterectomy	582 000	15
Myomectomy	64 977	70
Pelvic floor reconstruction	160 000	40
Removal of adnexal structures	350 059	65
Total	1 157 036	37
Urology		
Nephrectomy	44 863	75
Cystocele/rectocele	158 144	45
Pediatric urology (orchiopexy, vesicoreflux)	25 000	80
Adrenalectomy	20 000	60
Total	248 007	55
Plastic surgery		
Breast reconstruction	182 000	15
Face and forehead lifts	80 000	25
Total	262 000	18
Thoracic surgery		
Lung biopsy	90 000	75
Lung resection	47 124	60
Total	160 000	60
Cardiothoracic surgery		
Coronary artery bypass surgery	330 000	17
Heart valve replacement	81 000	15
Congenital defect surgery	25 000	20
Total	436 000	17
Vascular interventional surgery		
Saphenous vein harvest	220 000	35
Peripheral vascular bypass	80 000	2
Aortoiliofemoral bypass	75 000	1
Abdominal aortic aneurysm	51 000	10
Total	426 000	20

1.1.2 Evolution of the endoscopes

The first instrument developed to look into deeper cavities was probably the rectal speculum, mention in Hippocrates' treaty on fistula. Although open tubes were later designed, several hundred years passed before they could be made useful [7]. The earliest endoscope is attributed to Phillippe Bozzini whose "Lichtleiter" was demonstrated in Vienna in 1806 [8]. It consisted of a simple silver tube, which was illuminated proximally by candlelight and reflected by a mirror. Cigalas, Fisher, Guillon and Nelaton produced numerous other versions but in each case the lack of distal illumination severely limited the use of these early instruments. The first endoscope to

resemble a modern rigid instrument was produced by Max Nitze in 1877 [9]. It incorporated the three important principles of modern rigid endoscopes namely: distal illumination, a lens system and instrument channel. Johann von Mikulicz, used Nitze's telescopic system to design a rigid gastroscope with an angulation at the distal end. It had a globe for illumination at the tip and a channel for air insufflation (Fig. 1-1) [10]. Stoerk (1887) used reflected sunlight for illumination, and right-angled open tube to examine the esophagus (fig. 1-2) [11]. The advent of the Edison bulb in 1891 finally made cystoscopy feasible for ordinary clinicians. There were numerous improvements in cystoscopes including the Amici prism to correct the image inversion, the Albarron lever (1897) to assist instrumentation and finally prisms to achieve an angled field of view. With developments in urology, gastroenterologists were becoming interested in inspecting the alimentary tract. Kussmaul performed the first gastroscopy [12] in 1868 using a rigid tube with illumination from a Desormeaux source. However, the distal illumination was very restricted and the procedure could not be regarded as a success until the days of Schindler in the early 20th century when illumination had been improved. In 1930 Wolf [13] produced the first flexible scope but this was based on a conventional lens system. Taylor improved the design in 1941 by adding maneuverablility of the distal tip. In 1951 Professor Harold Hopkins, working on the original concept of Baird (1927) that glass fibers can transmit light, developed the clad fiber [14]. This resulted in the first practical flexible fibreoptic instrument, developed by Curtis and demonstrated by Hirschowitz in 1958 [15]. It was the first flexible gastroscope and the introduction of a completely new diagnostic and therapeutic modality in the field of gastroenterology [5]. In the 1970's gynecologic surgeons began using laparoscopic techniques to perform female sterilization, known as tubal ligations [16, 17]. The real advantage in laparoscopy did not come until 1989, when physicians in Atlanta and Nashville began applying laparoscopic techniques to gallbladder operation. In the year 2000, above 80% of gallbladders have already been removed, laparoscopically [1].

Figure 1-2 Esophaguscope (1887) [5]

Figure 1-1 Rigid gastroscope (1881) [5]

1.1.3 Modern endoscopes

Subjected to the visualizing system integrated, there are five basic types of endoscopes [18]:

- Conventional telescope (rigid)
- Rod lens telescope (rigid)
- Gradient optic (rigid)
- Fiberoptic (flexible)
- Microchip sensor (flexible)

Conventional telescope consists of a distal objective lens that forms an inverted virtual image, which is transmitted by relay lenses. The improvements, which have been introduced over the years, have included a distal prism to angulate the field of view, field lenses which improve light transmission and correction of image inversion by the prism at the eyepiece. These instruments are now largely obsolete, as they cannot compete with the improved rod lens system optic

Rod lens optic, developed by Hopkins, is now incorporated in all newly manufactured rigid endoscopes. It consists of a series of glass rods. The ends

4

of each rod are precisely ground to provide a refracting surface. The use of blooming and flint glass reduces external reflection and chromatic aberration. The resolution and light transmission of such systems is unrivalled.

Gradient optics has recently been considerably improved. They consist of a single glass element of different refractive indices and have the advantage that they can be turned into a viewing system a fraction of a millimeter in diameter. They are the basis of the so-called needle scope. There are some disadvantages of such needle endoscopes: the field of view is limited at 45°-56°, they suffer from varying degrees of chromatic aberration, relatively poor light transmission and extreme fragility. They are however cheap to produce and could be formatted in a disposable mode.

Fiberoptics have two roles in visualizing: to transmit light for illumination in all endoscope systems and to transmit images in the fiberoptic flexible endoscopes. The transmission of light down a glass fiber is by the process of internal refraction. Glass fibers are thus produced which contain a glass of high refractive index surrounded coaxially by glass of a lower refractive index. In this way, light is internally refracted along the central high refractive index core. When glass fibers are haphazardly arranged they transmit light only. However, when they are lined up in a coherent or parallel manner they can transmit an image. This is achieved in current fiberoptic endoscopes by having an objective lens, which is focused directly onto the distal tip of the fiber bundle. The image is then transmitted along the fiber bundle, the final image being appreciated and magnified by the eyepiece lens. The smaller the fiber, the less obvious is the pattern. Fiber diameter of modern endoscopes varies between 8 and 15 microns, packing is constantly improving and hence picture quality.

Microchip sensor has lead to the development of the 'video optic'. In this system a CCD microchip and electrical wiring have replaced the visual optics. The image is generated electronically and displayed on monitor.

Endoscopes are characterized upon their clinical orientation, the target site and the body path through which they're threaded. They can be of various lengths, thickness, flexible or rigid. Classification of some major types is listed below:

- Laparoscope: designed for the abdominal space; used in gallbladder operations, hernia repair, appendix removal, hysterectomies

- Arthroscope: designed for joints; used in arthroscopic knee and shoulder surgery

- Cystoscope: designed for the bladder; used in prostate surgery and other procedures related to the urinary and reproductive systems

- Gastroscope: designed for the upper digestive tract; gastroscope and gastroscopy are focused in this study.

- Other types: ureteroscope, pharyngoscopy, bronchoscopy, nephroscopy

Fig. 1-3 presents a typical gastroscope. The instrument has two flexible shafts. The distal (pic.1-1) is maneuverable and inserted into patient. It incorporates fiber bundles for illumination and viewing (recently done by CCD electronics instead), outlets for irrigation, aspiratory, suction, insufflation, and channels for surgical micro-tool or laser waveguides. The second shaft connects inlets' sources: light, water, suction, etc. The part in-between is the instrument control by which physician can guide the distal tip and activate the flows.
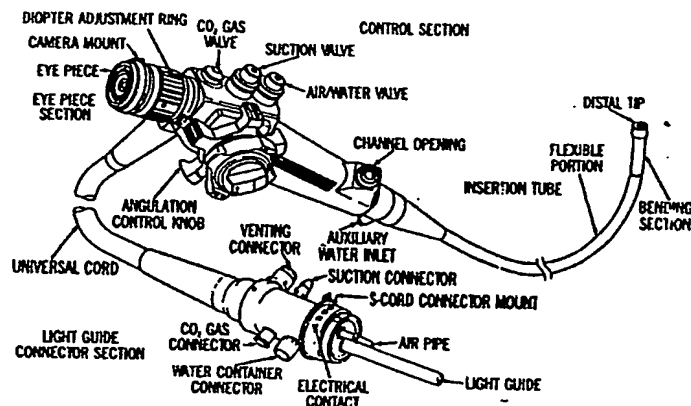
Figure 1-3 Schematic drawing of a gastroscope [19]

Picture 1-1 Gastroscope's distal tip: 2 illuminative fibers, viewing fiber, 4 open canals for flow, suction and surgical instrumentation

Surgical micro-tools make it possible to grasp, suck, clip, hold and cut endoscopically, but their overall size is miniature and therefore limits the amount that can be done. The advent of lasers, refinements to diathermy, shock wave generators, ultrasound devices and hydraulic devices have extended the surgical capabilities (e.g. coagulation, ablation). The mechanical

actions are a mere extension of conventional surgical work on a small scale at a distance. Fig. 1-4 demonstrates a micro-tool threaded through endoscope open channel. Open channels are utilized for various tool as well as laser waveguides.
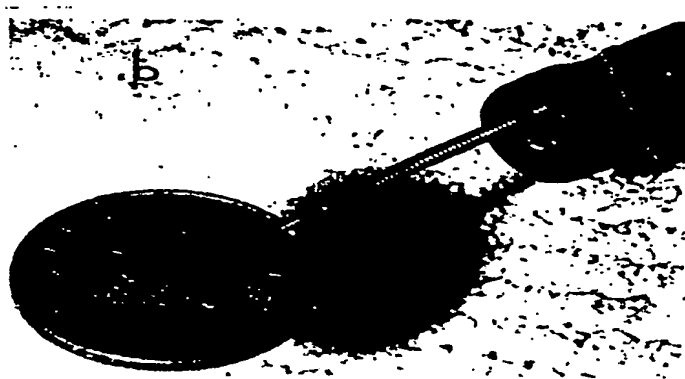
Figure 1-4 A coin held by micro-forceps threaded through an endoscope [20]

1.1.4 Gastroscopy and current laser-gastroenterology

Gastroscopy, also known as upper endoscopy, gastrointestinal (GI) endoscopy, panendoscopy or esophagogastroduodenoscopy (EGD), lets the surgeon examine and treat gastroscopically the lining of the upper part of the gastrointestinal tract, which includes the esophagus, the stomach and the duodenum [3, 21, 22].

Gastroscopy helps evaluating symptoms of persistent upper abdominal pain, nausea, vomiting or difficulty swallowing. It enables minimal invasive diagnosis of bleeding from the upper GI tract. It's more accurate than X-ray imaging for detecting inflammation, ulcers and tumors of the esophagus, stomach and duodenum. It is also used to obtain biopsies in order to distinguish between benign and malignant tissues or to test for Helicobacter pylori (bacterium that causes ulcers). In addition upper endoscopy is performed when a cytology test is needed for cell analysis.

One of the finest therapeutic means in gastroentroscopy is the laser. Gastroenterologists were the first to use lasers in conjunction with flexible endoscopes [18]. They first made their mark in the endoscopic control of

massive hemorrhage [23] in the GI tract. Today, Nd YAG lasers are used routinely and considered effective in controlling hemorrhage (via coagulation), treating benign, malignant or non-neoplastic stenosis (stenosis that is not related to cancer), such as peptic ulcers and vascular anomalies, and recanalization of dysphagia (obstructing cancers of the upper GI tract).

However, despite of early expectations concerning the potential of lasers in gastroenterology, they could have only partially been fulfilled so far [24]. It is quite obvious that the Nd:YAG laser at a wavelength of $1.064\mu m$ does not provide the optimum radiation for all GI diseases.

Dye lasers have been recently applied in this field, for Photo Dynamic Therapy (PDT). In GI PDT, tumors are exposed to a dye laser after the injection of photosensitizer and a time delay (24-72h). The clearance of the photosensitizer leads to a concentration gradient among benign and malignant tissue ranging from about 1:2 to 1:4.

Tumors of the stomach are often more difficult to access for PDT due to wrinkles of the mucosa. Thus, treatment of the stomach is frequently associated with the application of higher energy doses. One major advantage of PDT is that fewer endoscopic sessions are usually required compared to treatments with the Nd:YAG laser. Hence, the overall duration of a PDT treatment is significantly shorter and easier to tolerate, as well.

In general, PDT is applied at early stages of cancer and if alternative methods are associated with a high risk for the patient.

1.1.5 Additional elements of practical MIS, to be considered

Ablative endoscopy, within body cavities, incorporates means that must be considered in this study:

• Surgical suction

• Gas insufflator

Both outlet cavity space through endoscope's open canals.

• When using CO_2 laser - fiber cooling

The suction evacuates smoke, vapor and tissue particles, to unmask the treated area and to reduce the heat convection within cavity.

Insufflating the cavity, generally by CO_2 purge gas, allows the management of the endoscope tip inside. By circulating the atmosphere, insufflation averages heat dispersion with cavity, yet increases heat convection.

CO_2 gas minimizes the risk of embolism but also partially absorbs CO_2 laser energy. The phenomenon, known as resonant absorption, limits the power available for tissue ablation whenever [25]. Fournier [26] exhibited the attenuative effect of CO_2 purge gas on CO_2 laser power. Gannot [27] mentioned that in 30Watts laser power the loss is considerable and it grows as power climbs.

Cooling the CO_2 laser waveguide is obtained by injecting flow (air, N_2 or water) to cavity, through fiber's hollow core. In terms of heat dispersion, this flow has principally similar effect to that of insufflating gas, however typically in a lower scale.

1.2 The clinical problem

This section briefly reviews stomach anatomy, and subsequently demonstrates the problem of current MIS techniques to ablate superficial lining of a body cavity, such in mucosal gastric cancer and Barrett Esophagus.

1.2.1 Anatomy of the stomach

Stomach represents a major cavity along the GI tract. Fig. 1-5 exhibits its anatomical structure. Dimensions of the stomach, as in other digestive organs, are subject to great variation. The length of the lesser curvature averages about 10 cm in the adult, and that of the greater curvature is 30-40cm. The diameter varies exceedingly according to the amount of contents [28], with a maximal volume of 1-1.5 liters.

The diameter of the pyloric canal, which is the narrowest point in the digestive system below the esophagus, when constricted, is only about 1.5 cm. It is distensible, however, as hard bodies with diameters of 2 cm or more may readily pass through.
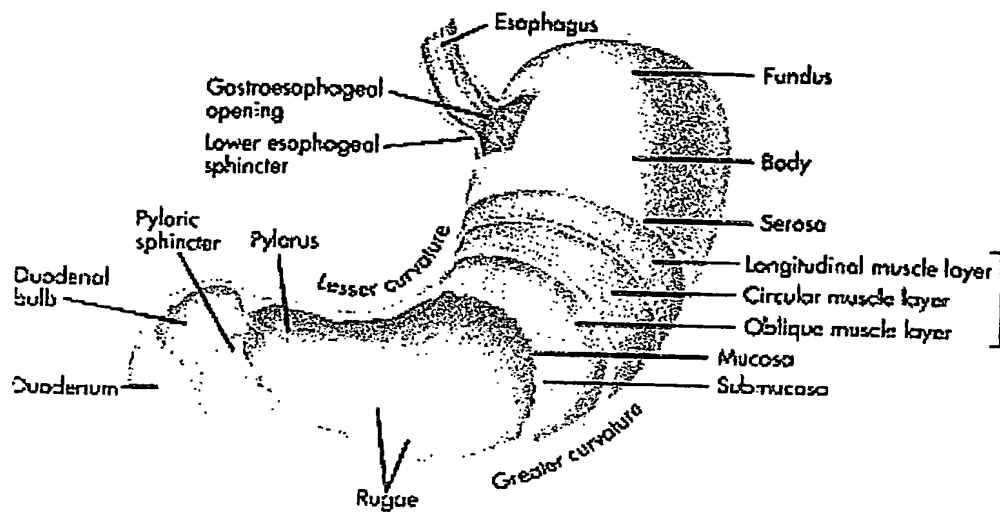
Figure 1-5 Stomach anatomy; a portion of the anterior wall has been cut away to reveal the layers. The mucosa lines the stomach and forms folds (Rugae) [28]

1.2.2 Gastric cancer

1.2.2.1 Characteristics

Tumors of the stomach may be benign or malignant. Benign tumors can be usually removed completely and are not likely to recur. Malignant stomach tumors invade neighboring tissues and organs [3, 21, 22].

While its cause is unknown, gastric cancer is often associated with gastritis (Inflammation of the stomach lining) and intestinal metaplasia of the mucosa. Peptic ulcer has not been proven as cancer precursor whereas polyps (a benign tumors of epithelium extending above the surface) of the gastrointestinal tract may have a tendency to become a cancer generally removed. Biopsy of stomach lining can be obtained gastroscopically for diagnosis.

Known types of stomach carcinomas can be classified according to gross appearance:

- Protruding (polypoid or fungating)

- Penetrating; the tumor has a sharp, well-circumscribed border and may be ulcerated

- *Spreading, either superficially along the mucosa* or infiltrating within the wall

- Miscellaneous, showing characteristics of 2 of the other types; this is the largest group

1.2.2.2 Treatment techniques

Treatment for stomach cancer is generally prompt removal of the tumor by surgery. This may require removing part or all of the stomach, by either conventional surgery or MIS, via micro-knives, diathermy, ablative lasers (Nd YAG, Ho YAG) or PDT. If the stomach cancer has started to spread, removing affected parts of neighboring organs is needed (e.g. spleen, pancreas). If all of the cancer present in the body cannot be removed by surgery, chemotherapy may be given. Radiotherapy plays a limited role in the treatment of stomach cancer since radiation doses strong enough to destroy these cancer cells could seriously damage the surrounding healthy tissue. Thus, treating gastric cancer in its very first stage is essential. However, when early cancer spreads superficially, thin slices of mucosa layers needed to be ablated. None of these techniques has definitively demonstrated high specificity, yet efficacy, in doing so. A study conducted between 1981 and 1990, stated certain success in treating endoscopically superficial esophageal cancer and early gastric cancer lesions by photodynamic therapy (PDT) with argon and excimer dye lasers (630nm wavelength) [29]. Another study reported selective ablation of submucosal gastric wall with diode laser (Indocyanine green), by applying real-time spectral monitoring of ablation depth. It additionally claimed that ablation depth could be roughly judged through a gastroscope by surface color change [30].

1.2.3 Barrett Esophagus

1.2.3.1 Characteristics

Barrett esophagus is defined by the metaplasia of existing squamous mucosa into a specialized intestinal-type mucosa. In simple words the esophageal lining changes, and becomes similar to the mucosa that lines the intestine. The importance of this metaplasia is the association of this condition with the

11

development of adenocarcinoma of the esophagus. It is more likely to occur in patients who experienced GERD, had nighttime symptoms or had complications such as bleeding or stricture (a narrowing due to scarring)[31-36]. Barrett's tissue is visible during endoscopy, although a diagnosis by endoscopic appearance alone is not sufficient. The definitive diagnosis of Barrett's esophagus requires biopsy confirmation.

1.2.3.2 Treatment techniques

Elimination of the metaplastic mucosa may decrease the cancer risk. Currently, several forms of therapy have evolved with the goal of replacing the specialized mucosa with normal squamous mucosa. These proposed treatments include PDT and thermal techniques. The effectiveness of PDT varies depending on the pharmaceutical photosensitizer used and the wavelength of light applied to activate the drug. Thermal techniques include multipolar coagulation, argon plasma coagulation, KTP YAG laser therapy, Nd: YAG laser therapy, and argon laser therapy. Mucosal resection has been attempted through the endoscope to remove large areas of the Barrett mucosa [33]. All of these ablative strategies attempt to destroy the metaplastic mucosa and promote the re-growth of squamous epithelium. These therapies have demonstrated the ability to "reverse" the metaplasia to varying degrees, *but a decrease in cancer risk has not been demonstrated conclusively with any of these treatment methods.*

1.3 The laser

1.3.1 Introduction

This section outlines medical lasers: wavelengths, transmission mode and principal parameters. It emphasizes CO_2 laser and its hollow fiberoptic.

1.3.2 Medical lasers for thermal interactions

Lasers are now used routinely in medical therapy and surgical technique to incise, coagulate, or vaporize tissues. The laser energy is emitted as a narrow collimated beam of very high intensity, which makes it eminently suitable for

surgical applications, introducing desirable features as increased precision, improved homeostasis, less tissue manipulation and mechanical trauma and easily maintaining sterility. When used transendoscopically, they provide a means of delivering energy to precise sites inside the body under exact control [18].

Medical applications make use of three fundamental mechanisms of laser-tissue interactions: photochemical, photothermal and photomechanical. The biological effects of laser energy depend on the laser wavelength, the irradiance, the exposure duration, and the opto-thermal properties of the tissue involved (see sec. 1.5.4 for details). Surgical procedures that involve coagulation or ablation of tissue are thermal. In this interaction, laser light is partially absorbed by tissue and converted into heat energy, which rises tissue temperature. Initially, this causes thermal contraction of the treated area. As tissue shrinks, small vessels are sealed, which can stop hemorrhage, obtaining coagulation. Higher energies, such that used for ablation, kill the cells in situ and ultimately vaporize cellular material, leaving a crater.

The types of laser currently in widespread use for their photothermal effects are: CO_2 (10.6μm) and Er: Yag (Erbium Yttrium Aluminum Garnet, 2.94μm) in the mid IR, Nd (Neodymium) YAG (1064nm) in the near IR and Argon ion, which has 2 main lines (488 and 514 nm) in the blue and green regions of the visible spectrum. The CO2 and the Er: YAG laser beams are strongly absorbed in water (fig. 1-12 in sec. 1.5.2) hence in soft tissue (contents 70-90% water). The other two are absorbed more in pigmented cells. Er: YAG lasers are used to evaporate both soft and hard tissues (e.g. teeth).
The differences between these wavelengths arise substantially in the extent of milder damage in surrounding areas. In soft tissue, such as bladder, applying sufficient energy, to vaporize solely the surface cells, only causes lesser damage to a depth of 0.1mm with the CO_2 laser. When the same surface effect is produced with the Argon laser, milder damage extends for 1mm and with the Nd: YAG, it extends for 5mm.

1.3.3 CO_2 Lasers

The volume heated by the CO_2 laser outside the area of vaporized tissue is so small that it has little practical value for stopping major hemorrhage, although it can seal capillary oozing. In contrast, the highly localized effect of this laser makes it eminently suitable as a laser knife, the cells immediately under the beam being vaporized with minimal damage to adjacent areas. This beam can cut through tissue or scan across the surface of an organ to vaporize the superficial layers to any desired depth [18]. *This merit could be of great value when treating superficial carcinomas such as Barrett esophagus and mucosal gastric cancer.* However, neither CO_2 nor Er: YAG laser beam are yet transmitted via flexible endoscopes.

CO_2 lasers are the primarily and most used in the IR region. They have a major role in therapy applied through rigid endoscopes such as gynecology, otolaryngology and airway obstruction surgeries. They are also used in genitourinary, plastic, dental, hepatic, orthopedic, and cardiovascular surgery and considered the mainstay of laser neurosurgery. Since IR emittance is invisible, CO_2 laser is combined with low power, helium-neon (He-Ne) or diode laser-pointer.

At the present, applications of CO_2 lasers are limited to "straight lines". Their beam is maneuvered with a series of articulated mirrors (within the machine's arms), and straight rigid waiveguides (used for rigid endoscopes). The recent development of flexible mid-IR waveguides [37-39] could virtually target these wavelengths to body cavities via flexible endoscopes. *This technological innovation together with the clinical value highlighted earlier* (sec. 1.2.2, 1.2.3) *has driven our investigation.* Further discussion on laser waveguides is presented in section 1.4.

1.3.4 Power Density and Energy

The ability of a surgical laser to incise, coagulate, or vaporize tissue will depend on the concentration of power in the laser beam. Power density (expressed in W/cm^2) describes the amount of laser power that is distributed over the cross-sectional area of the laser beam on the tissue being treated.

In general, during surgical applications, power densities below 500 mW/cm² tend to be used for tissue coagulation, whereas power densities of 1 kW/cm² and above are needed for vaporization and incision of tissues.

Fig 1-6 shows the relationship between laser power, beam diameter, and average power density. Changing the distance between the tissue being treated and the focusing lens of the optic fiber varies spot size.
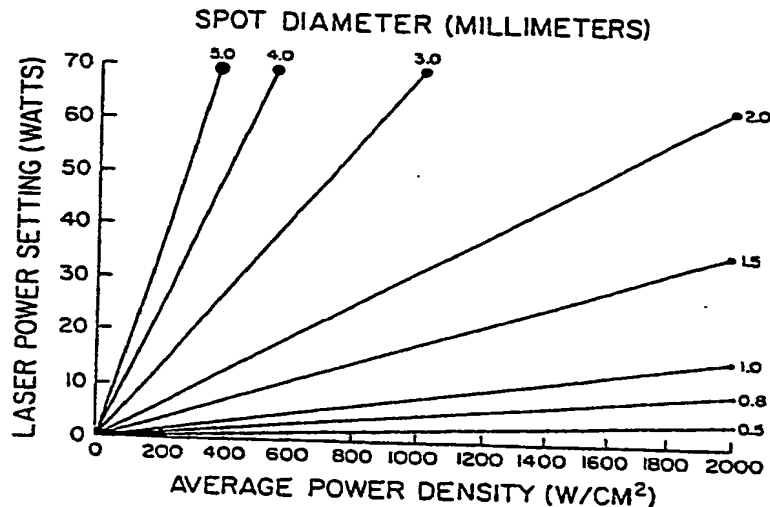
Figure 1-6 Relationship of laser power, beam diameter, and average power density. Power density increases by a factor of 4 when beam diameter is halved [40]

As formulated below, the duration tissue exposed to laser beam is crucial:

$$Energy\ (Joules) = power\ (W) \times time\ (s)$$

When using extremely high-power densities to obtain tissue ablation, the depth of vaporization will be linearly correlated to exposure time.

1.3.5 Continuous Wave (CW) vs. Pulsatile Wave (PW)

CO_2 lasers have mainly two modes of operation: CW and PW. In the CW mode the laser delivers same energy as long as the laser is activated. This mode releases the highest average power. However, it byproducts a zone of thermal coagulum at the cut edge, which impedes the biological healing process [41]. Fig 1-7 illustrates the thermal effects inside biological tissue. In

15

order to let the inner tissue repair itself, the unwanted carbonization process must be avoided.

PW mode reduces this thermal side effect, by minimizing the heat conduction effect, during which heat is transferred from irradiated volume to adjacent areas, all within tissue. This is managed by transmitting pulse train or "Superpulse" whereat each pulse lasts mili or microsecond. During ablative therapy, the short-energetic pulse enables instant evaporation of matter, such that heat conduction is further minimized. The technique of Q-switched laser enables extremely high power output, (megawatts), over a very short time (nanosecond) [42]. The rationale for favoring PW modes is summarized below:

- Minimizing damage zone
- Minimizing surgical duration
- Delivering ablative energy within every pulse, so that cells will vaporize instantly, before heating the surrounding tissue.

Two classes of pulsed lasers are vying to be the laser of choice for ablation in medical applications: the UV laser ($\lambda < 300$ nm) and the mid-IR laser ($\lambda > 2.0$ μm). The UV light is highly absorbed by lipids, proteins, and nucleid acids whereas mid-IR light (2.94μm and 10.6μm) is strongly absorbed in water.

The UV laser has the potential to precisely ablate tissue, leaving a little thermal damage but it may cause significant mechanical damage to the tissue and is potential mutagenic. Mid-IR lasers are easy to maintain, compact, and less expensive, yet may produce mechanical and thermal damage to the adjacent tissue.
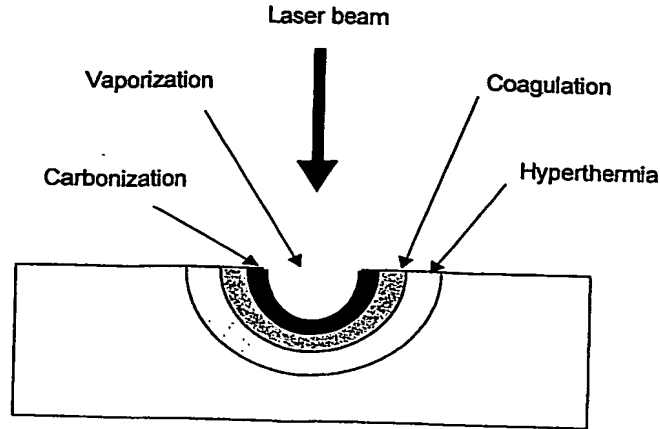
Figure 1-7 Schematic location of thermal effects inside biological tissue

1.3.6 PW laser thermal relaxation time

The clinical success of PW treatment is often limited by the extent of damage that is caused to the tissue in the vicinity of the ablation crater. In general, pulsed ablation seems to be a trade off between thermal damage to the surrounding tissue, caused by relatively long pulses (>100 ms), and mechanical damage to surrounding tissue, caused by relatively short pulses (< 1 ms).

Photothermal interactions are due to conversion of the laser energy into heat, and diffusion of heat within the tissue. When laser penetration depth is less than the laser spot radius, the thermal relaxation (also called diffusion) time t_p can be defined as:

$$t_p = \frac{Z^2}{4\alpha_1}$$

(1.3.6.1)

where Z is the thermal penetration depth (explained in section 1.5.3) of laser light in tissue and α_1 is the thermal diffusivity [24, 43].

For laser pulses shorter than the thermal relaxation time, the distribution of thermal energy is determined by the light distribution, as explained in [44].

If the pulse duration is larger than the thermal relaxation time, the thermal energy propagates into tissue during the laser pulse.

The thermal relaxation time is, in fact, a constructed parameter, emerged from the tissue parameters, and varies as the tissue varies at a constant laser light.

A high repetition rate for the laser pulses can evoke and additional increase in temperature if the rate of heat transport is less than the rate of heat generation. Vangemert and Welch [45] have modeled the correlation of temperature upon pulse repetition rate, by considering its effect during the heat accumulation.

The thermal relaxation time, for instance, in water, with an optical penetration depth D=0.013mm (shorter than spot diameter) and a thermal diffusivity α_1 = 0.0015cm²/sec, for CO_2 laser, is:

$$t_p = \frac{D^2}{4\alpha_1} = \frac{0.0013^2}{4*0.0015} = 281.6\mu \sec$$

(1.3.6.2)

1.4 Optical waveguides for the IR

1.4.1 Introduction

In order to utilize the laser advantages within body cavities, the beam must be delivered via waveguide, threaded through the endoscope. Flexible endoscopes entail flexible waveguides, which have been recently developed. According to Gannot et al. [37] such waveguides should meet the following requirements:

i.   Minimal energy losses to avoid damage of the endoscope or tissue.

ii. The output beam should be as close as possible to a smooth Gaussian beam, in which most of the energy is centralized

iii. Fiber substances should be biocompatible

iv. Fabrication must be repeatable, employing small tolerance

For surgical applications the best choice of mid-IR delivery system is the hollow waveguides, as they can transmit high peak laser power (megawatts) and up to 100 watts of CW radiation with losses less than 1dB/m (endoscopical applications only require short distances).

1.4.2 Hollow waveguides (HWG)

General structure of a HWG (fig. 1-8) consists of a hollow tube, internally coated with a metal layer and a thin dielectric layer [46]. The optical radiation is guided through reflection and refraction from the inner layers.
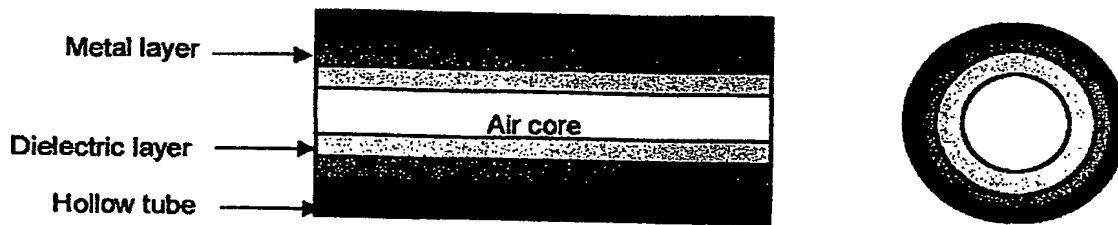
Figure 1-8 General structure (left) and cross section (right) of a HWG [46]

HWGs are characterized by guiding mechanism of the radiation. The main attenuation mechanisms are reflection from a thin layer and scattering due to surface roughness. Reflection and refraction determine the wavelength to be transmitted and its attenuation, whereas scattering changes ray's propagation angle and energy distribution, and thus causes to losses [47].

Croitoru and Gannot et al. [48-52] as well as Miyagi et al. [53] and Harrington et al. [54-56] have developed HWG for a large range of wavelengths, mainly for CO_2 and Er: YAG lasers (those lasers are widely used in surgical applications). Tube's substance (fused Silica, Teflon or Polyimide) is selected upon desired characteristics e.g. flexibility, roughness and chemical inertness. Fused silica tubes are very smooth [52] and flexible (at small bore radius), yet have poor thermal conductivity. A sample graph of attenuation vs. bending radius for a fused silica HWG is shown in fig. 1-9 [46, 57]. Fig 1-10 shows losses versus bore diameter for straight glass HWG using CO_2 laser beam. Harrington [56] pointed out the heating problem of glass HWGs. Daoning et al. [58] concluded that it is reasoned by two factors: losses caused by fiber coupling and attenuation due to beam distribution inside the waveguide. These effects produce a temperature that is highest at the input face and decreases along the waveguide, and may be reduced by injecting inert gas through the bore.
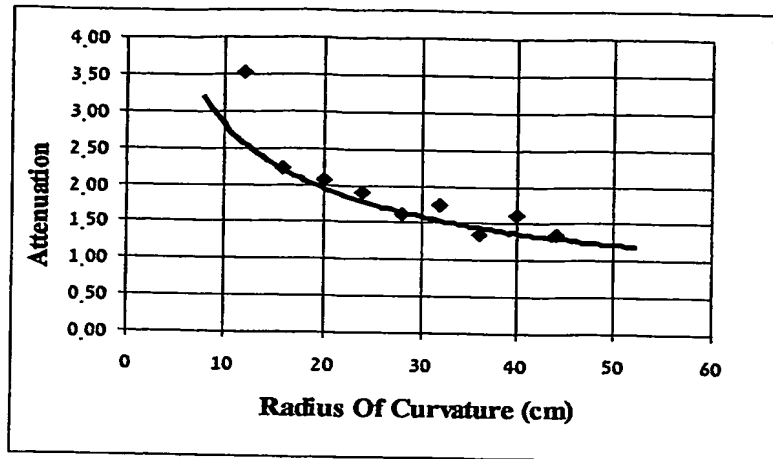
Figure 1-9 Theoretical and experimental attenuation, bent fused silica, ID=0.5mm, L=1m, λ=10.6 µm [46]

Bore diameter (micron)
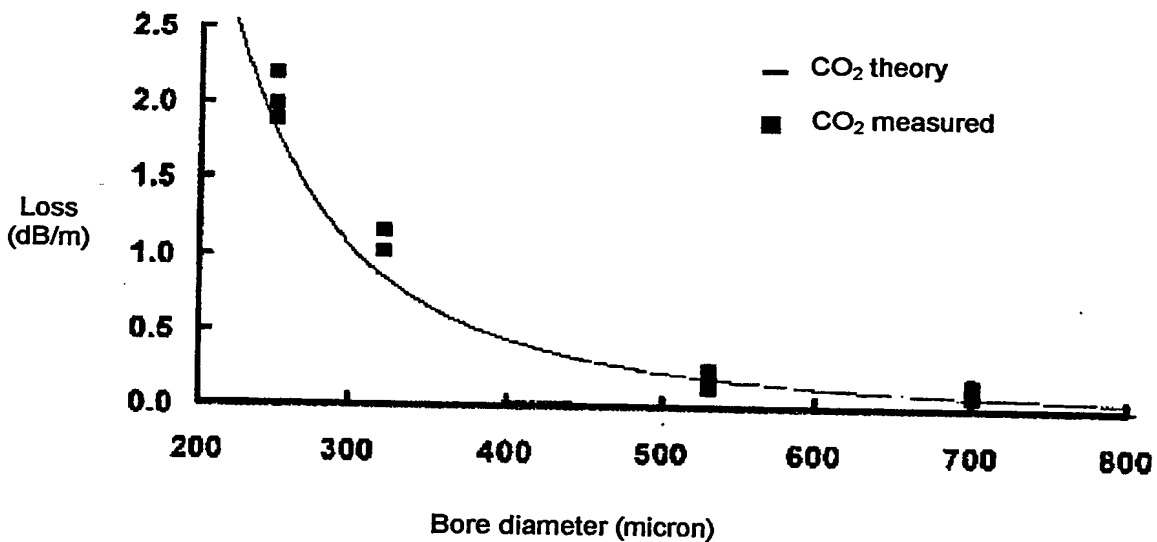
Figure 1-10 Loss vs. bore diameter in straight glass HGW, λ=10.6µm [54]

The optical HWG are fabricated in our laboratories and are made according to the needs of this investigation.

1.5 The tissue

1.5.1 Introduction

Laser irradiation of tissue leads to thermal energy deposition into the tissue. When a laser beam irradiates a tissue, part of its energy is reflected from the

20

surface. The rest of the laser energy penetrates into inner layers where it is absorbed and scattered by the tissue. Eventually the incident energy is distributed into backscattered, absorbed, and transmitted portions. The three fundamental occurrences of reflection, absorption and scattering are defined below. Fig 1-11 illustrates a typical situation, where light incidents a matter.

Reflection is defined as the returning of electromagnetic radiation by surfaces upon which it is incident. There are two kinds of reflection: the *specular* reflection, when the surface itself is assumed to be smooth, like in wet surface, and the reflected light is spread in the same angle of the incidence angle. The *diffuse* reflection is when the surface has irregularities comparable or even larger than the wavelength of radiation, and the reflected light doesn't necessarily reflect in the same angle of incidence.

Absorbency of a medium is defined as the ratio of absorbed and incident intensities, and is due to a partial conversion of light energy into heat motion or certain vibrations of molecules of the absorption material. An opaque media is a media in whom incident radiation is reduced to zero, and all the radiation is converted into heat. In contrast, a transparent media permits the passage of light without any absorption.

Scattering is the basic origin of dispersion of the beam into the matter. Because physical processes, e.g. electromagnetic waves, a laser beam penetrating into a media is attenuated and deflected into directions other than the intended forward direction. Scattering reduces laser beam power density by increasing its effective cross-sectional area as it penetrates into tissue.
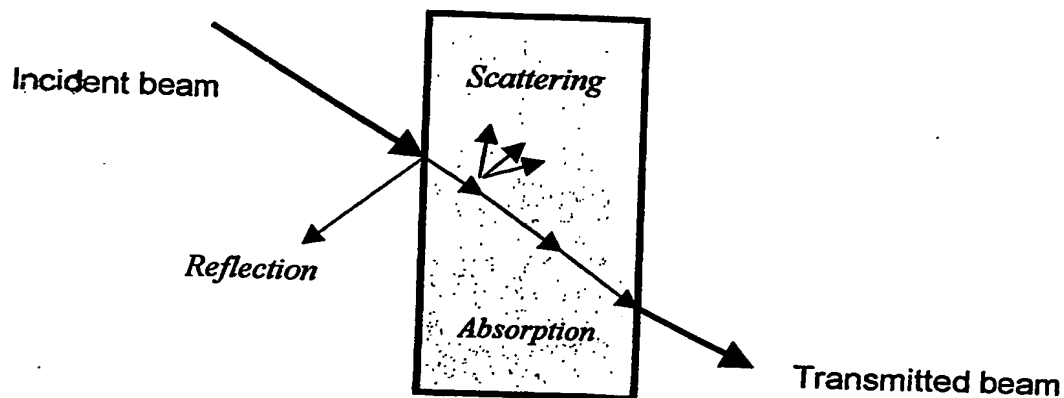
Figure 1-11 Geometry of reflection, absorption, and scattering

1.5.2 Optical penetration depth

The term *optical penetration depth* denotes the depth within which scattering and absorption processes, in a biological tissue, attenuates an incident laser beam. Within this depth the beam energy can induce significant biological effects. If one processes, however, substantially more dominant it will determine the penetration depth, namely it will be either absorption depth or a scattering depth (this depends on the type of biological effects discussed). Absorption depth is the physical process by which atoms and molecules that comprise tissue convert light energy (laser energy) into other forms of energy, such as heat. Assuming that the cross-sectional area of the beam is constant, at certain depth, the power in the forward-directed laser beam is diminished and eventually cannot produce a significant biological effect. Fig 1-12 shows the absorption depth, or the penetration depth according to the type of the biological effect, versus IR wavelength for water. From the optical penetration depth can be referred the *absorption coefficient* α as:

$$\alpha = \frac{1}{D}$$

where D is the optical penetration depth.

The absorption coefficient strongly depends on the wavelength of the incident laser radiation.
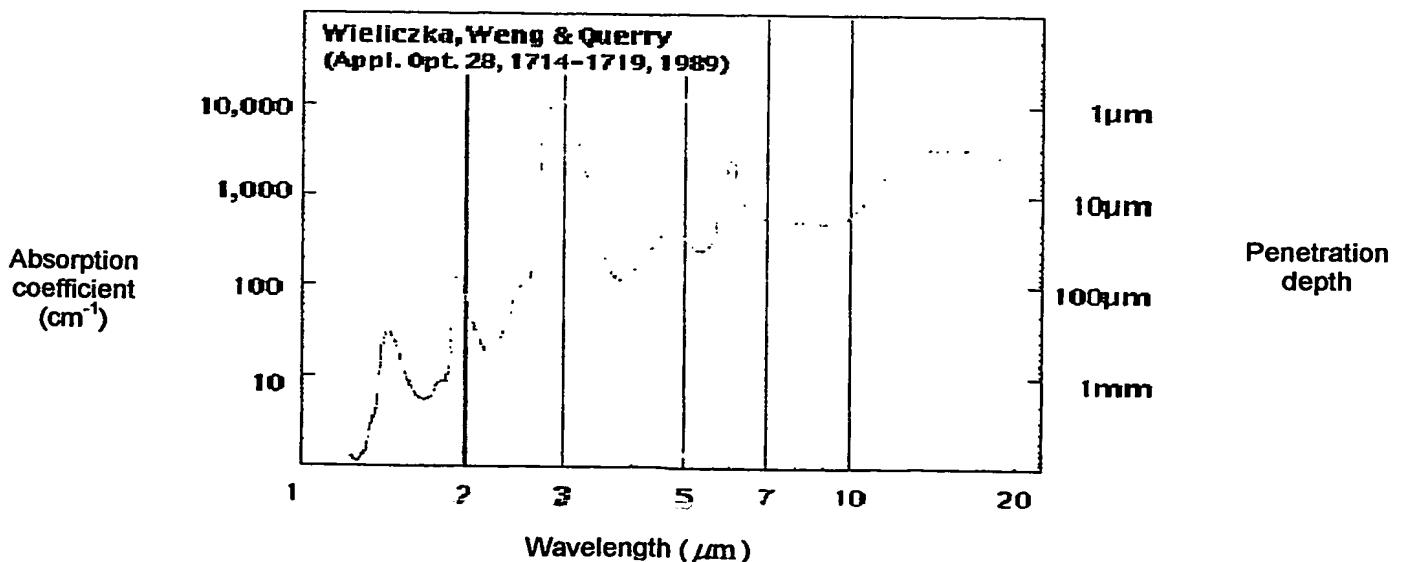
Figure 1-12 Absorption coefficient and penetration depth vs. IR wavelength in water

1.5.3 Thermal penetration depth

Niemz [24] defined the thermal penetration depth as the distance in which the temperature has decreased to 1/e of its peak value:

$$Z_{thermal}(t) = \sqrt{4\alpha_1 t_p}$$ (1.5.3)

where t_p is the pulse duration and α_1 is the thermal diffusivity for water (α_1 = 0.0015 cm^2/sec as mentioned in the next section). For example, if supposed pulse duration of 200 μsec :

$$Z_{thermal} \approx 0.011 \text{ mm}$$

The 200μsec pulse duration is chosen according to the thermal relaxation time (explained in section 1.3.6).

1.5.4 Tissue opto-thermal parameters

Analytical models frequently use opto-thermal parameters of water to represent those of internal soft tissues. Such representations are based on the following:

- The content of stomach tissue is approx 75% water [59]
- CO_2 laser light is highly absorbed in water, almost without scattering

Table 1-2 presents the water parameters set:

Table 1-2 Opto-thermal parameters of water

Symbol	Value	Units	Definition	Reference
D	0.013	mm	Penetration depth	[24]
C	4.2	$J/g\,^0C$	Specific heat	[24]
ρ	1	g/cm^3	Density	[24]
K	0.0063	$W/cm\,^0C$	Thermal conductivity	[40]
α_1	0.0015	cm^2/sec	Thermal diffusivity	[60]
L_v	2.26×10^3	J/g	Latent heat of vaporization	[43]

23

1.5.5 Heat effects in tissue

1.5.5.1 Biological effects

Laser-induced heating has biological implication, results in tissue alterations. The ultimate local fate of such heated tissue falls into one of the following categories [18, 24]:

1. 37-42°C: local warming only - no biological alternations
2. 42-50°C: *hyperthermia*: structural changes of molecules, accompanied by bond destruction and membrane alterations of the cells; edema is observed; for long exposure time (several minutes) necrosis may start.
3. 50-60°C: reduction in enzyme activity, cellular energy transfer and repair mechanisms (i.e. repair of mistakes in DNA producing); inflammation may occur.
4. 60°C: permanent denaturation of proteins and collagen leads to tissue coagulation and shrinkage (generally in blood vessels); necrosis with healing by regeneration
5. 80-100°C: permeabilization of the membrane is drastically increased, destroying the chemical concentration equilibrium; necrosis with healing by scarring or later sloughing
6. 100°C: water molecules, contained in most tissues, start to vaporize; cavitation bubbles cause ruptures and thermal decomposition of tissue fragments, whereby adjacent tissue is preserved.
7. 150°C: carbonization; observable by the blackening of tissue and smoke escape.
8. 3000°C and up: melting

Irreversible damage is subjected not only to tissue temperature but also to the duration it induced. The combined effect, of critical temperature and the duration it induced, on the biological tissue is illustrated in fig. 1-13.
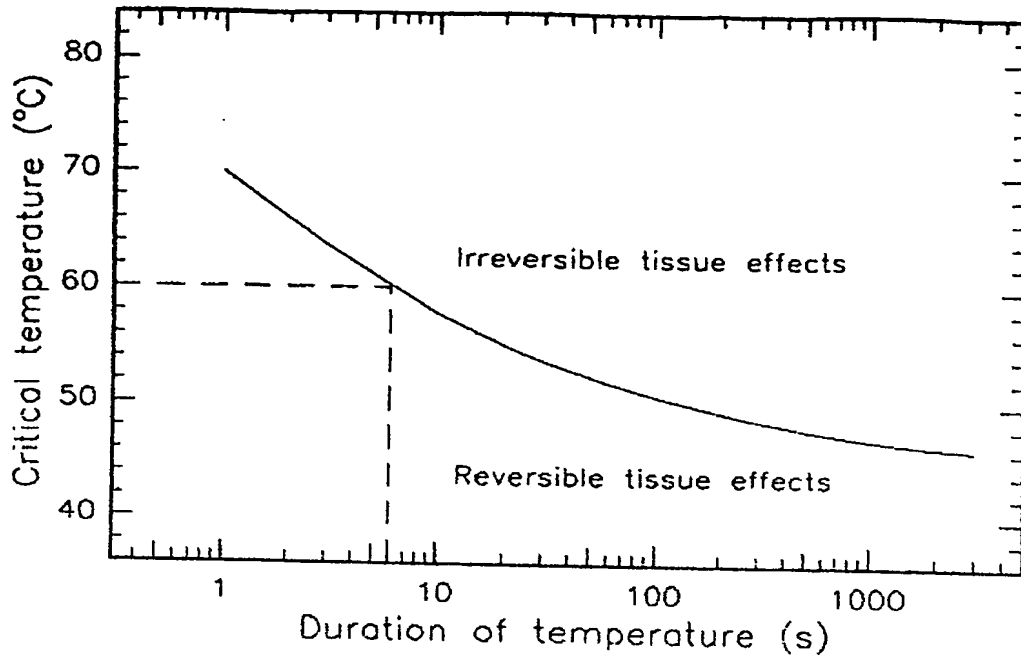
Figure 1-13 Critical temperature for the occurrence of cell necrosis [24]

1.5.5.2 Mechanical effects

Ablation of soft tissues via high-energy laser pulses may generate mechanical side effects as shock wave and cavitations [24]. Cavitations occur if plasmas are generated inside soft tissues or fluids. By means of the high plasma temperature, the focal volume is vaporized. Thereby, work is done against the outer pressure of the surrounding medium, and kinetic energy is converted to potential energy being stored in the expanded cavitation bubble (typically water vapor and carbon oxides). Cavitation bubble usually performs several oscillations of expansion and collapses within a period of a few hundred microseconds. A significant mechanism is formed when such a bubble collapses near a solid - the jet effect.

1.5.5.2.1 Jet Formation

Jet formation was first investigated and described by Lauterborn (1974) and Lauterborn and Bolle (1975) when producing single cavitation bubbles by focusing Q-switched laser pulses into fluids. When cavitation bubbles collapse in the vicinity of a solid boundary, a high-speed liquid jet directed toward the wall is produced. It is reasoned by an asymmetric collapse due to lower fluidic pressure in the bubble side, which is closer to the solid. If the bubble contacts

the solid during its collapse, the jet can cause a high impact pressure against the solid wall.

The temporal behavior of cavitation and jet formation is shown in Fig. 1-14. A cavitation bubble was generated near a solid, located at the bottom of each frame, and captured with high-speed photography. Jet formation toward the solid is observed during the collapse of the bubble. Vogel et al. [61] reported jet velocities of up to 156m/s. The water pressure corresponding to such a velocity is approximately 2kbar. If the distance between the cavitation bubble and solid boundary is further decreased as seen in the bottom sequence, a counter jet is formed, which is pointing away from the solid boundary.
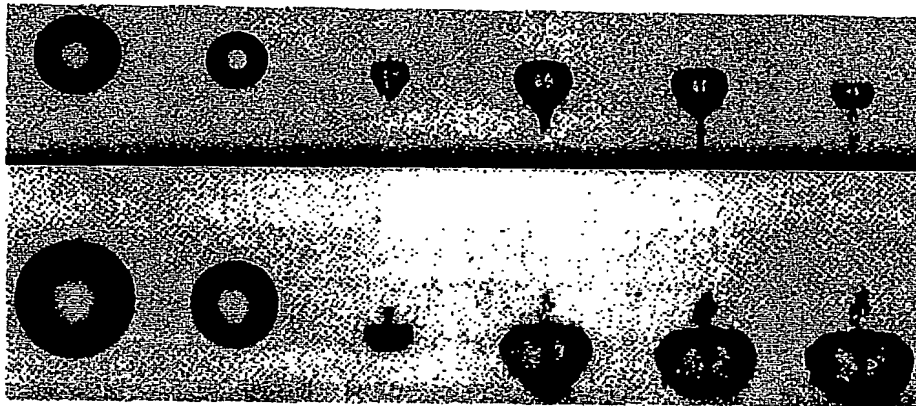
Figure 1-14 Top: bubble collapse with jet formation; bottom: bubble collapse with counter jet formation; pictures taken at 20000 frames per second (frame size: 7.3mm X 5.6mm) [61]

1.5.6 Bioheat transfer

Heat flows in biological media whenever a temperature difference exists. Three modes of heat transfer describe the thermal energy, gained through heat exchange with adjacent structures: conduction, convection, and radiation [62].

Radiation is defined as thermal energy transfer via electromagnetic wave action between non-contacting systems at different temperatures. Unlike either conduction or convection heat transfer, no medium is required for energy transport.

Heat conduction is the transfer of thermal energy through a solid or fluid medium due to an internal temperature gradient. Direct physical contact between interacting systems is required for conduction to happen. The transfer of thermal energy occurs at the molecular and atomic levels without net mass motion of the material. In stationary fluids, random translational and internal rotational and vibrational motions of molecules cause collisions to transfer heat from regions of high temperature to regions of low temperature [43].

Convection is the transfer of thermal energy through a fluid due to bulk motion of the fluid. This is the most important mechanism for thermal energy transfer between a solid and a moving fluid. Heat convection is important for laser irradiation studies in the following settings: PDT, irrigation of surface tissues during irradiation, irradiation of surface and near-surface regions for extended periods, and post-irradiation heat transfer. Convection typically involves four simultaneous intermediate processes:

1. Conduction of heat from the solid surface to the immediately adjacent fluid particles.

2. Absorption and storage of the conducted energy by these fluid particles with elevation of their internal energy.

3. Migration of these higher-energy fluid particles to regions of lowers temperature, with mixing and transfer of part of the stored energy.

4. Transport of the energy by bulk movement of the fluid.

The combined effect is referred to as the convection heat transfer. There are two different types of convection, depending on the driving force for fluid motion:

"Forced convection" is the result of positive fluid motion caused by external mechanical means, and is most important for studies involving flowing blood, irrigation fluids or gas.

In "free convection", fluid motion is caused by density differences in the fluid itself. The density differences result from temperature differences in the fluid. They are most relevant for modeling gas convection currents and plumes above the irradiated tissue.

The biological surface loss process was investigated by Loze and Wright [63]. They found a combined convective-evaporative loss in surface, whereat evaporation was the major, representing an important surface-heat-loss mechanism. This study employed several laser wavelengths, yet excluded 10.6µm.

1.5.7 Heat exchange with the environment

An organism exchanges energy and mass with the environment through a combination of convection, radiation, evaporation, and conduction. The driving forces of these exchange mechanisms are the temperature and water vapor partial pressure differences between tissue and surroundings. The amount of heat transferred by each mechanism varies with atmospheric conditions.

Air circulation will increase the *convectional* heat transfer by a large factor. Calculations demonstrate the ability of the circulatory system to selectively modify the tissue temperature [43].

1.6 Tissue-like Phantoms

Phantom is a vital component in this investigation. It needs to simulate reliably tissue thermal properties and to fit experimental course under certain constraints. The fundamental types noted in this regard are: Polyacrylamide gel, Agar gel and in-vitro biological specimens, taken from porcine and caw organs. Theses various phantom types are summarized below.

1.6.1 Biological phantoms

Using actual tissue is sometimes impractical due to the constraints of accessibility and storage of fresh samples. Reproducibility of results may also be poor because of the difficulty in finding identical specimens. Nonetheless, biological phantoms are widely used prior to animal studies. Following are two relevant examples of such phantoms utilization:

Exploring temperature distribution for combined laser hyperthermia-PDT therapy in the esophagus by means of cow muscle [64].

Thermal events during CW argon laser ablation were investigated using porcine aorta [65].

1.6.2 Tissue-equivalent materials

An alternative approach is to use tissue-equivalent materials or phantoms. Phantoms are usually homogeneous, and therefore do not normally possess the complex structures that exist throughout tissue. Therefore, tissue substitutes do not necessarily reflect the true complexity and hence response of tissue during laser therapy. However, they do provide a qualitative means of testing the parameters and assumptions made in mathematical models and may indicate generally important features of opto-thermal processes in tissue. Phantoms may also be used to demonstrate and elucidate the transient effects of interstitial laser heating. For instance, heating of tissue during interstitial laser photocoagulation produces a coagulated region surrounded by healthy tissue. This occurs in a dynamic fashion, which depends upon a variety of factors such as the temperature dependent changes in optical

properties of the tissue and changes in blood perfusion. Phantoms may therefore be used to investigate these effects in a controlled fashion where the complexities of in vivo studies can be avoided [66].

1.6.2.1 PolyAcrylAmide (PAA)

PAA gels, used as tissue phantoms, give a more realistic simulation of tissue compared to water. This gel has structural integrity, which can be varied by varying the water concentration (typically between 60 and 95 %, i.e. 40 to 5% PAA). In addition the gel is optically transparent which allows visualization of the ablation process. Compared to other gels such as agar or gelatin, the biggest advantage is, that PAA does not melt at elevated temperatures, which is important in ablation studies [67]. However, Acrylamide as a monomer is considered toxic, directly affecting the nervous system, and it may reasonably be considered to be a carcinogen. Acrylamide is readily absorbed through intact skin from aqueous solutions [68].

PAA phantoms have been used during near IR laser photocoagulation studies [66], evaluation of hyperthermia utilization [69], studies in laser interstitial thermal therapy for treating breast tumors [70], investigation of thermal events during CW argon laser ablation [65], etc.

1.6.2.2 Agar

Arag / Agrose gels is generally used to simulate tissue optical properties. Yet it has served some thermal investigations [66, 71, 72], and considered safe to work with. For instance, an Agar phantom, possessing a cavity, for simulating the stomach, was employed to evaluate temperature distribution upon RF-heating. Such therapy was aimed at patients with advanced gastric cancer.

The gels are frequently combined with substances as Intralipid and Naphthol green dye to imitate tissue properties. Intralipid is a weakly absorbing, highly scattering liquid emulsion that can be diluted with water to yield tissue-like scattering in the near IR. Naphthol green dye is an organic powder that can be dissolved in water and added to Intralipid suspension to yield absorption properties of tissues in the near IR [73].

Additional related information can be noticed in [66, 74, 75].

1.7 Thermography

1.7.1 Introduction

William Herschel, an astronomer, discovered the Infra Red (IR) in 1800. Knowing that sunlight was made up of all the colors of the spectrum, and that it was also a source of heat, he wanted to find out which colors were responsible for heating objects. He devised an experiment using a prism, paperboard, and thermometers with blackened bulbs where he measured the temperatures of the different colors. Herschel observed an increase in temperature as he moved the thermometer from violet to red in the rainbow created by sunlight passing through the prism. He found that the hottest temperature was actually beyond red light. The radiation causing this heating was not visible; Herschel termed this invisible radiation "calorific rays." Today, we know it as IR.

1.7.2 IR thermography

Nearly everything that uses or transmits energy gets abnormally hot before it damaged. That includes human tissues and fiberoptics. IR thermography is an effective predictive and the only diagnostic technology that lets an instantly visualize and verify thermal performance. IR cameras show thermal problems and quantify them with precise non-contact temperature measurement. IR camera is a non-contact device that detects IR energy (heat) and converts it into an electronic signal, which is then processed to produce a thermal image on a video monitor and perform temperature calculations. Heat sensed by an IR camera can be precisely quantified, or measured, allowing monitoring thermal performance and identifying and evaluating the relative severity of heat-related problems.

1.7.3 IR in Medicine

IR thermal imaging has been used for several decades to monitor the temperature distribution of human skin. Abnormalities such as malignancies, inflammation, and infection cause localized increases in temperature, which show as hot spots or as asymmetrical patterns in an IR thermogram. Even though it is nonspecific, IR thermology is a powerful detector of problems that

affect a patient's physiology. Digital IR cameras have much improved spatial and thermal resolutions, and libraries of image processing routines are available to analyze images captured both statically and dynamically. If thermographs are captured under controlled conditions, they may be interpreted readily to diagnose certain conditions and to monitor the reaction of a patient's physiology to thermal and other stresses. Some of the major areas where IR thermography is being used successfully are neurology, vascular disorders, rheumatic diseases, tissue viability, oncology (especially breast cancer), dermatological disorders, neonatal, ophthalmology, and surgery [76]. Cadeddu et al. [77] have recently combined IR imaging during laparoscopic clinical and animal studies. They concluded it could improve differentiation and localization of anatomic structures and allow, for the first time, to assess laparoscopically physiologic features, such as perfusion and tissue viability.

1.7.4 The Theory of Thermography

1.7.4.1 IR wavelength

Thermography makes use of the IR spectral band [78, 79]. At the short-wavelength end the boundary lies at the limit of visual perception, in the deep red. At the long-wavelength end it merges with the microwave radio wavelengths, in the millimeter range. The IR band is often further subdivided into four smaller bands, the boundaries of which are also arbitrarily chosen. They include: the near IR (0.75-2 μm), the mid IR (2-20 μm), the far and the extreme IR (20-100 μm) [38, 80].
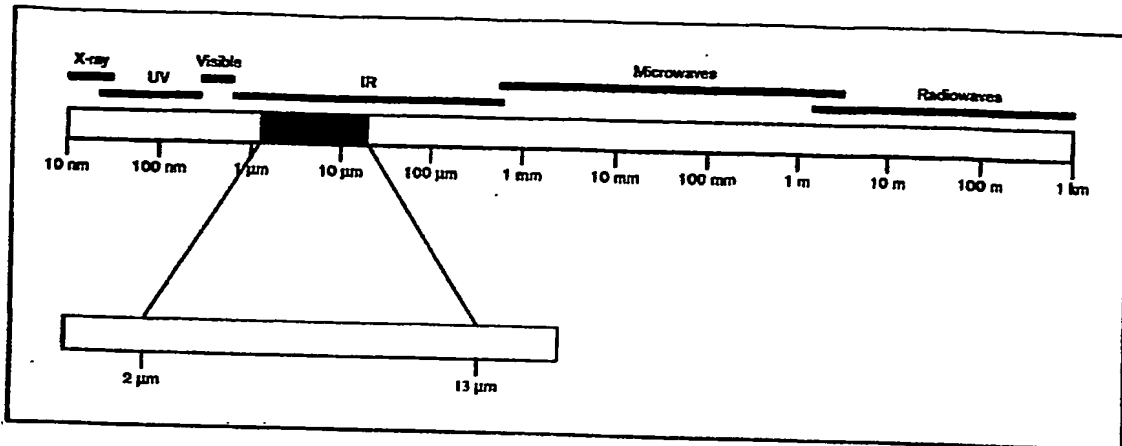
Figure 1-15 The electromagnetic spectrum. Thermography typically uses wavelengths between 2 and 13μm.

1.7.4.2 Blackbody radiation

A blackbody is defined as an object, which absorbs all radiation that impinges on it at any wavelength. The apparent misnomer 'black' relating to an object emitting radiation is explained by Kirchhoff's Law (after *Gustav Robert Kirchhoff*, 1824-1887), which states that a body capable of absorbing all radiation at any wavelength is equally capable in the emission of radiation.

The radiation characteristics of an aperture in an isotherm cavity made of an opaque absorbing material represents almost exactly the properties of a blackbody. By providing such an isothermal cavity with a suitable heater it becomes what is termed a 'cavity radiator'. An isothermal cavity heated to a uniform temperature generates blackbody radiation, the characteristics of which are determined solely by the temperature of the cavity. Such cavity radiators are commonly used as sources of radiation in temperature reference standards in the laboratory for calibrating thermographic instruments as IR camera.

If the temperature of blackbody radiation exceeds 525°C, the source begins to be visible so that it appears to the eye no longer black. This is the incipient red heat temperature of the radiator, which then becomes orange or yellow as the temperature increases further. In fact, the definition of the so-called 'color temperature' of an object is the temperature to which a blackbody would have to be heated to have the same appearance.

Three expressions describe the radiation emitted from a blackbody:

1.7.4.3   Planck's law

Max Planck (1858-1947) was able to describe the spectral distribution of the radiation from a blackbody by means of the following formula:

$$W_{\lambda b} = 2\pi hc^2\, 10^{-6} /\, \lambda^5(e^{hc/\lambda kT}-1) \quad (Watts/m^2\mu m)$$

(1.7.4.3)

where:

$W_{\lambda b}$ = the blackbody spectral radiant emittance at wavelength λ.

c   = the velocity of light = 3×10^8 m/sec.

h   = Planck's constant = 6.6×10^{-34} Joule sec.

k   = Boltzmann's constant = 1.4×10^{-23} Joule/K.

T   = the absolute temperature (K) of a blackbody.

λ = wavelength (m).

Planck's formula, when plotted graphically for various temperatures, produces family of curves (1-16). Following any particular Planck curve, the spectral emittance is zero at λ = 0, then increases rapidly to a maximum at a wavelength λ_{max} and decreases exponentially back to zero. The higher the temperature, the shorter the wavelength at which maximum occurs.
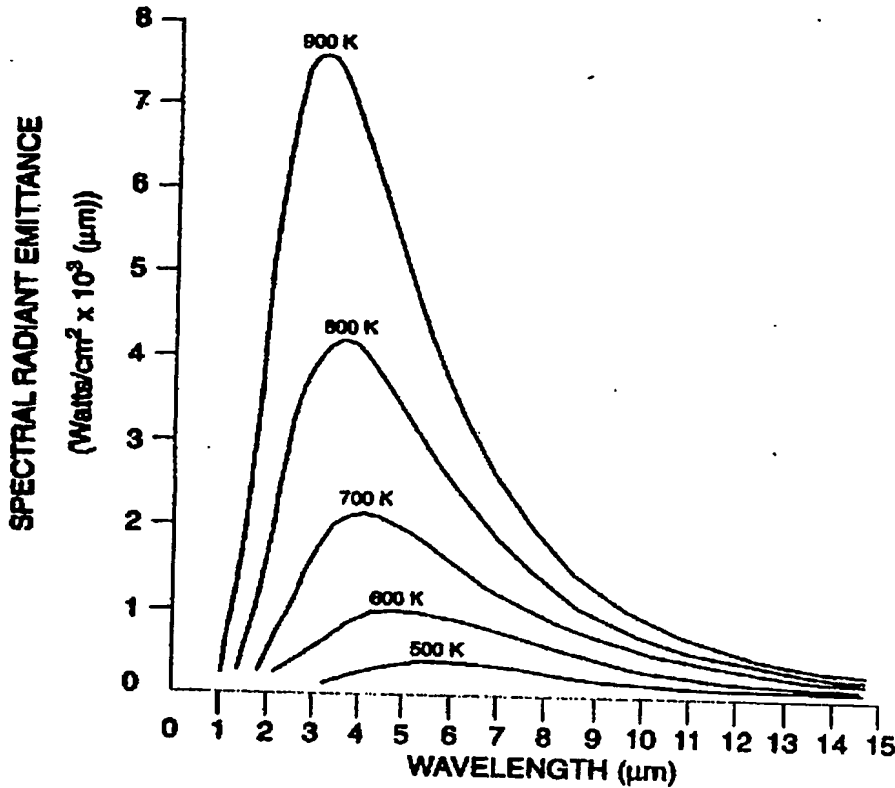
Figure 1-16 Blackbody spectral radiant emittance according to Planck's law, plotted for various absolute temperatures [78]

1.7.4.4   Wien's displacement law

By differentiating Planck's formula with respect to λ, and finding the maximum, we have:

$$\lambda_{max} = 2898/T \text{ (µm)}$$

(1.7.4.4)

This is Wien's formula (after *Wilhelm Wien*, 1864-1928), which expresses mathematically the common observation that colors vary from red to orange or yellow as the temperature of a thermal radiator increases. The wavelength of the color is the same as the wavelength calculated for λ_{max}. A good approximation of the value of λ_{max} for a given blackbody temperature is obtained by applying the rule-of-thumb 3000/T µm. For instance, the sun (~6000K) emits yellow light, peaking at ~0.5µm in the mid visible spectrum, while at room temperature (300K) the peak of radiant emittance lies at 9.7µm, in the mid IR.
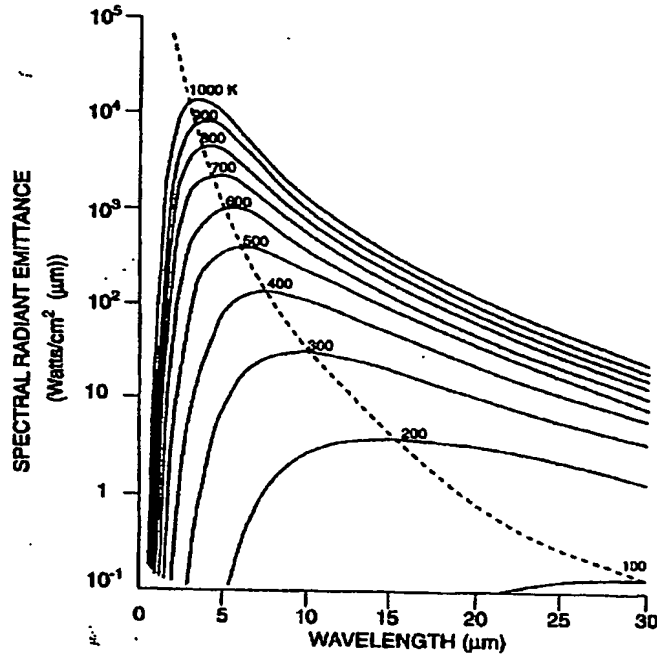
Figure 1-17 Planckian curves plotted on semi-log scales from 100K to 1000K. The dotted line represents the locus of maximum radiant emittance at each temperature as described by Wien's displacement law

1.7.4.5 The Stefan-Boltzmann law

Integrating Planck's formula from $\lambda = 0$ to $\lambda = \infty$, obtains the total radiant emittance (W_b) of a blackbody:

$$W_b = \sigma\, T^4 \;(\text{Watts/m}^2)$$

(1.7.4.5)

where:

$\sigma =$ the Stefan-Boltzmann constant $= 5.7 \times 10^{-8}\,\text{Watt/m2}$

This is the Stefan-Boltzmann formula (after Josef Stefan, 1835-1893, and Ludwig Boltzmann, 1844-1906), which states that the total emissive power of a blackbody is proportional to the fourth power of its absolute temperature. This means that even slight temperature differences between adjacent areas of a blackbody will result in large differences in radiant emittance.

Graphically, W_b represents the area below the Planck curve for a certain

temperature. It can be shown that the radiant emittance in the interval $\lambda = 0$ to λ_{max} is only 25% of the total.

Using the Stefan-Boltzmann formula to calculate the power radiated by the human body, at a temperature of 300K and an external surface area of approx. 2m^2, we obtain 1kW. This power loss could not be sustained if it were not for the compensating absorption of radiation from surrounding surfaces, at room temperatures, which do not vary too drastically from the temperature of the body.

1.7.4.6 Non-blackbody emitters

Real objects almost never comply with these laws over an extended wavelength region - although they may approach the blackbody behavior in certain spectral intervals (fig. 1-18). For example, white paint appears perfectly 'white' in the visible light spectrum, but becomes distinctly 'gray' at about 2 μm, and beyond 3 μm it is almost 'black'.

Three processes can prevent a real object from acting like a blackbody: a fraction of the incident radiation α may be absorbed, a fraction ρ may be reflected, and a fraction τ may be transmitted. Since all of these factors are more or less wavelength dependent, the subscript λ is used to imply the spectral dependence of their definitions. Thus:

- The spectral absorbance $\alpha_\lambda =$ the ratio of the spectral radiant power absorbed by an object to that incident upon it

- The spectral reflectance $\rho_\lambda =$ the ratio of the spectral radiant power reflected by an object to that incident upon it

- The spectral transmittance $\tau_\lambda =$ the ratio of the spectral radiant power transmitted through an object to that incident upon it

The sum of these three factors must always add up to the whole at any wavelength, so we have the relation:

$$\alpha_\lambda + \rho_\lambda + \tau_\lambda = 1$$

(1.7.4.6.1)

For opaque materials $\tau_\lambda = 0$, and the relation simplifies to:

$$\alpha_\lambda + \rho_\lambda = 1$$

<div align="right">(1.7.4.6.2)</div>

Another factor, called the emissivity, is required to describe the fraction ε of the radiant emittance of a blackbody produced by an object at a specific temperature. Thus, we have the definition:

The spectral emissivity ε_λ = the ratio of the spectral radiant power from an object to that from a blackbody at the same temperature and wavelength. Expressed mathematically, this can be written as the ratio of the spectral emittance of the object to that of a blackbody as follows:

$$\varepsilon_\lambda = W_{\lambda o} / W_{\lambda b}$$

Generally, there are three types of radiation source, distinguished by the ways in which the spectral emittance of each varies with wavelength.

• A blackbody, for which $\varepsilon_1 = \varepsilon = 1$.

• A graybody, for which $\varepsilon_1 = \varepsilon$ = constant less than 1.

• A selective radiator, for which ε varies with wavelength.

According to Kirchhoff's Law, for any material the spectral emissivity and spectral absorption of a body are equal to any specified temperature and wavelength. That is:

$$\varepsilon_\lambda = \alpha_\lambda$$

From this we obtain, for an opaque material (since $\alpha_\lambda + \rho_\lambda = 1$):

$$\varepsilon_\lambda + \rho_\lambda = 1$$

For highly polished materials ε_λ approaches zero, so that for a perfectly reflecting material (i.e. a perfect mirror) we have

$$\rho_\lambda = 1$$

For a graybody radiator, the Stefan-Boltzmann formula becomes

$$W = \varepsilon \sigma T^4 \text{ (Watt/m}^2)$$

<div align="right">(1.7.4.6.3)</div>

This states that the total emissive power of a graybody is the same as a blackbody at the same temperature reduced in proportion to the value of ε from the graybody.
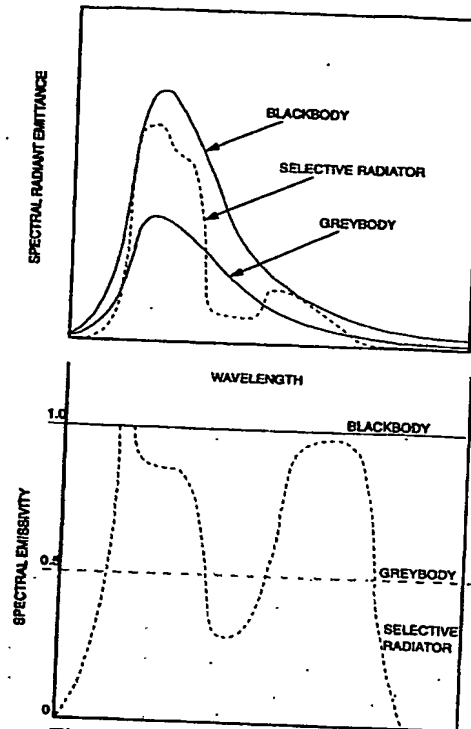

Figure 1-18 Spectral radiant emittance and spectral emissivity of three types of radiators

1.7.4.7 IR semi-transparent materials

Consider a non-metallic, semi-transparent body, in the form of a thick flat plate of plastic material. When the plate is heated, radiation generated within its volume must work its way toward the surfaces through the material in which it is partially absorbed. Moreover, when it arrives at the surface, some of it is reflected back into the interior. The back-reflected radiation is again partially absorbed, but some of it arrives at the other surface, through which most of it escapes; part of it is reflected back again. Although the progressive reflections become weaker and weaker they must all be added up when the total emittance of the plate is sought. When the resulting geometrical series is summed, the effective emissivity of a semi-transparent plate is obtained as

$$\varepsilon_\lambda = (1-\rho_\lambda)(1-\tau_\lambda)/(1-\rho_\lambda \tau_\lambda)$$

(1.7.4.7.1)

When the plate becomes opaque ($\tau_\lambda = 0$) this formula is reduced to the single formula:

$$\varepsilon_\lambda = 1-\rho_\lambda$$

(1.7.4.7.2)

This last relation is a particularly convenient one, because it is often easier to measure reflectance than to measure emissivity directly.

1.7.4.8 IR Camera measurement formula

When viewing an object, camera receives radiation from three sources:

- The object itself
- The surroundings, reflected by object surface
- The atmosphere

The atmosphere along the viewing medium attenuates contributions of the first two. This description of the measurement situation (illustrated in fig. 1-19) neglects other emitters such as sun light scattering in the atmosphere or stray radiation from intense radiation sources outside the field of view. These disturbances are difficult to quantify, however, in most cases they are small enough to be neglected. In case they are not, the measurement configuration is likely to be such that the risk for disturbance is obvious. Changing the

40

viewing direction or shielding off intense radiation sources will avoid them. Using this model, we can derive a formula for the calculation of the object temperature from the calibrated camera output.
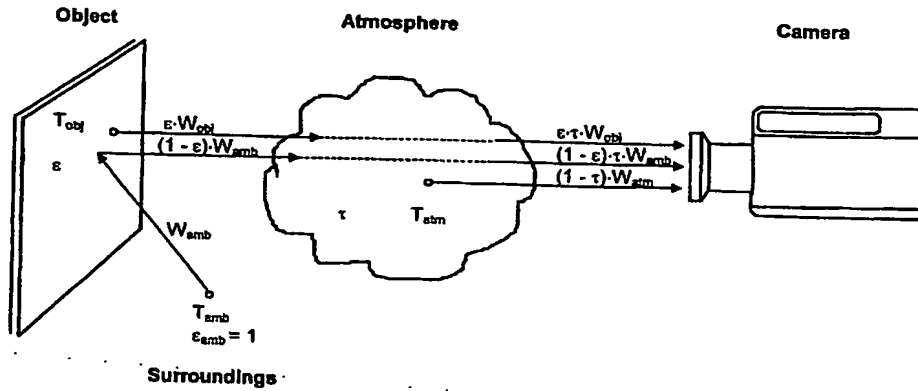

Figure 1-19 A schematic representation of the general thermographic measurement situation.

Assuming the received radiation power W from a blackbody source of temperature T_{source} on short distance generates a camera output signal U_{source} that is proportional to the power input (power linear camera), we can write:

$$U_{source} = C \cdot W\ (T_{source})$$

or, with simplified notation:

$$U_{source} = C \cdot W_{source}$$

(1.7.4.8.1)

where C is a constant.

Should the source be a graybody with emittance $\mathcal{E}$, the received radiation would consequently be $\mathcal{E} \cdot W_{source}$

The three collected radiation power terms:

(1) Emission from the object = $\mathcal{E} \cdot \mathcal{T} \cdot W_{obj}$

where $\mathcal{E}$ is the emittance of the object and $\mathcal{T}$ is the transmittance of the

41

atmosphere. The object temperature is T_{obj}.

(2) Reflected emission from ambient sources = $(1- \mathcal{E}) \cdot \mathcal{T} \cdot W_{amb}$

where $(1 - \mathcal{E})$ is the reflectance of the object. The ambient sources have the temperature T_{amb}

It has here been assumed that the temperature T_{amb} is the same for all emitting surfaces within the hemisphere seen from a point on the object surface. This is sometimes a simplification of the true situation. It is, however, a necessary simplification in order to derive a workable formula, and T_{amb} can theoretically be given a value that represents an efficient temperature of a complex surrounding.

We have additionally assumed that the emittance for the surroundings = 1. This is correct in accordance with Kirchhoff's law: All radiation impinging on the surrounding surfaces will eventually be absorbed by the same surfaces. Thus the emittance = 1.

(3) Emission from the atmosphere = $(1- \mathcal{T}) \cdot \mathcal{T} \cdot W_{atm}$

where $(1- \mathcal{T})$ is the emittance of the atmosphere. The temperature of the atmosphere is T_{atm}

..The total received radiation power can now be written:

$$W_{tot} = \mathcal{E} \cdot \mathcal{T} \cdot W_{obj} + (1- \mathcal{E}) \cdot \mathcal{T} \cdot W_{amb} + (1- \mathcal{T}) \cdot W_{atm}$$

Each term is multiplied by the constant C of eq. 1.7.4.8.1 and the products C· W is replaced by the corresponding U according to the same equation:

$$U_{tot} = \mathcal{E} \cdot \mathcal{T} \cdot U_{obj} + (1- \mathcal{E}) \cdot \mathcal{T} \cdot U_{amb} + (1- \mathcal{T}) \cdot U_{atm} \qquad (1.7.4.8.2)$$

or:

$$\boxed{U_{obj} = U_{tot} / \mathcal{E} \cdot \mathcal{T} + U_{amb}(\mathcal{E} -1)/ \mathcal{E} + U_{atm}(\mathcal{T} -1)/ \mathcal{E} \cdot \mathcal{T} \qquad (1.7.4.8.3)}$$

where:

U_{obj} - Calculated camera output voltage for a blackbody of temperature T_{obj} i.e.

voltage that can be directly converted into requested object temperature.

U_{tot} - Measured camera output voltage for the actual case

U_{amb} - Theoretical camera output voltage for a blackbody of temperature T_{amb} according to calibration

U_{atm} - Theoretical camera output voltage for a blackbody of temperature T_{atm} according to calibration

This is the measurement formula of the thermal camera we have used.

Additional references: [81-86]

2 Study goal

As discussed in the introduction chapter, CO_2 and Er YAG lasers are considered best for treating such cases as mucosal gastric cancer and Barrett Esophagus, where ablating superficial tissue layer is needed. They are not yet applied endoscopically to the lining of body cavities as their flexible waveguides have only been developed recently. Furthermore, irradiating tissue within a closed space, using wavelengths that are highly absorbed in water, will cause the dispersion of hot steam, and thus may thermally damage healthy tissues that line the cavity. Hence, studying the potential side effects during such MIS should precede the practical procedure. Investigating thermal side effects as well as ways to manage them have motivated our research and its two goals, respectively:

א. To investigate experimentally heat distribution, thermal effects and maximal temperature of the surrounding tissue, in a closed body cavity, during transendoscopical, CO_2 laser based surgery.

ב. To explore the relative effect of every controllable component (i.e. parameters of laser, suction and gas insufflator), during such an MIS, by the means of software-controlled setup that simulates practical conditions.

3 Experimental investigation

3.1 Experiment strategy

3.1.1 Determining the controllable parameters

Investigating heat dispersion within cavity-like human tissues, during laser irradiation is a multi-parameter problem. Most of them are listed below (some are correlated), classified into three categories, assuming the use of 10.6µm laser and a hollow fiber:

1st category – The Energy Transmission System

- Laser power
- Continuous mode: duration of laser transmission
- Pulse mode: pulse duration, shape and frequency, duty cycle
- Fiber characteristics: straightened / angulated, beam diameter and profile, perfusion and attenuation (transmission ratio)
- Hit angle

2nd category – The Cavity Medium

- Cavity volume and geometry of surrounding tissue
- Distance between fiber edge and the irradiated tissue
- Gas content
- Atmospheric pressure (or vacuum), gas flow rate and mode

3rd category – Tissue dynamic characteristics during the irradiating

- Composition (mainly the water percentage of every layer induced)
- Crater deepness and shape
- Initial temperature

The parameters of the first two categories (excluding organ geometry) govern the effective power profile that applied to tissue. Given the applied power at a certain time, the heat distribution will be characterized by the last two categories (excluding the distance fiber-tissue). Hence the medium parameters play a double role in this issue and should be considered thoroughly.

We had to decide which parameters are the ones to be modified in this experimental study. Doing so we based on three criteria:

א. Our technical capabilities and limitations

ב. Relative contribution to heat build up and distribution

ג. Clinical aspect - in practice, the surgeon controls the laser power, the transmission duration, the pulse mode, the CO_2 insufflating and the suction volume. He also has a limited control on the angle and the distance between endoscope and tissue.

The following parameters were accordingly selected:

1st category

- Laser power (when fiber was used - power that exits the fiber)
- Transmission mode: continuous / pulse
- Transmission duration
- When pulse mode: pulse rate, duty cycle
- Hollow fiber types: 1.6mm rigid, 0.67mm flexible*, 0.3mm flexible (*)
- Beam diameter: 6.5mm (no fiber), 1.6mm (rigid fiber)
- Hit angle: perpendicular, diagonal (45-70°)

2nd category

- Cavity roof: flattened, domed, roofless
- Distance fiber-irradiated tissue
- Injected gases: air, CO_2, suction, combinations of them, none

- CO_2 gas flow and vacuum rate

3rd category

- Tissue types: Agarose gel phantoms, in-vitro samples of porcine stomach
- Crater deepness

(*) Both flexible fibers were damaged shortly after laser had been activated, due to imperfect coupling and fiber coating. The rigid fibers lasted longer but couldn't be threaded through gastroscope. These lessons are taken into consideration in our subsequent investigation (see prospective research, chapter 5).

3.1.2 The Monitoring strategy

Exploring the temperature development of the surrounding tissue was the study goal. The location of tissue hottest areas is parameter-dependable. In order to "cover" the whole area an IR camera was used. It further enabled an online feedback by acquiring raw or analyzed thermal data.

We additionally used a video camera to visually record the smoke (and the steam) distribution, as it is the cause to the heat build up along the surrounding tissue.

3.1.3 Phantom selection

As mentioned in section 1.6 polyacrylamide (PAA) gels commonly simulate the thermal properties of human tissues. However this material is considered being cancerous, fast hardened and fractured and thus difficult to work with. During our preliminary trials we used Agarose gel instead (see sec 3.2.4.1 for recipe). It gave us a ballpark estimation of the heat distribution. We then replaced it by porcine gastric samples to finely imitate the thermal response of human stomach. The biological phantoms were combined with various plastic hemispheres to construct cavity-like phantoms.

3.2 Setup components

Scheme in fig. 3-20 describes the comprehensive setup, which has been used in the software-controlled stage. During earlier stages, we have adopted relevant parts of this setup. It consists of four subsystems:

- Transmittance
- Control
- Feedback
- Phantoms
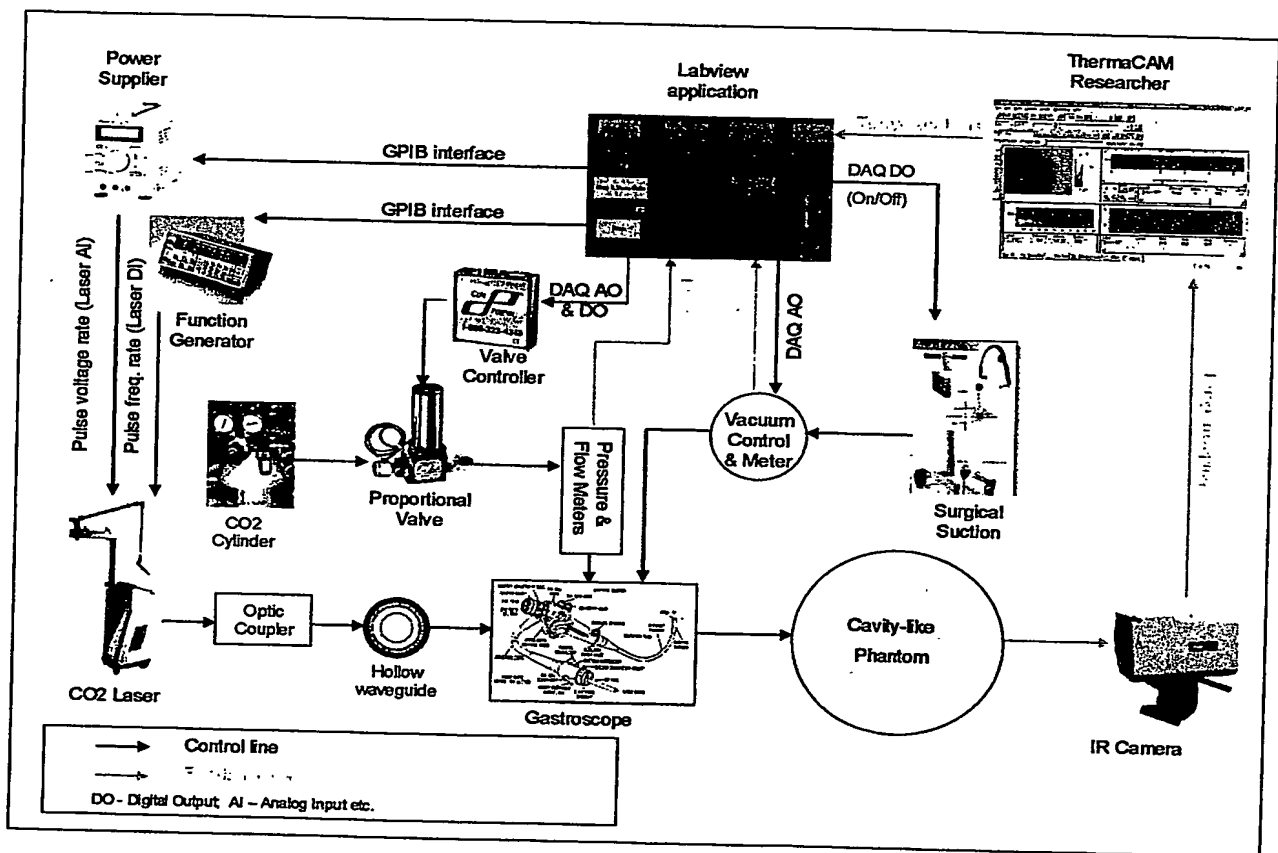
Figure 3-20 Inclusive setup scheme

Setup components are listed in the following sections.

3.2.1 Transmittance: Mid IR Energy, Insufflating and Suction

Devices: Laser system, Insufflating system, Suction system
Transmittance Media: Gastroscope, Fiberoptics, Optic Couplers, Mirrors

Laser System

- Sharplan 1041S CO_2 Laser Generator 0-100w
- Goodwill PPT-3615 Programmable Power Supply
- Stanford Research System DS335 Synthesized Functions Generator

The laser user interface is bypassed. Laser generator is activated and controlled by two input channels, wired directly to laser electronics: analog channel and digital channel.

- Analog Channel - determines laser pulse amplitude
- Digital channel - determines laser pulse rate and duty cycle

Power Supplier - wired to laser analog channel

Functions Generator - wired to laser digital channel

Both instruments are controlled and monitored by Labview based drivers through GPIB.

Alternatively, we've managed to control laser parameters by the means of DAQ hardware and Labview programs as follows:

- Labview sub VI - direct control of pulse rate and duty cycle through NI-DAQ and external connection board, wired to laser digital channel
- Labview sub VI - direct control of pulse amplitude and on/off through NI-DAQ and external connection board, wired to laser analog channel

Insufflating System

This system functions as a CO_2 gas insufflator, used for MIS, such as Laparoscopy. Its main role is to insufflate the sphere in which the surgery is performed. It additionally enables to use the gas for cooling.

Components:

- CO$_2$ Gas Cylinder
- Low Pressure Regulator
- Pressure Gauge
- Proportional Electrical Valve
- Valve Controller (on/off; flow rate)
- Electrical Flow meter
- Pipeline
- NI DAQ hardware for PC
- Labview Drivers that monitor the actual flow and control it according to the main application

Suction System

- Acu-E-Vac II Surgical Suction
- Proportional Vacuum Valve
- Electrical Vacuum Meter
- Pipeline
- NI DAQ hardware for PC
- Labview Drivers that monitor the actual vacuum and control it according to the main application

Optics

- Focusing lens, mirrors, tailor-made optic couplers, SMAs, Iris Diaphragm

Fiberoptics

- Rigid hollow 1600 μm
- Flexible hollow 700 and 300 μm
- None (focused laser beam)

Pic 3-2 and fig 3-21,22 present the fibers and their structure, made by our group:
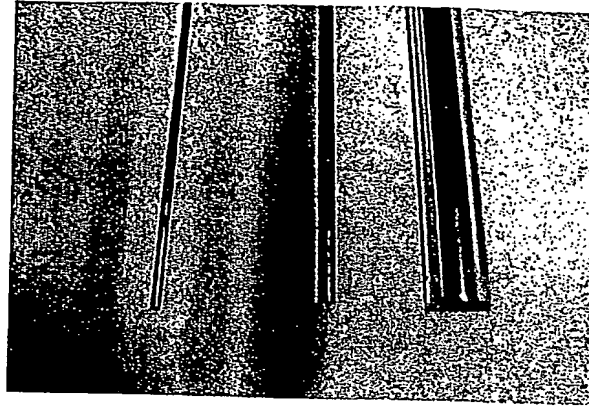
Picture 3-2 From left to right: 300μm flexible,
700μm flexible and 1600μm rigid fiberoptics
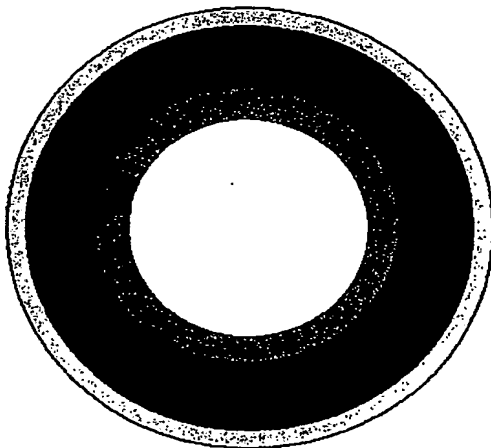
Figure 3-21 Principle structure of the
hollow fiberoptics: black - hollow tube
(fused silica, glass); blue - metal layer
(silver); green - dielectric layer (AgI); red
- optional jacket (flexible fibers only)
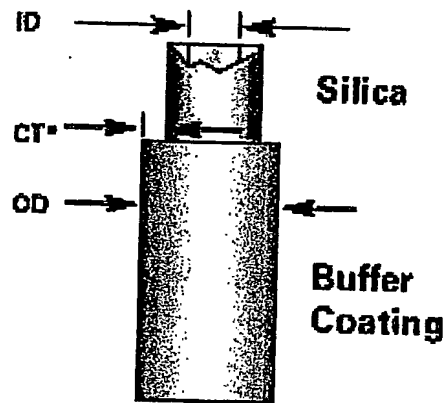
Figure 3-22 Fused Silica capillary
tubing; CT* - coating thickness (red
layer on left figure), for flexible
fiberoptics

The flexible fibers got overheated in the mid and the high ranges of laser
powers and therefore abandoned at the very beginning. Consequently, the
use of the gastroscpoe was limited.

Gastroscope

Olympus GIF type 2T10 (pic 3-3);
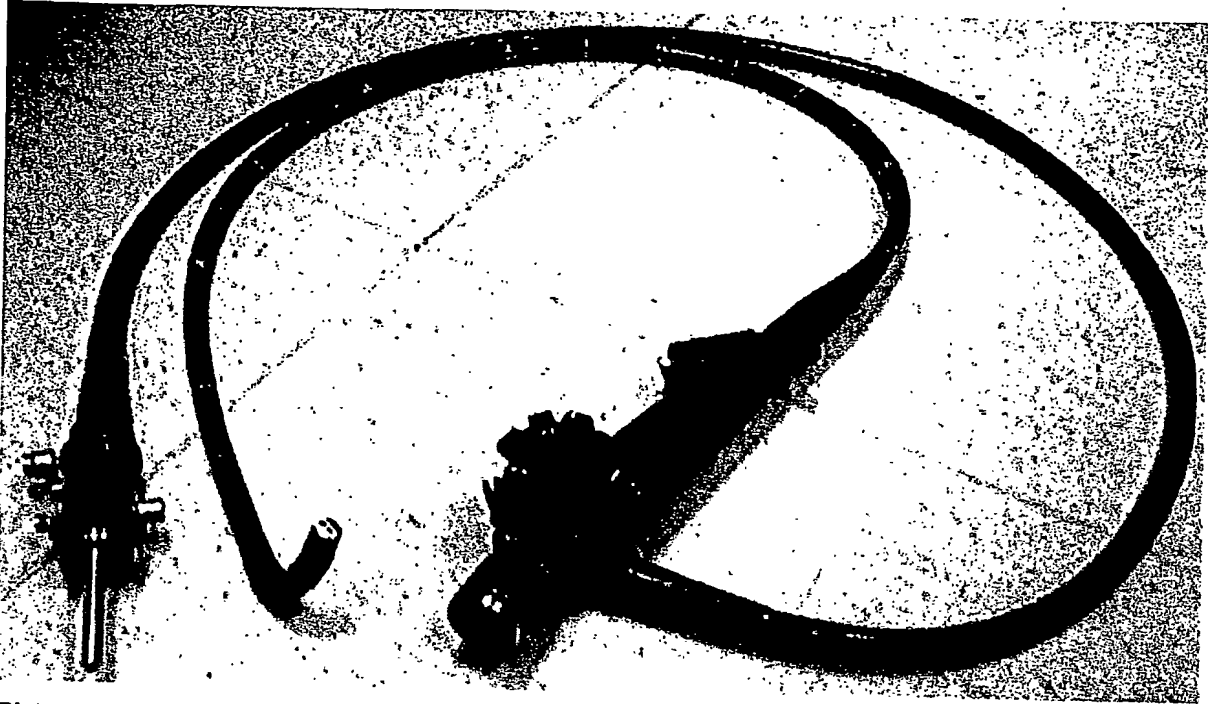
Picture 3-3 Olympus gastroscope

Refer section 1.1.3 and figure 1-3 for details.

3.2.2 Control

Software Application

All drivers have been developed using NI Labview application.
Top Virtual Instrument (VI) - Main panel (fig. 3-23): control, data acquisition and optimization
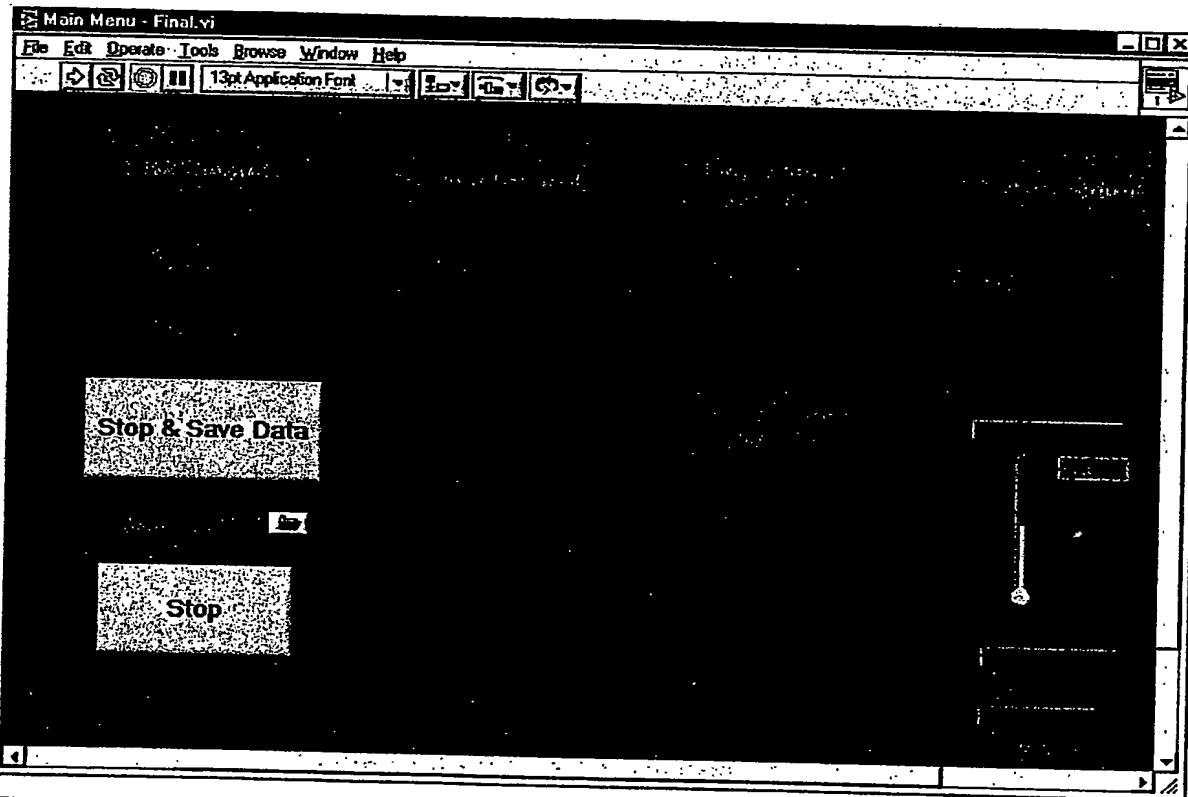
Figure 3-23 Main control panel of the Labview application

Sub VIs (see Appendix A for codes and user interfaces):

- Laser pulse amplitude control (DAQ)
- Laser pulse amplitude control (GPIB)
- Laser pulse rate and duty cycle control (DAQ)
- Laser pulse rate and duty cycle control (GPIB)
- Vacuum control
- CO_2 flow control
- IR camera control

Hardware & Interfaces

- NI PCI-GPIB Hardware and GPIB cables (IEEE 488)
- NI DAQ PCI-6024E Hardware and its external cable and connection board type CB-68LP

3.2.3 Feedback

Thermal Imaging

- Infrared camera FLIR ThermaCam SC500 (7.5-13µm) with an optional 10.6µm cutoff filter embedded (10µm and up)
- Breakout box
- Frame grabber - PC card interface Agema Multifunction Device THV550
- PCI PCMCIA Card reader
- ThermaCAM Researcher Application version 2001
- Labview drivers, controlling the IR camera (i.e. camera parameters, image acquisition and recording) and the image analysis

Visual Recording

Video Camera Logitech QuickCam Pro 3000

3.2.4 Cavity-like Phantoms

Various combinations of plastic hemispheres and nylon constructions; some were internally layered with Agarose gel or in-vitro porcine stomach. Pic 3-4 - 3-9 demonstrate various components of the phantoms.
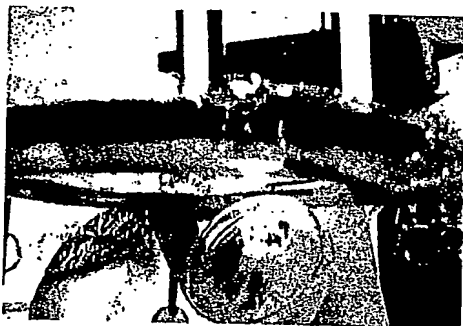
Picture 3-4 Tissue-like phantom, made of Agarose
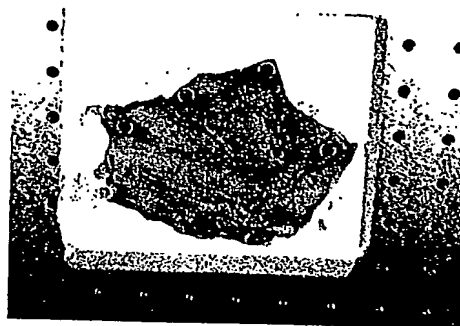
Picture 3-5 Sample of porcine gastric tissue
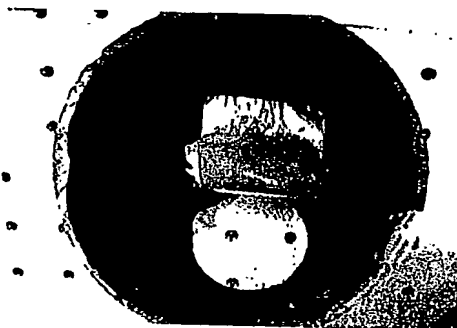
Picture 3-6 Tissue sample at the bottom of the lower plastic hemisphere, and a nylon wrapped window for the IR camera
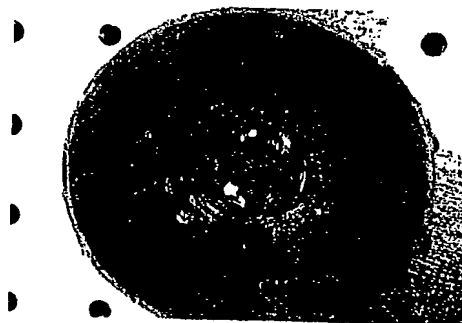
Picture 3-7 Upper plastric hemisphere with tissue sample at the center and inlets for fiberoptic, suction and insufllation tips
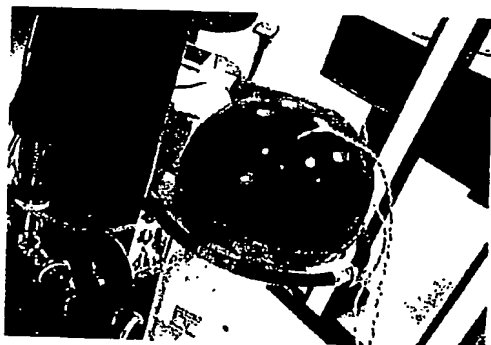
Picture 3-8 one version of the closed sphere; external view
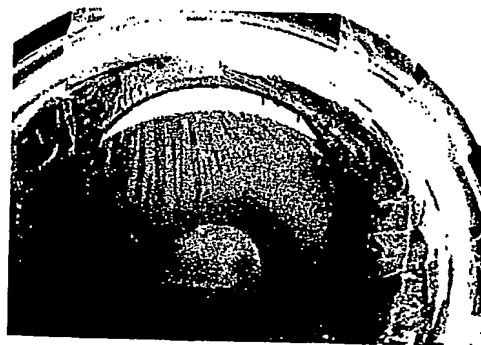
Picture 3-9 The closed sphere as seen by IR camera

Specific configurations are embedded throughout the results (section 3.4).

3.2.4.1 The Agarose slabs recipe

A quantity of 0.8g agarose (Seakern HE agarose, FMC Bioproduct) and 36.6ml PBS-phosphate buffered saline (J. T. Baker, cat. No. 5656) are heated and boiled while stirring to dissolve the agarose [72]. The solution obtained was clear and free of bubbles. After cooling to 70°C, 3.4ml Intralipid (Intralipid 20%, Pharmacia & Upjohn, cat. No. 406563A) was added to the solution while shaking the tube gently. The solution was then poured into petri plates.

3.3 Preparations

3.3.1 Setting the IR camera

3.3.1.1 Focus

The IR camera's focus distance is 0.5m and up. We placed it 0.52m beneath objects (pic. 3-10,11).
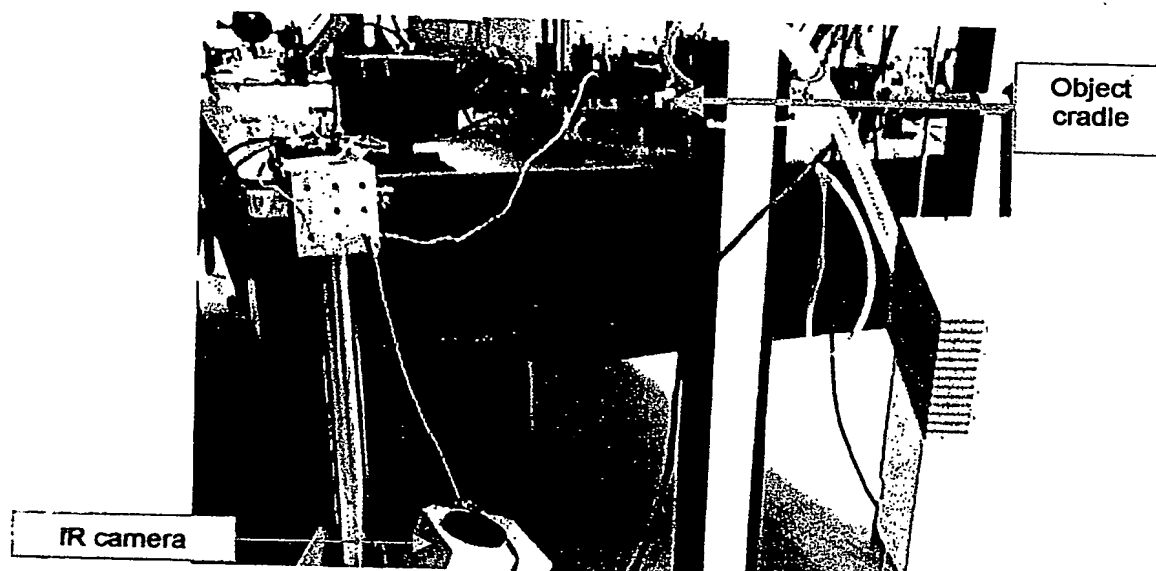
Picture 3-10 Positioning the IR camera; side view

Picture 3-11 Top view

3.3.1.2 Emissivity

When IR images were taken from tissue samples, emissivity was set to 0.95 [78, 87].

3.3.1.3 Temperature correction

During the cavity-like phantom trials, camera recorded through a nylon wrapped window, which attenuated the temperature. The temperatures shown in the graphs below are the actual ones minus 2°C.

3.3.2 Measuring the beam diameter

Measuring the laser beam diameter partially based on the "razor-blade" technique [88], in which a knife-edge is slowly inserted into the beam. Doing so, we used a 0.5mm iris diaphragm and a 0.5mm steps. The beam diameter defined as the distance between two X-axis values of the gaussian profile. A 6.5mm diameter resulted without fiber (graph 3-1) and a 1.6mm diameter with a 1.6mm rigid fiber, at three different powers (graph 3-2).
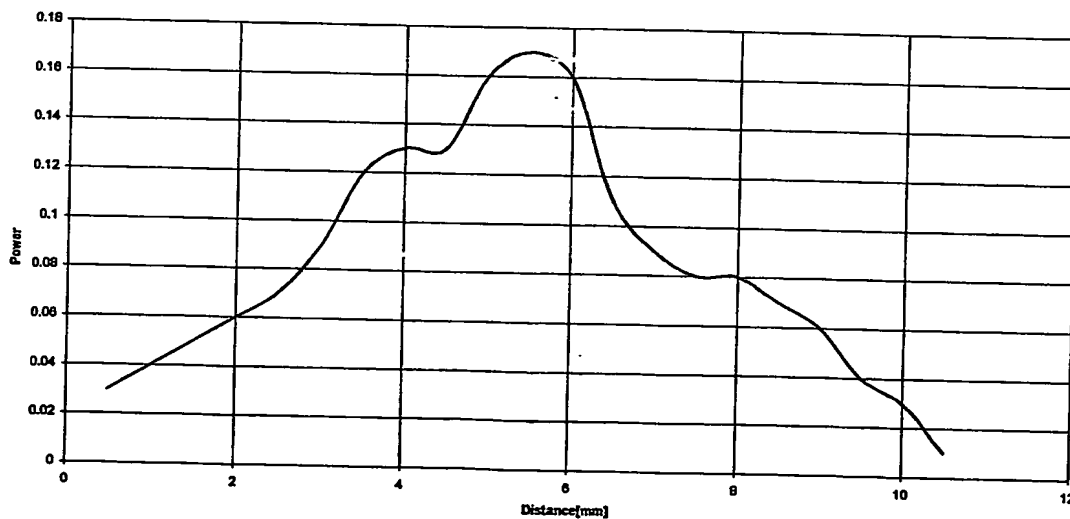
Graph 3-1 Fibreless laser beam gaussian (10w); max. power 0.17/2.72=0.0625w, thus Beam Diameter is approx 6.5mm
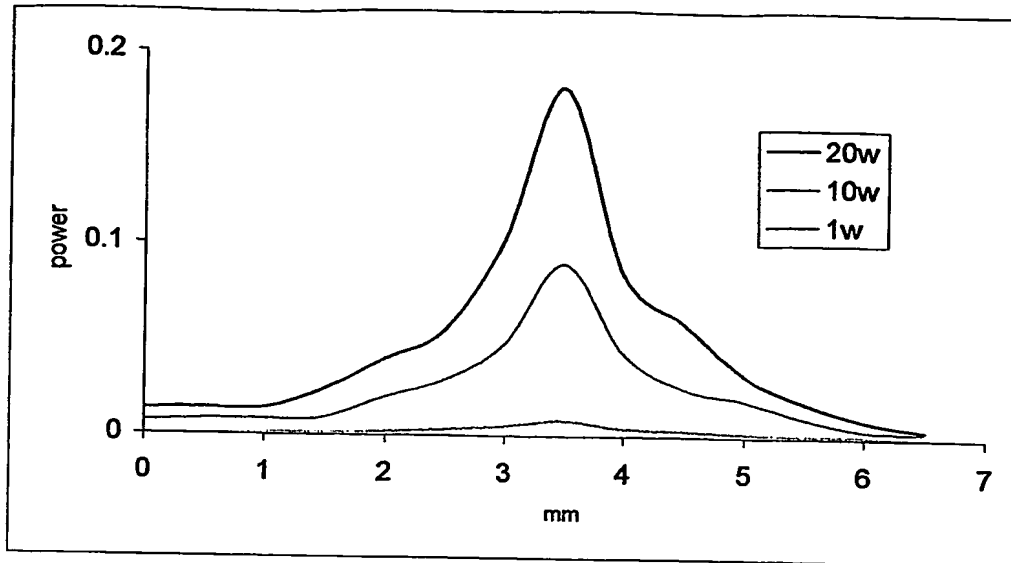
Graph 3-2 - 1.6mm fiber beam gaussian (1,10,20w); beam diameter ~ 1.6mm

Given beam diameter, the Average Power Density (APD) can be calculated (see sec 1.3.4):

R = 0.08cm

$$APD= power/(\pi R^2) = power \times 50 \qquad\qquad (3.3.2)$$

Table 3-3 APD for varying power rates, using 1.6mm fiberoptic

Power (w)	1	3	5	10	15	20
APD (w/cm^2)	50	150	250	500	750	1K

3.3.3 Transmission ratio and fiber coupling

Picture 3-12 demonstrates the fibreless setup we have used during the Agarose sessions, to obtain a relative high transmission ratio (~84%) and a certain beam diameter, via focusing lens and iris diaphragm.
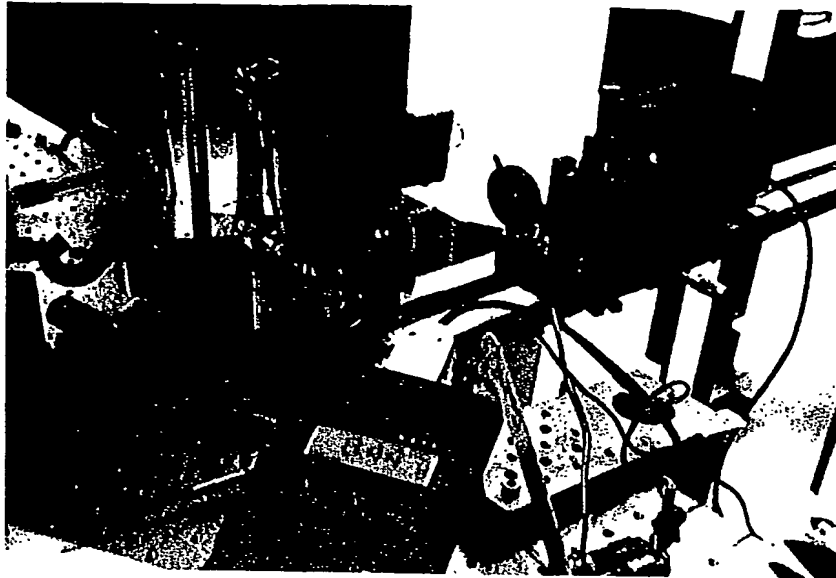
Picture 3-12 The fibreless setup incorporates focusing lens and 0.8mm iris diaphragm; 8.44w delivered out of 10w provide transmission ration of 84.4%

This setup allowed high power irradiations, up to 50watts. This ratio dramatically declined down to 8% when a glass coupler was examined (pic. 3-13), in order to wave-guide the laser beam through a fiberoptic.
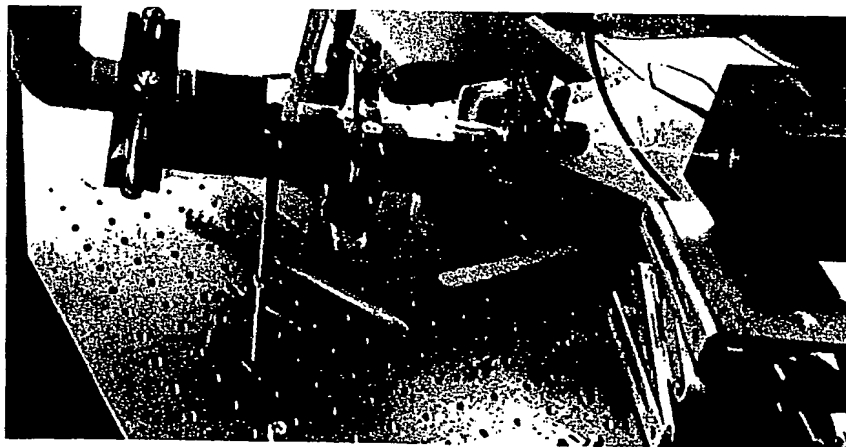
Picture 3-13 Glass coupler attenuates 25w to 2w - an 8% ratio

Consequently, we used custom-made coupler, displayed in pic. 3-14 where we achieved transmission ratio that ranged between 60 to 80% with the 1.6mm fiberoptics.
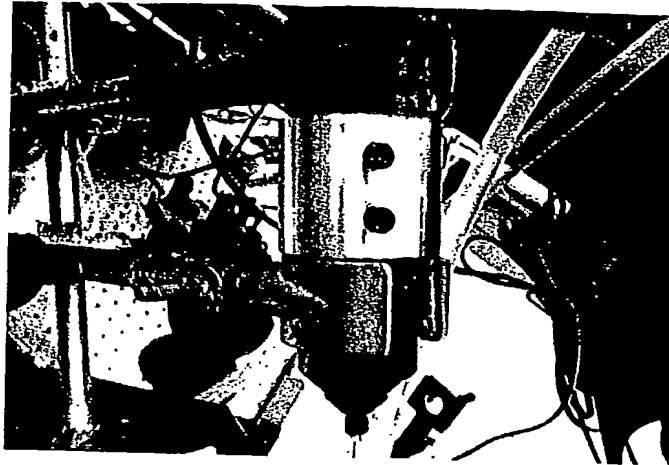
Picture 3-14 Custom-made coupler and adaptor
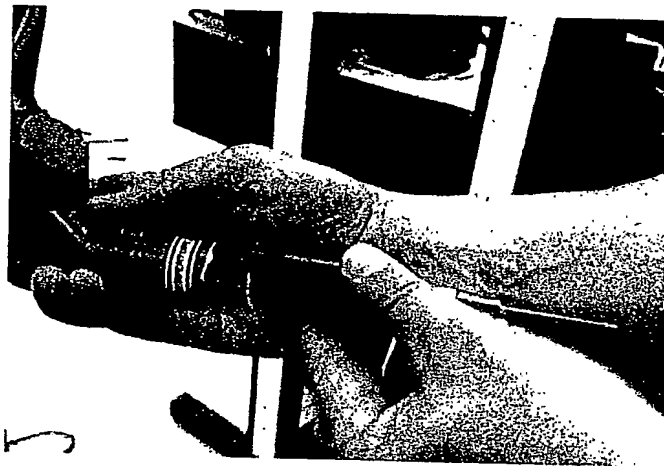
Picture 3-15 Custom-made coupler, SMA and 0.7mm flexible fiberoptic

The ratio of the 0.7 (pic. 3-15) and the 0.3mm flexible fiberoptics decreased rapidly in mid-range powers (8-12w) and therefore neither one was applicable to this study, nor the flexible gastroscope.

3.4 Experimental stages: method and analyzed results

Over the course of this investigation, quite a few dilemmas have emerged. Some are phenomenon to be considered when designing the practical procedure, while others where obstacles that we had to overcome, in order to accomplish study goals. Research stages were often redesigned accordingly.

Visual documentation, thermal images and analysis, when relevant, accompany most experimental steps. Results are exhibited, analyzed and discussed throughout this section, and summarized in chapter 4.

3.4.1 Exploring the heat distribution

3.4.1.1 Getting a ballpark estimation of the steam thermal effect in a hemisphere

In order to focus on the hotspot of the surroundings, during the irradiating process, we needed to figure where and what to look for. The "where" is strongly depended on the manner the steam distributes while the "what" relates to a general estimation of the thermal gradient. In this section, the "what" question has been focused. For our first attempt of steam spreads into a hemispheric plastic roof, we used boiled water vaporized from a kettle as shown in pic. 3-16. The kettle was placed beneath the hemisphere and then removed.
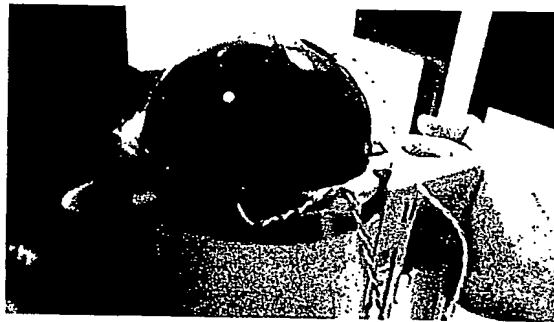
Picture 3-16 Steam from kettle rises up into the hemisphere

IR camera recorded thermal images of the hemispheric interior (image 3-1).
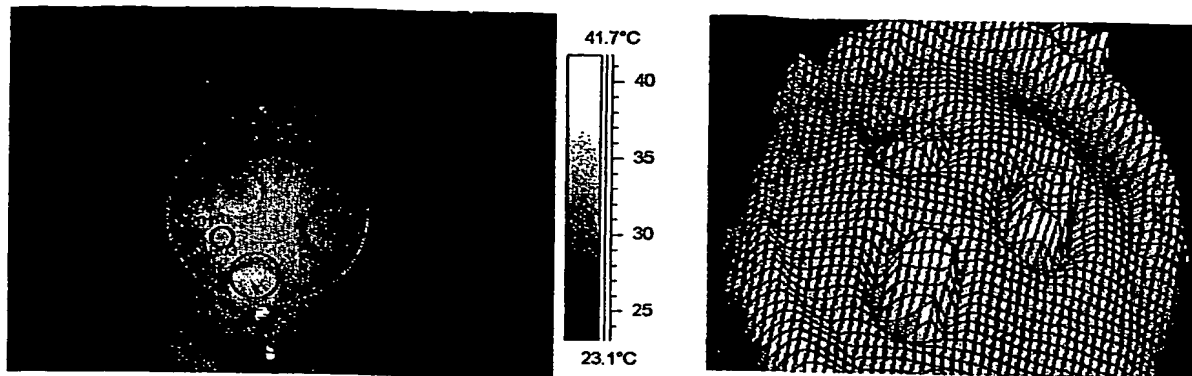
Thermal image 3-1 Temperature mapping of hemisphere interior after a burst of steam (left-2D, right-3D); Areas 1- area3 (AR01-3) demarcate three areas respectively: in the vicinity of the dome center; inclusive; flattened-lowered;

Although the steam rises up uniformly from the circuital water surface, the higher temperatures are seen in the in the region of the dome center. Another hot area is marked as ARO3. It protrudes approx 3cm down the domed surface and thus much closer to the kettle.
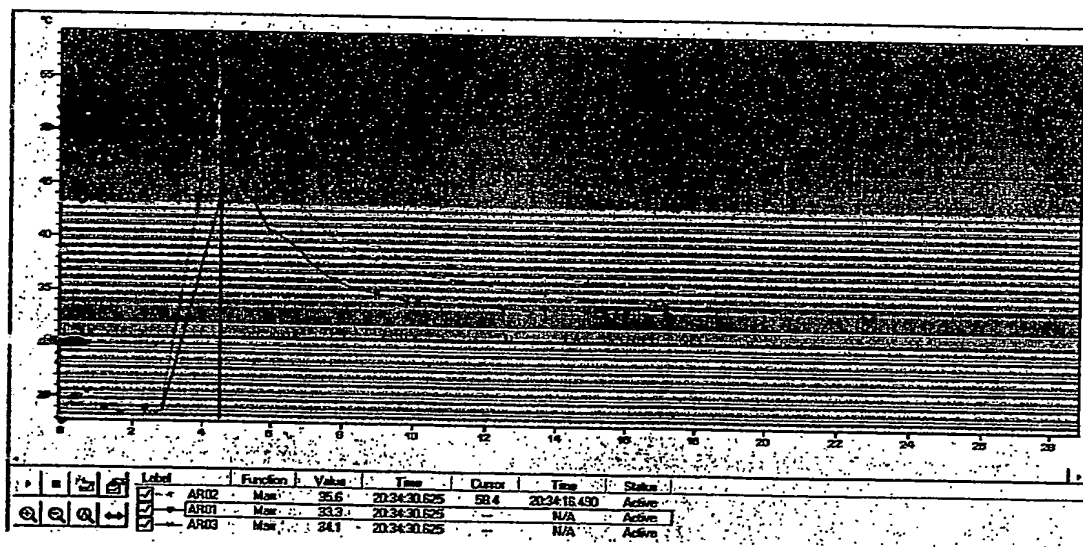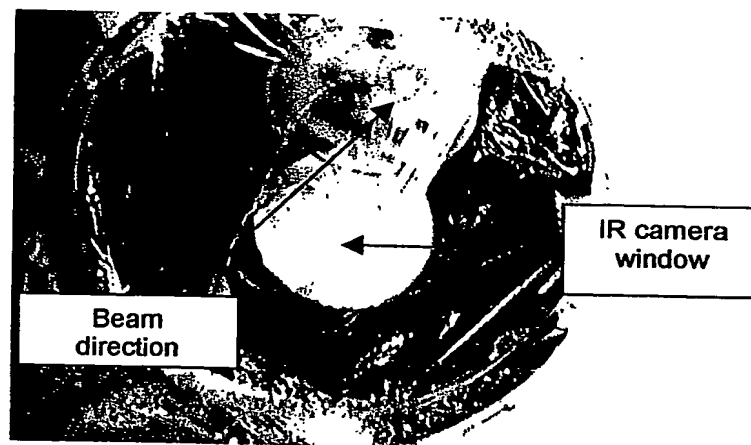

Graph 3-3 - Max. temperature (°c) vs. time (seconds) of the 3 marked areas in thermal image 3-1

Three findings resulted in this preliminary experiment:

• Significant heat build-up was caused by water steam
• Higher temperatures occurred in the center of the dome
• Higher temperature were also noticed in closer flat areas

63

3.4.1.2 Initial trials with Agarose Gel in a Closed Sphere

In this section we used a tissue-like phantom made of Agarose gel, a wide range of laser powers and a flat nylon roof, which enabled videoing the smoke as well as obtaining thermal images of the roof through a hole at the bottom (picture 3-17). The laser beam was focused on the Agarose surface. No fiber was used. During the IR imaging, we measured the temperature of the whole roof, thus obtained the maximum temp at all times.
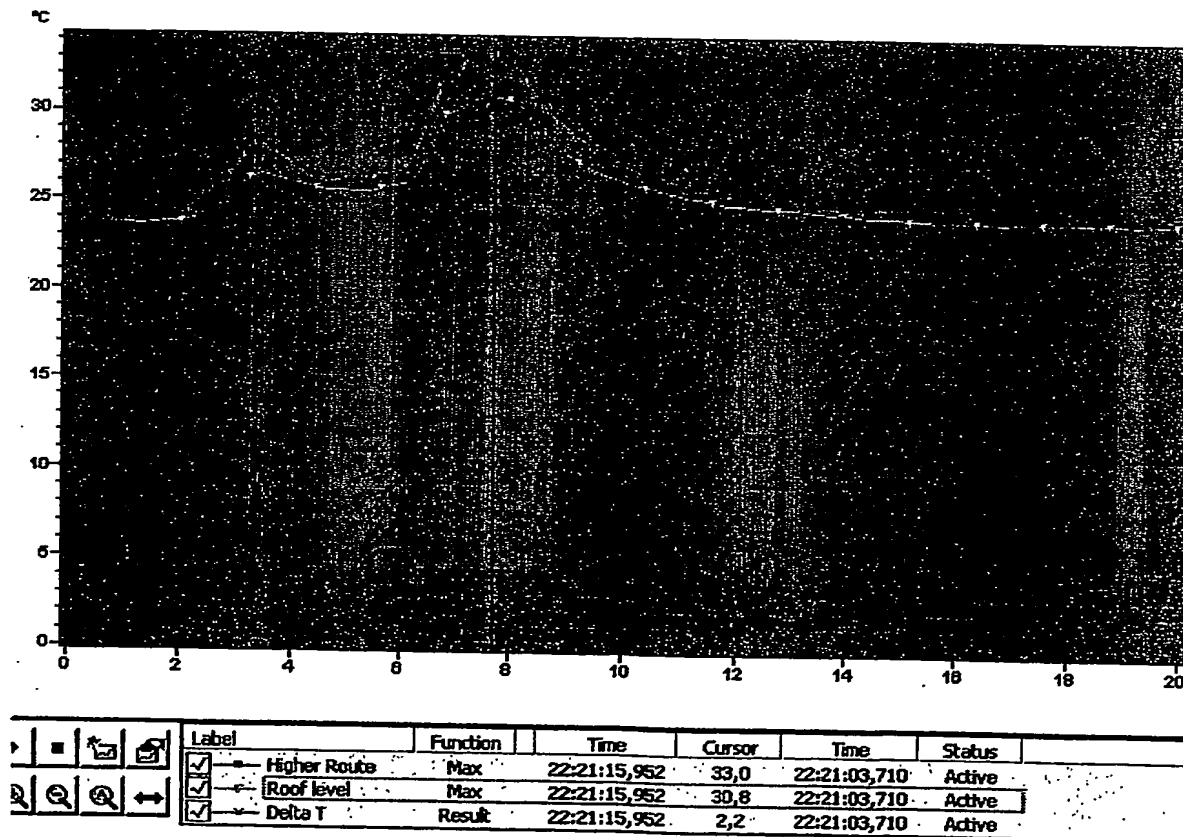

Picture 3-17 Agarose gel phantom setup; fibreless setup
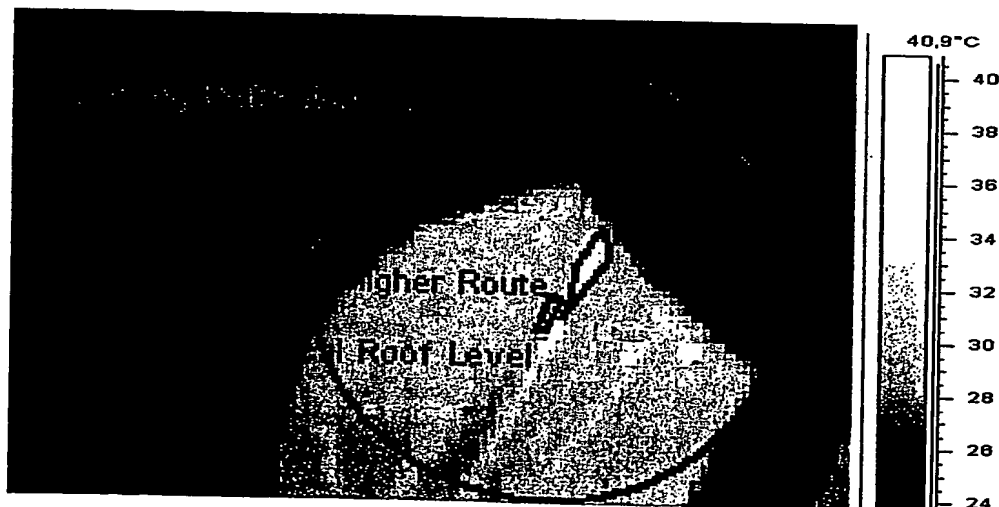
Thermal image 3-2 - 20watts

Label		Function	Time	Cursor	Time	Status
☑	Higher Route	Max	22:19:27,593	44,8	22:19:15,419	Active
☑	Typical Roof Level	Max	22:19:27,593	38,4	22:19:15,419	Active
☑	Including Reflections	Max	22:19:27,593	44,8	22:19:15,419	Active
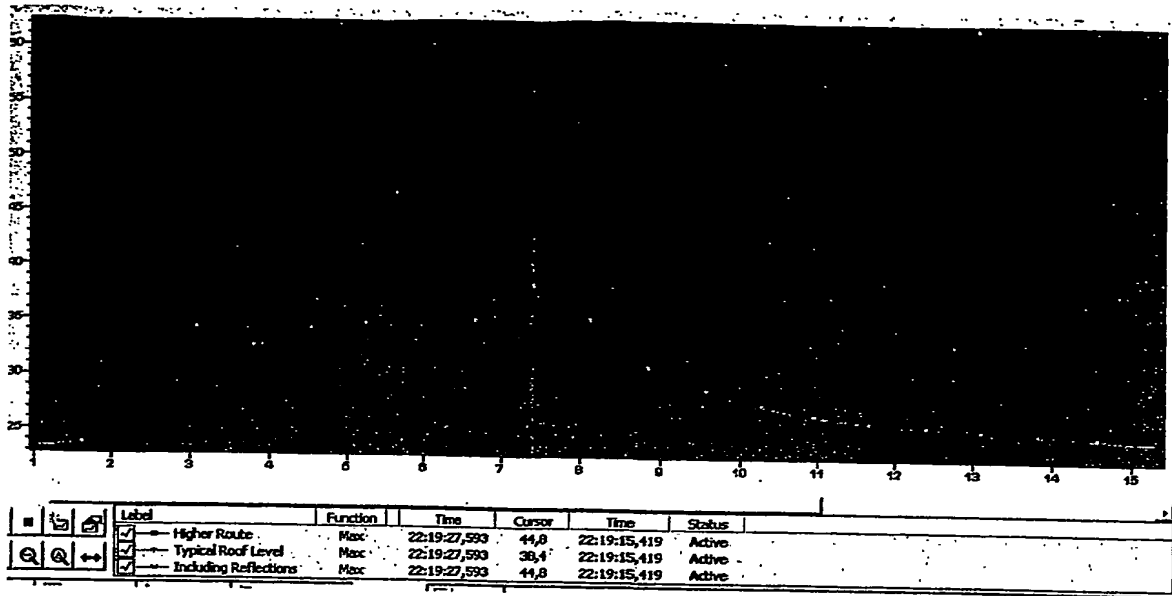
Graph 3-4 Max. temperature in the marked areas vs. time; 20watts; ΔT = (roof level temp)-(fold temp); Max ΔT =6.40°C

Label		Function	Time	Cursor	Time	Status
☑	Higher Route	Max	22:21:15,952	33,0	22:21:03,710	Active
☑	Roof level	Max	22:21:15,952	30,8	22:21:03,710	Active
☑	Delta T	Result	22:21:15,952	2,2	22:21:03,710	Active

Graph 3-5 - 10watts; Max ΔT (blue line) =2.20°C

Label	Function	Time	Cursor	Time	Status
Highest Route	Max	22:22:46,233	25,3	22:22:39,639	Active
Roof level	Max	22:22:46,233	24,6	22:22:39,639	Active
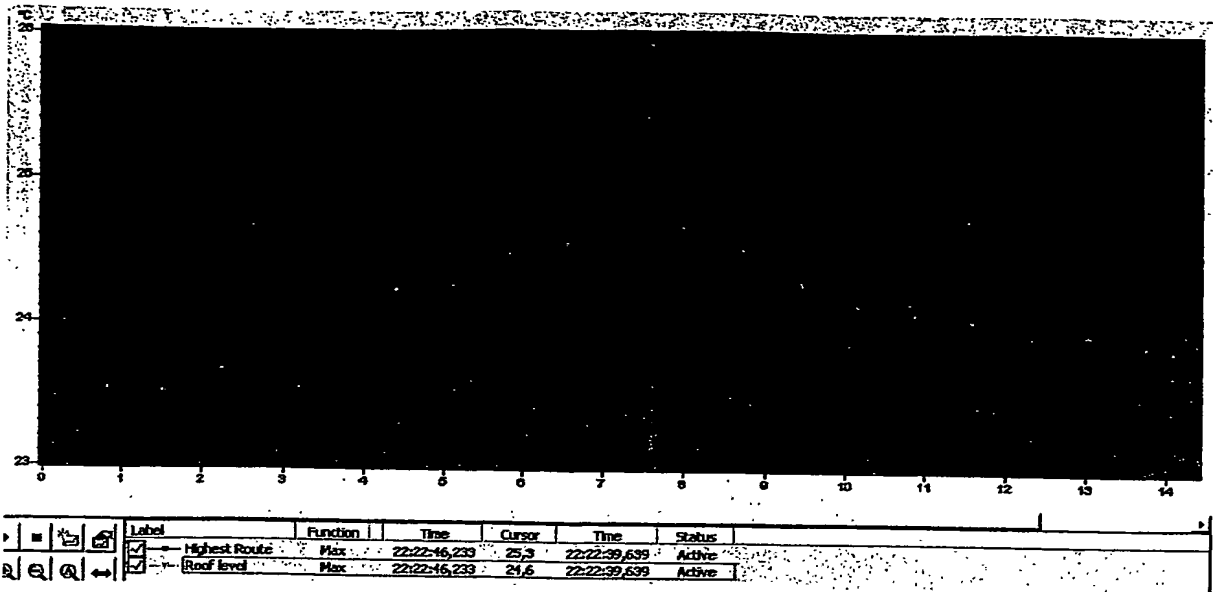
Graph 3-6 - 5watts; Max ΔT =0.70°C
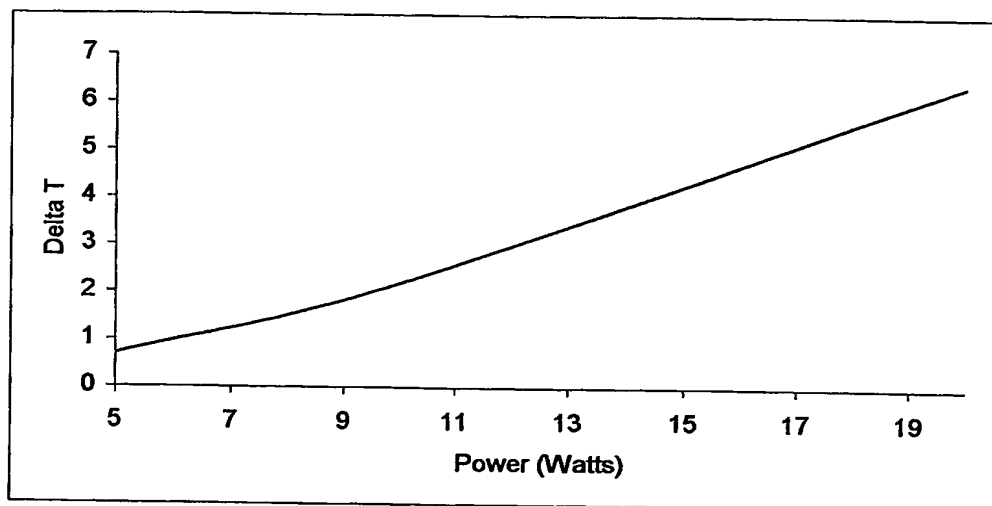
Graph 3-7 Thermal gradient (fold level minus roof level) vs. laser power

Three major observations came up here:

- Highest temperatures resulted in the highest routes along the nylon folds. The temperature gradient - between roof level and folds level - increases when laser power climbs. Nylon folds virtually represent tissue wrinkles.

- Formation of jet (smoke and steam) directed contrary to laser beam, at high laser powers; "Plume" (a smoke column) headed up in low powers.

- Laser reflections interrupt the IR readings but do not contribute to the heat build-up.

3.4.1.3 Exploring the smoke distribution during the irradiation of porcine stomach samples

In this section we used roofless as well as transparent-roof spheres, to explore three major factors - induced power, gas circulation/vacuum and distance between fiber and tissue - that govern the directions and the velocity of steam. Another related aspect was the cavity geometry. Surrounding tissue can be domed, curved or flattened. In practice, it is frequently domed due to the artificial insufflation of the organ. We explored the heat and smoke dispersion in both cases: flat (sec. 3.4.1.5-6) and domed (3.4.1.7).

3.4.1.4 Irradiating tissue in open space

A fresh gastric sample was placed on a bottom of a plastic hemisphere (pic. 3-18,19,20), partitioned by wood and metal slices. The metal blocked the laser beam when drilled throughout the tissue, and the wood functioned as a thermal isolator between metal and plastic. Otherwise plastic got heated and interfered IR readings. The mucosal layer (stomach's lining) was up, so as irradiation hit it first.

Picture 3-18 - 6w, plume   Picture 3-19 - 12w, jet   Picture 3-20 - 24w, jet

- Two modes of smoke distribution were noticed: plume and jet.

- The plume headed straight up while the jet was directed to fiber.

- The jet formation occurred at higher laser powers (approx. 10watts and up in this settings).

3.4.1.5 Varying laser power and fiber-tissue distance in closed space with flat roof
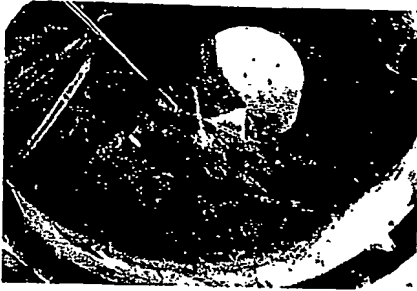
Picture 3-21 - 3watts, *plume*

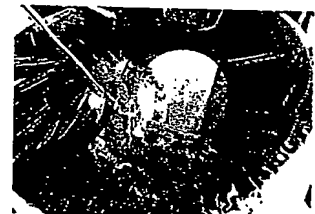Picture 3-22 - 6watts, *plume* and smoke rings

Picture 3-23 - 9watts, *plume*

Picture 3-24 - 9watts after longer period of 4sec, *jet*


Picture 3-25 - 5watts at shorter distance, *jet*

Picture 3-26 - 12watts; top: *jet;* bottom (after 20sec): *plume*

- In the absence of gas and vacuum, in certain distance and low laser powers, the hotspot was above the irradiated tissue, while at high powers it was contrary to the beam direction as a result of the jet.
- Jet was created at higher powers but also in low powers if irradiation had lasted long enough (due to deeper crater).
- When smoke hit the roof, the effect of "smoke rings" is observed [89].

In the 2nd 12w trial the jet has turned into plume. It is reasoned by decline of actual output power to 8w after 20sec.

- The longer time elapses and the higher power is used, while no cooling air is running through fiber, the more hot smoke and steam penetrate in and attenuate fiber's power transmission.

69

3.4.1.6 Distribution in the presence of gas flow and vacuum in a closed space with flat roof

Obviously the effect of gas circulation or vacuum depends on parameters such as the rate of gas flow or vacuum, the cavity volume etc. We explored the principle effect of airflow, CO_2 flow and suction by using the lower range of typical values that are being set in practice.
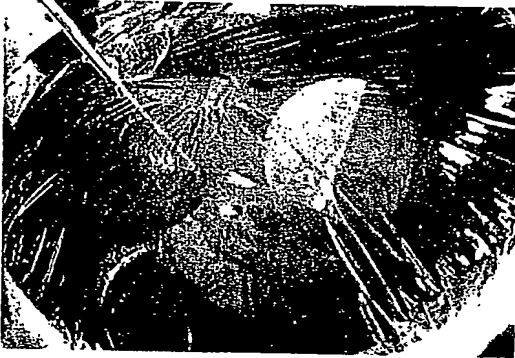
Picture 3-27 Air flow (3lpm)

Picture 3-28 CO_2 gas flow (2lpm)

Picture 3-29 Suction (40mmHg vacuum)

Picture 3-30 Air and suction

Pic. 3-27 - 30 - 12watts; top: homogeneous smoke distribution; bottom: no smoke; no jet in any case

- Air and CO_2 flow caused a uniform distribution of smoke.
- The suction, even when combined with CO_2 flow, has significantly purged the smoke.
- No jets or smoke rings were seen at any of theses cases.
- Gas insufflating helps "blurring" hotspots (i.e. reducing the maximal temperature) not only by circulating the steam but also by straightening the folds.

3.4.1.7 Smoke distribution and velocity in closed space, with a domed see-through roof
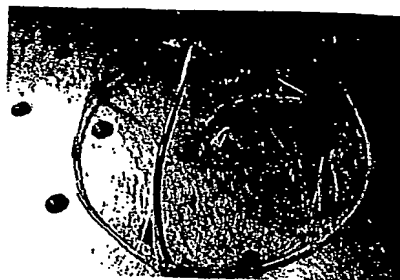
Picture . 3-31   Transparent domed hemisphere

Picture 3-32 - 0.5sec

Picture 3-33 - 0.6sec
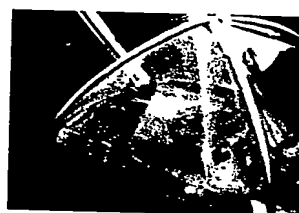
Picture 3-34 - 1sec

Picture 3-35 - 3sec

Picture 3-36 - 0.8sec

Picture 3-37 - 3.1sec

Picture 3-38 - 4.3sec

Picture 3-39 - 5.6sec

Top series: 5w, bottom: 9w

- Smoke plume rises straight up until it hits the roof. Then it spreads, mainly along the highest routes, toward bottom, and gets turbulence.
- Plume's velocity, in the 5w setting (top series), can be roughly computed: The distance between tissue and top was approx 5.3cm, and the smoke hit it after 0.5sec. Thus the averaged velocity in this interval was 0.053/0.5 ~ 0.1m/sec.

3.4.1.8 Summary of distribution types

Three principle modes were noticed - plume, jet and homogeneous - and the conditions at which they occurred.
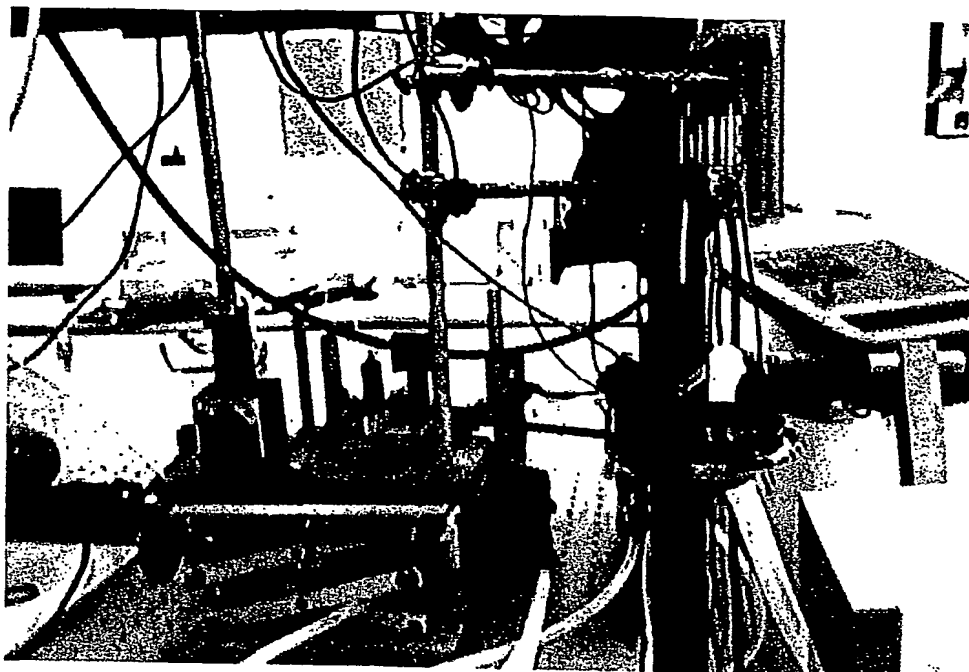
Picture 3-40 General view of setup using perpendicular fiber
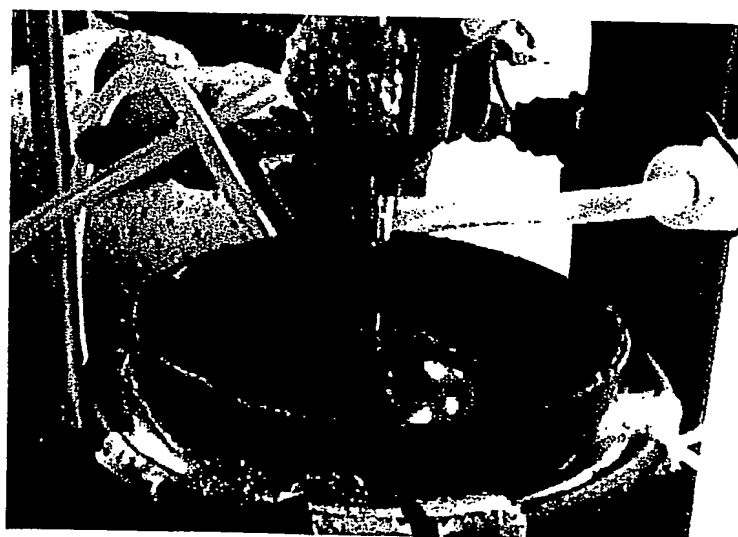
Picture 3-41 External view of the cavity-like phantom; air inlet
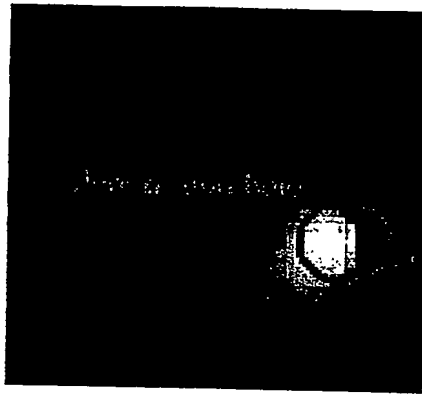

Picture 3-42
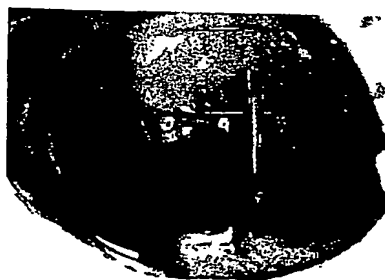
Picture 3-43

Picture 3-44

Pic. 3-42,3,4 Phantom internal view at varied distances between tissues

3.4.2.2 Fiber gets heated and heats its surroundings

All along gasless trials in this section, thermal images (exampled by 3-3) showed that the hotspot is created in the area we expected it to be - around the fiber entrance hole. Yet, that area seemed to be exceptionally demarcated, overheated and, in some cases, carbonized (pic 3-45). Moreover, fiber transmission ratio declined rapidly when airflow was shut down. A suspicion came up that the hotspot was created not by steam hit, but mainly by the fiber, of which hollow core got heated. Since our goal was to investigate the sole effect of steam (in practice the endoscope "isolate" fiber from tissue), these two heat sources had to be distinguished. To do so, we needed to explore the reason the fiber heats.

Thermal image 3-3 Hotspot is around fiber entrance hole

Picture 3-45 Carbonization around fiber entrance hole

## 3.4.2.3 Exploring the cause of fiber heating

We considered two potential causes:

- Penetration of hot steam into the hollow core
- Perfusive coating along fiber

Preventing from steam to penetrate into fiber was done by two means: injecting air through fiber and removing the bottom. We firstly used a bottomless setup (pic 3-46,47), with and without air, recorded (image 3-4) and analyzed the thermal gradient (graph 3-8). We then returned bottom to compare (table 3-4) the gradients (graph 3-9) resulted, to the one obtained from the bottomless setup.
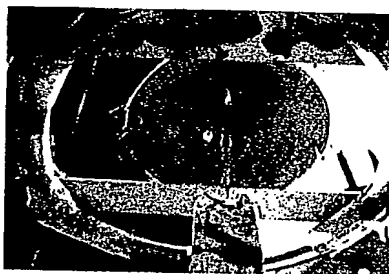
Picture 3-46
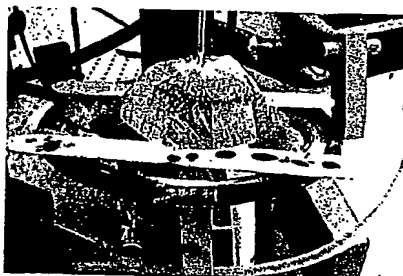
Picture 3-47

Thermal image 3-4

The bottomless setup and the thermal image resulted
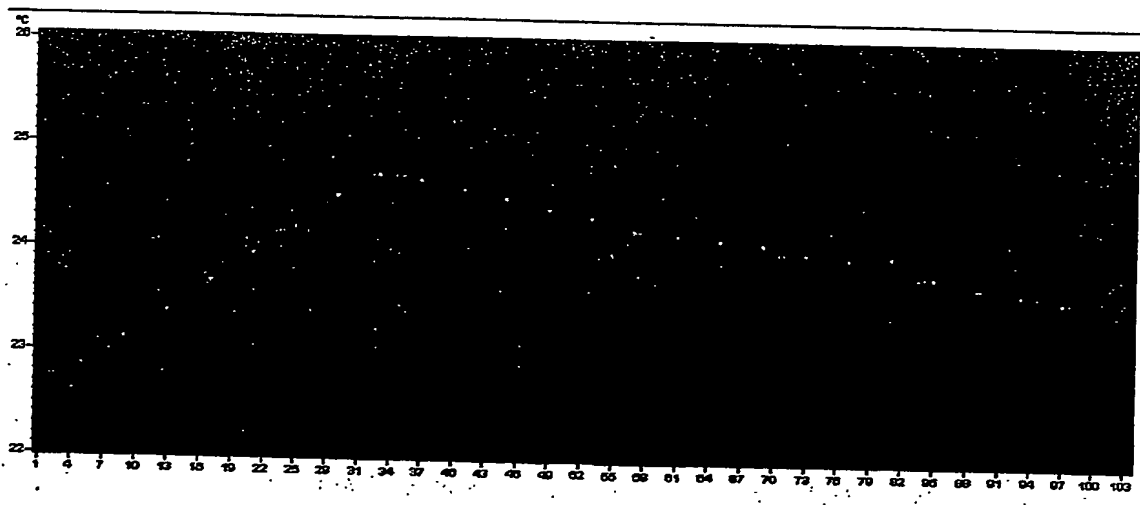
Graph 3-8 Bottomless setup; max. temperature of fiber in penetration area vs. time (secx4), (6w CW, 8sec)

75
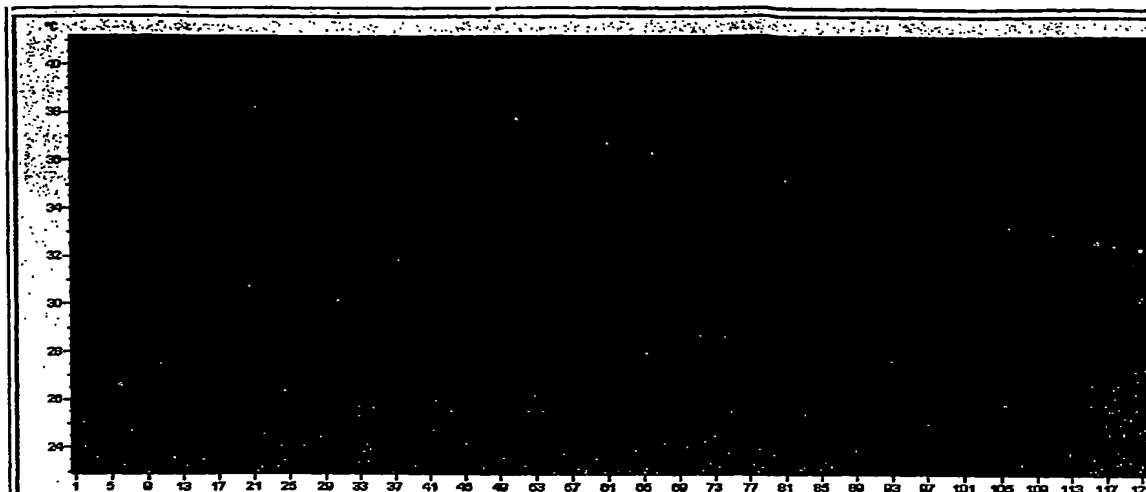
Graph 3-9 Original setup (pic 3-41); max. temperature of fiber in penetration area vs. time (secx4), (6w, CW, 8sec, 1.5cm between tissues)

After transmission is stopped (second 8th) fiber's temperature declines faster when air ran through it.

Table 3-4 Comparison of thermal gradients

6watts (300w/cm^2), CW, 8sec elapsed	Bottomless setup	Original setup	ΔT
No air	Max T = 25.2^{0}C	Max T* = 40^{0}C	14.8^{0}C
Air injected	Max T = 24.7^{0}C	Max T* = 34^{0}C	9.3^{0}C
ΔT	0.5^{0}C	6^{0}C	

*These values incorporate two temperature corrections: nylon wrap attenuation (-2^{0}C) and normalization to initial temperature (23^{0}C)

The bottomless experiment shows that in the absence of steam, fiber is slightly heated (approx. 20^{0}C after 8 sec), probably due to absorption along its perfusive coating. Another notice is that the air cools the fiber when transmission is stopped. Further investigation of the perfusive areas is visualized and thermally analyzed in pic 3-48,9 and fig. 3-24.

The ΔT of 14.80^{0}C (form table 3-4) vs. 9.30^{0}C, and the ΔT of 60^{0}C vs. 0.50^{0}C imply that fiber is heated mostly due to the hot steam. Visual and thermal recording of the fiber edge during the interaction (pic. 3-50,1,2) have verified this when air is not running through fiber, steam and smoke raises up into the

hollow core and overheat fiber. Shortly after it results a burned edge (pic 3-53).

We thus conclude that any other protection from steam penetration will avoid this undesired result. For instance: gas circulation or suction; 10.6μm transparent substance that will block the fiber edge; core fiber (for other wavelengths). However the last two may be masked by steam, smoke and particle, and thus attenuate transmission rate. That may occur in the lack of suction or adequate gas circulation, when fiber edge is close or above the tissue, or when high power is used, such that creates jet toward the fiber.

Picture 3-48 Severe leakage

Picture 3-49 See analysis below

Pic. 3-48,9 Imperfect coating
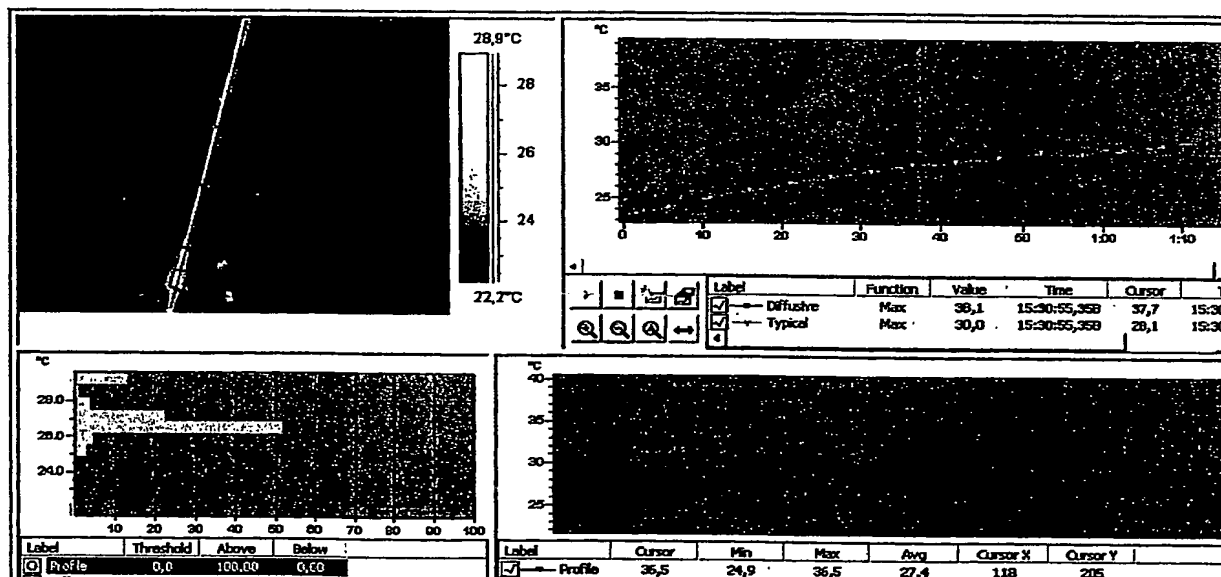
Figure 3-24 Thermal analysis of the fiber shown in pic 38, using 7w and CW. Air cooling was activated between second 37th and 63rd. Left-top: thermal image, with two areas (diffusive and non-diffusive) and a profile line to be analyzed; right-top: max. temperature of the two area vs. time (sec); left-bottom: histogram of temperatures along fiber; right-bottom: temperature along fiber profile. Difference in IR emission between the two areas is interpreted by camera to the substantial ΔT of approx. 10°C. *This technique virtually demonstrates a QA test by which coating defects can be located and evaluated.*
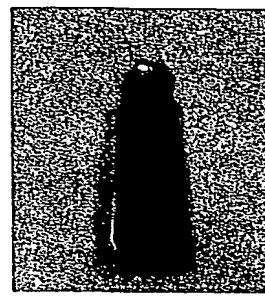
77

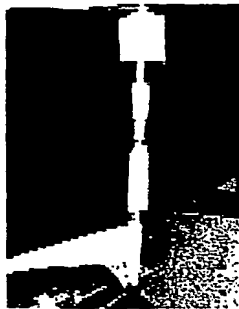| Picture 3-50 | Picture 3-51 | Picture 3-52 | Picture 3-53 The result |

Pic. 3-50 - 3-52 Fiber edge burns while "swallowing" hot smoke and steam
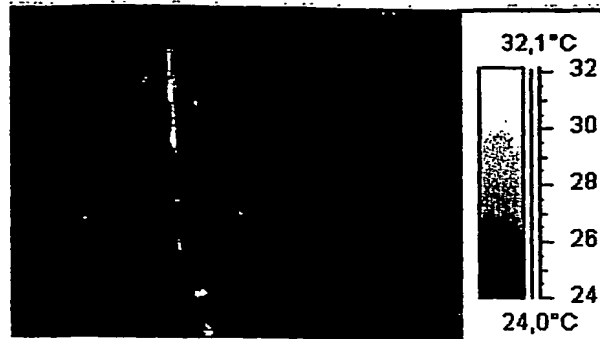
3.4.2.4 Thermal Isolators

One way to quarantine the heat contributed purely by fiber is to thermally isolate it. Such isolation should have the following capabilities:

- To ring the fiber
- To have a high isolation capability, so even a thick slice of it will be adequate. Thickness is important as isolator profile is in the area of interest (the hotspot being explored in the surrounding tissue).
- To seal the gap between fiber and tissue so steam will not spread through.
- To be uninflammable

We have conducted a preliminary study of 4 substances: ceramic, cigarette filter, plastic and wood. Fiber was threaded through all theses potential isolators (pic. 3-54). The thermal images acquired during laser transmission (3-5) were analyzed (graph 3-10). The thermal gradient (ΔT) was determined here as the difference between fiber temperature in the vicinity of each isolator and the average temperature measured from the external surface of that isolator.
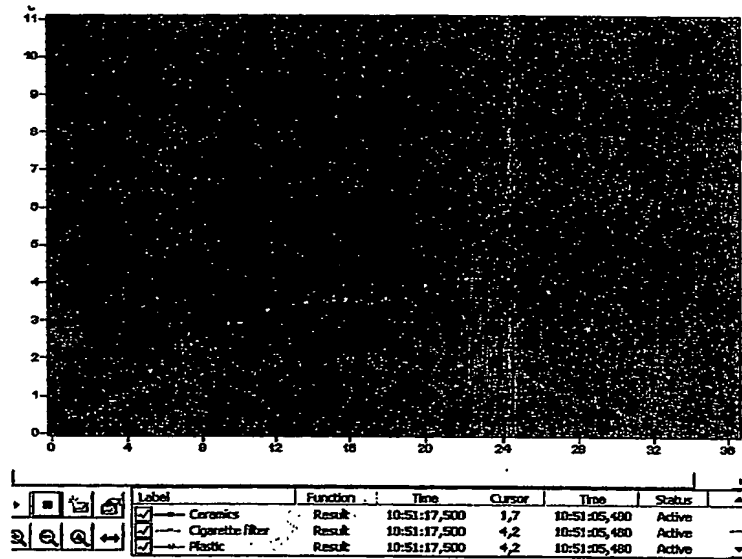
Picture 3-54

Thermal Image 3-5

Pic. 3-54 & Thermal Image 3-5 Testing the thermal isolation of four substances along fiberoptic

Graph 3-10 Each line represents ΔT of thermal isolator. In theses settings, wood (gray line) seems to be the finest isolator.

Is should be noticed that ΔT is affected by isolator thermal properties but also by the absolute temperature of the fiber at that point. The latter was neglected when we used a perfectly coated fiber and airflow, to obtain a uniform temperature along fiber.

In these conditions, results pointed out wood as the only one attenuates more than 6°C (refer table 3-4). Nonetheless wood might burn in higher laser power, when hot steam penetrates into fiber. Hence other solution has been sought (phase 2). We did utilize wood as a buffer between the metal layer and the plastic hemisphere (as described in section 3.4.1.4).

3.4.3 Exploring the thermal effect along the surrounding tissue-phase 2

We decided to overcome the issue presented in previous stage by inserting the fiber diagonally (pic. 3-55), so that fiber heat will not affect the area of interest. The compromise here was limiting the laser power to the mid-range, above which the jet effect turns dominant. When this happens, the most heated area of the surroundings is no longer the upper tissue but the one surrounds the fiber entrance or in-between. During this phase we have dealt with some more problems such as laser reflections interference.

3.4.3.1 Setup redesign

We used a similar setup to the one described in section 3.4.2.1 except the fiberoptic was inserted diagonally (pic 3-55,6,7).
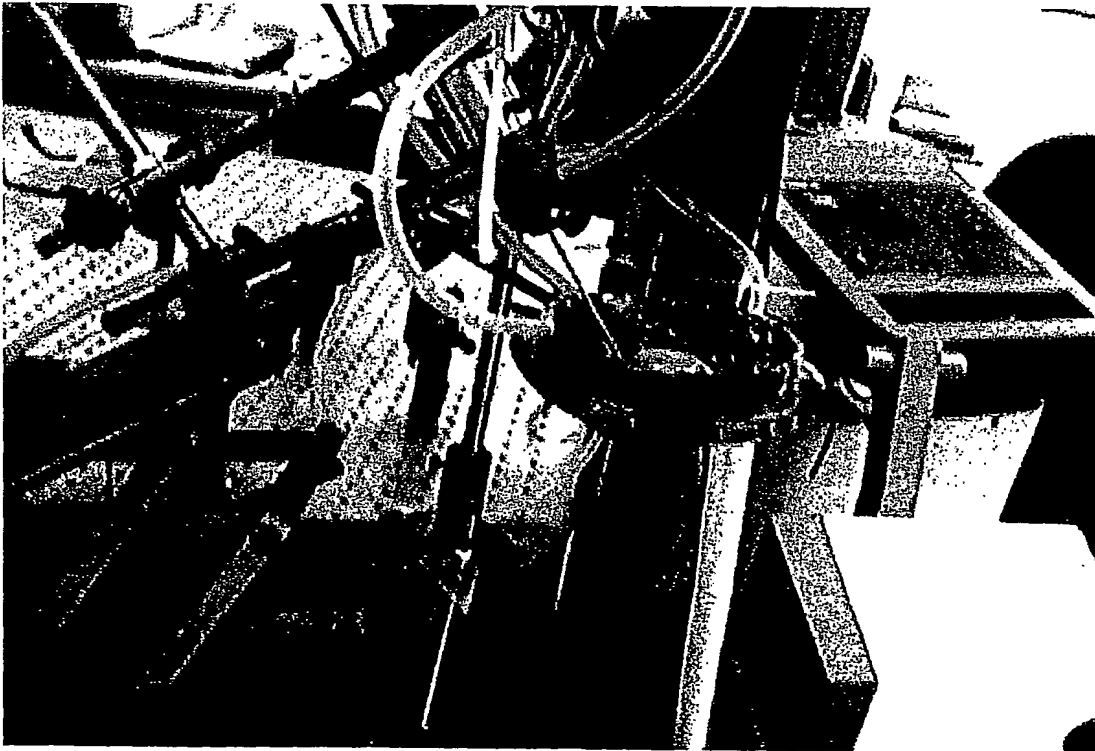
Picture 3-55 General overview of setup in which fiber was inserted diagonally
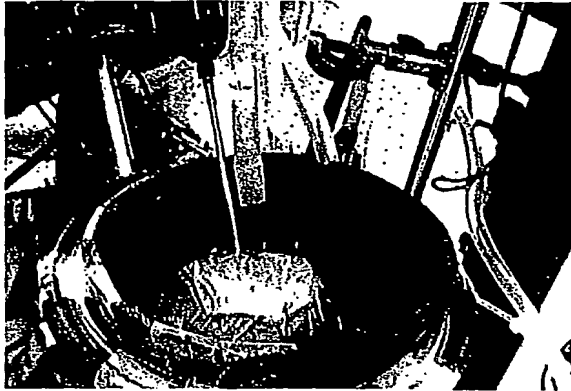
Picture 3-56 Top view

Picture 3-57 IR camera point of view; no direct contact between fiber and tissue sample. Upper tissue diameter is 2cm
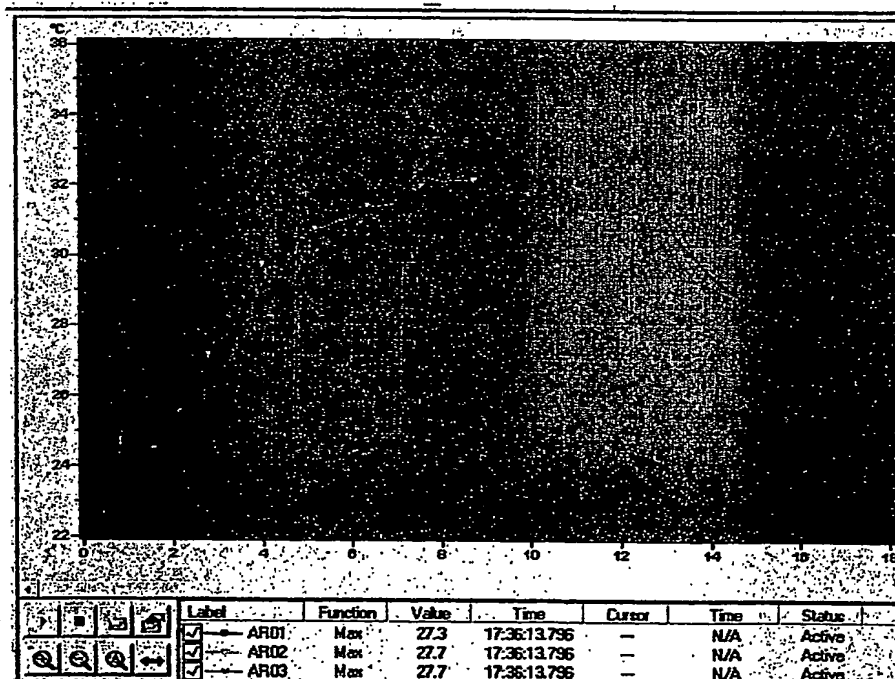
3.4.3.2 Managing additional concerns

3.4.3.2.1 IR emission of tissue vs. IR emission of plastic

In this configuration, it was harder to target the hotspot to the center of the upper hemisphere, where the tissue sample was attached. In some cases the spot deviated to the plastic area. We managed a few experiments to figure out how differ IR readings when emitted by plastic, and to estimate the possible error. In thermal image 3-6 the hotspot incorporates both - tissue and plastic areas. Area 1 (ARO1) and ARO2 indicate tissue and plastic areas respectively, whereas ARO3 represents the inclusive area.
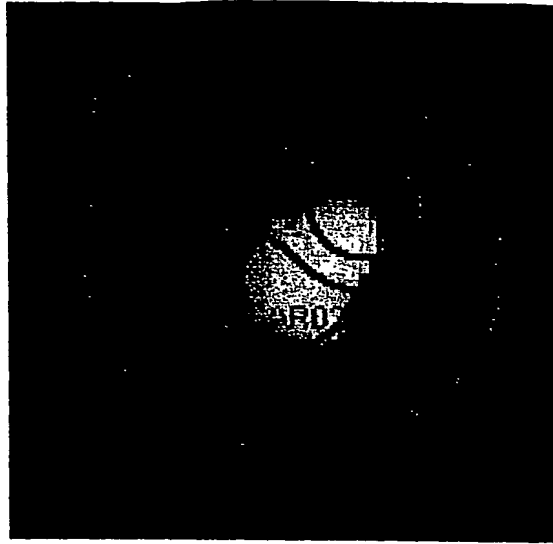
Thermal Image 3-6 Hotspot incorporates tissue and plastic areas. ARO1 indicates tissue area, ARO2 - plastic, and ARO3 - the inclusive area; 6w, CW

Label	Function	Value	Time	Cursor	Time	Status
ARO1	Max	27.3	17:36:13.796	—	N/A	Active
ARO2	Max	27.7	17:36:13.796	—	N/A	Active
ARO3	Max	27.7	17:36:13.796	—	N/A	Active

Graph 3-11 Max. temperature of ARO1-3 vs. time (sec); spikes represent laser reflections and should be ignored; (6watts, CW)

Analysis (graph 3-11) shows that *for our purposes*, the thermal behavior was similar. Nevertheless in next sections we recorded and analyzed when the hotspot was mainly within tissue boundaries.

### 3.4.3.2.2 Overcoming the problem of IR emission caused by Laser Reflections

By using IR camera with internal 10.6µm filter (optional) we intended to exclude laser reflections in the thermal analysis. Unfortunately, it turned out that when filter is in, sensitivity below 80^0C is too poor. We therefore examined two alternatives. The first was to use pulsate transmission and to record the thermal images in-between pulses (i.e. to synchronize laser with camera). The second was to keep out reflection graphically, when analyzing images.

3.4.3.2.3 Synchronized IR measurements

Due to the technical configuration, synchronizing IR camera externally, limits its sampling rate to 1 per second. Otherwise 4 images per second can be acquired. The laser pulse mode was then cycled to 1 second, and the duty cycle was altered. Thermal image were taken between pulses (3-7). Thermal image 3-8 was recorded during laser pulse, as a reference. Graphs 3-12 - 3-15 present several cases of synchronized vs. unsynchronized recordings.
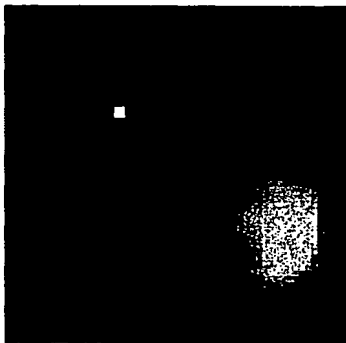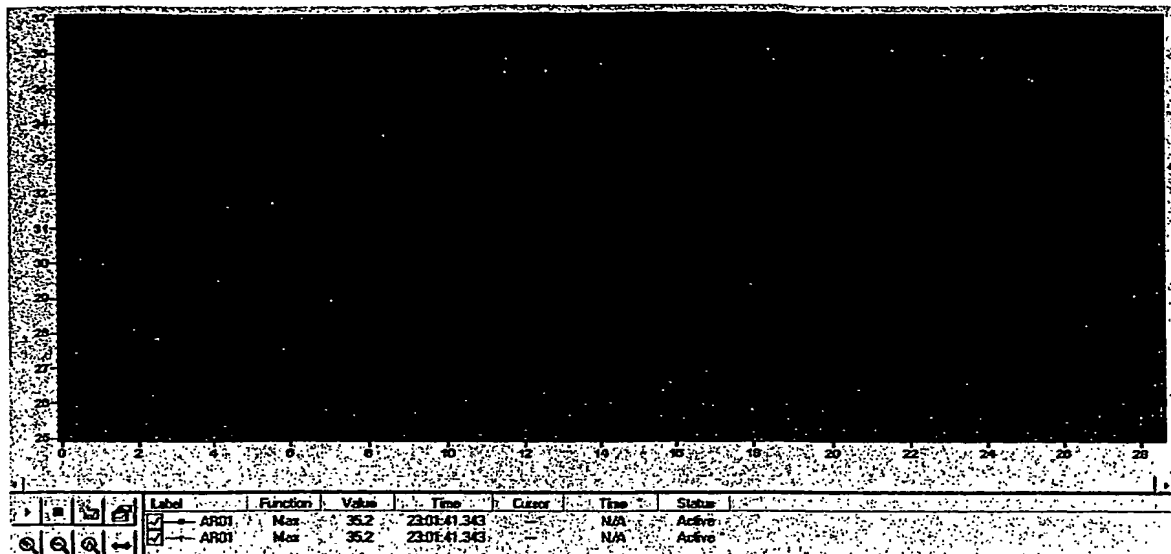

Thermal Image 3-7 Recording between laser pulses (Synchronized)
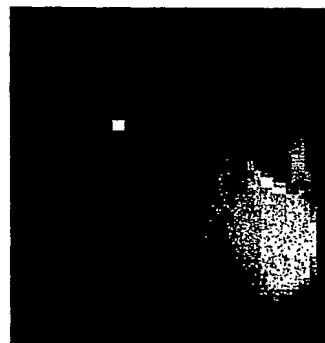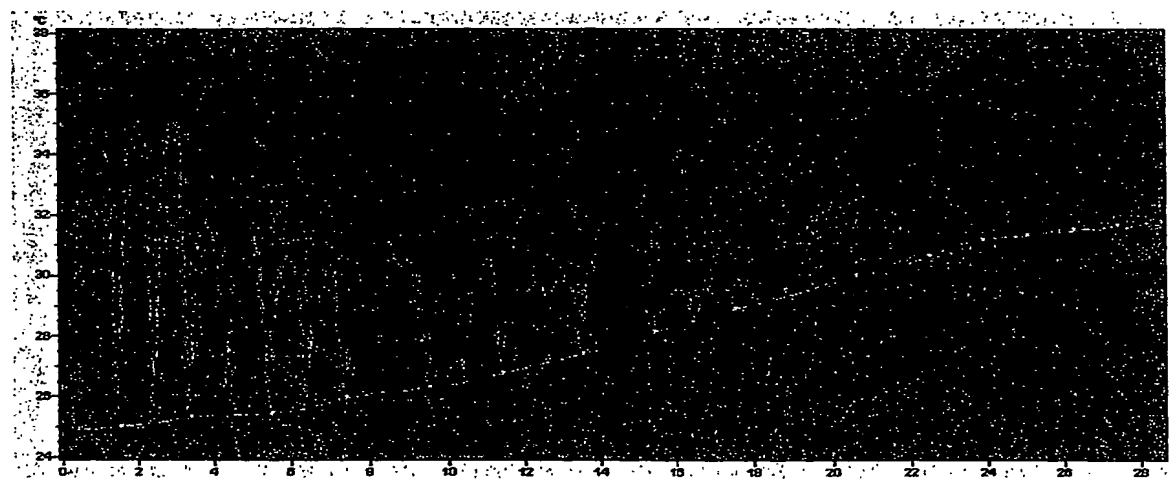

Thermal Image 3-8 Recording during laser pulse (unsynchronized)

Conditions are identical in both cases: 12watts, pulse mode: 0.9s on/0.1s off)

Graph 3-12 Sync (red) and unsync. (black) recording vs. time (sec); 6watts, pulse mode: repeated, 0.9 sec on/ 0.1sec off

Graph 3-13 Sync (red) and unsync. (black) recording vs. time; 6w, pulse: repeated , 0.8 on/0.2 off

84

Graph 3-14 Sync (red) and unsync. (black) recording vs. time; suction is activated; 6watts, pulse: repeated, 0.8 on/ 0.2off
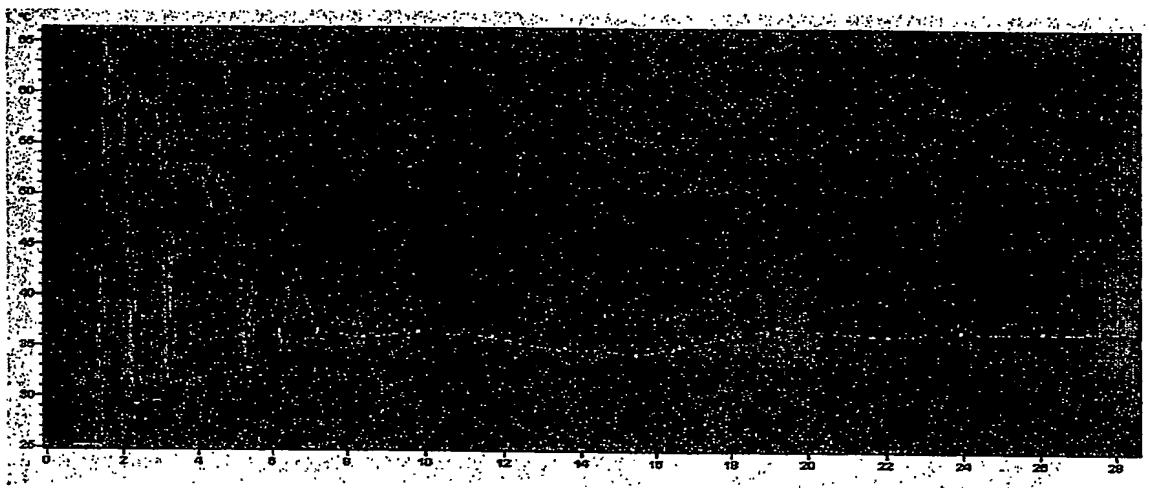
Graph 3-15 Sync (red) and unsync. (black) recording vs. time; 12watts, pulse: repeated, 0.8 on / 0.2off

3.4.3.2.4 Graphical filtering during analysis

Synchronization between laser pulses and IR camera, as an alternative to 10.6μm filtering, not only reduces the sampling rate by 4, but also has a major drawback - continuous mode is not applicable. Since the latter is commonly used, the method follows is suggested as an alternative. In most cases the reflected areas are small, noticeable and demarcated thus can be distinguished and excluded graphically from the analyzed area. Graph 3-26 demonstrates the efficiency of graphical filtering.

85
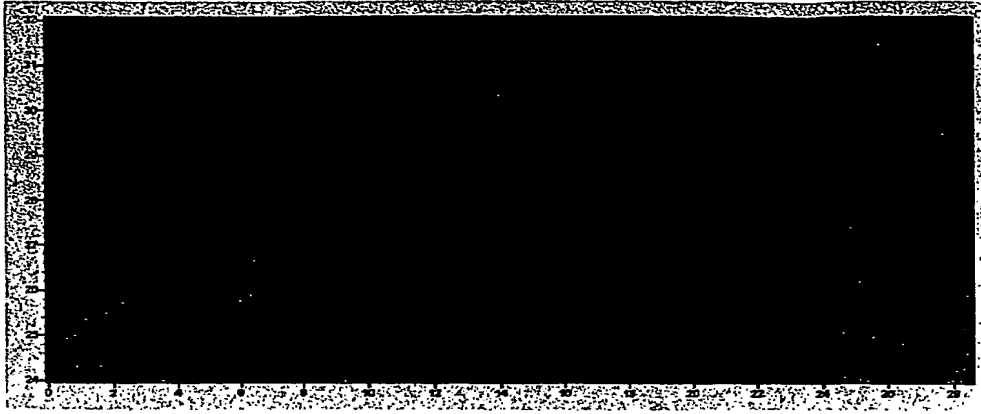
Graph 3-16 Temperature analysis using graphical filtering; 6w, pulse mode: repeated, 0.9 sec on/0.1 sec off;

Consequently, we used graphical filtering or synchronization during CW or PW experiments respectively.

3.4.3.3 Heat build-up in the surrounding tissue

We recorded and analyzed temperatures created in the upper tissue sample at varying conditions: different powers and pulse modes, gas circulations and vacuum.

3.4.3.3.1 The effect of airflow, suction and continuous/ pulsatile wave (CW/PW)
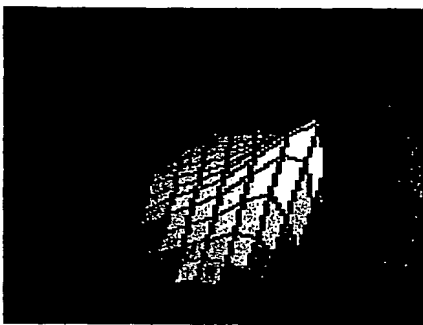
Using a fixed laser power, we have changed the conditions titled above, to explore each one's individual effect on the heat dispersion. Results, analysis and comparisons are shown below.
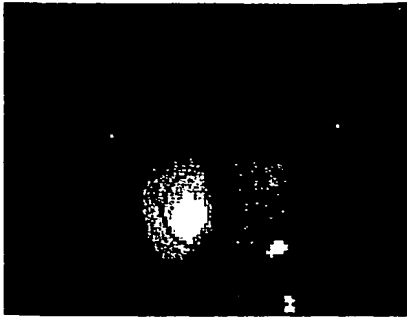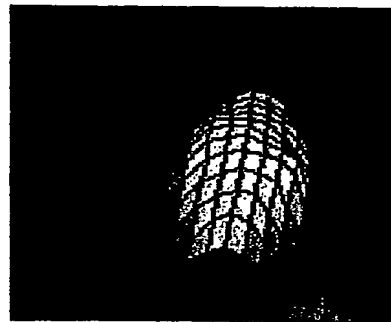
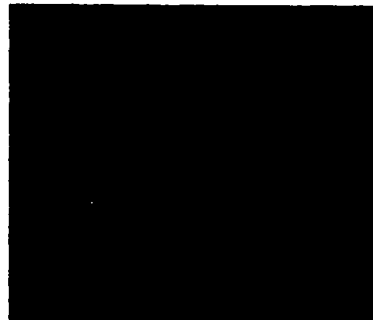Thermal image 3-9 Hotspot created in the upper tissue area. 15w, CW

Thermal Image 3-10 Heat cloud is created in the sphere when airflow (3lpm) runs through fiber. 15w, CW
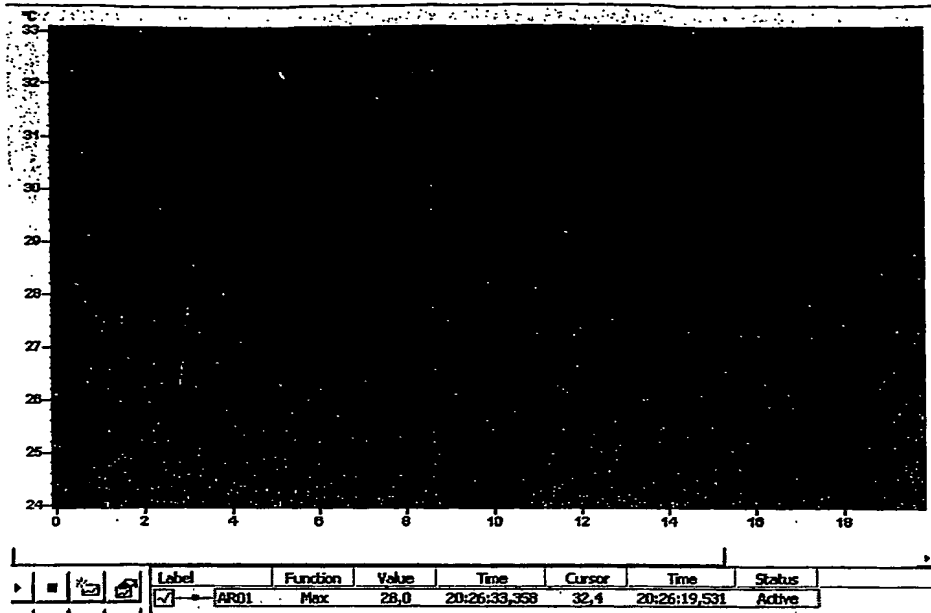

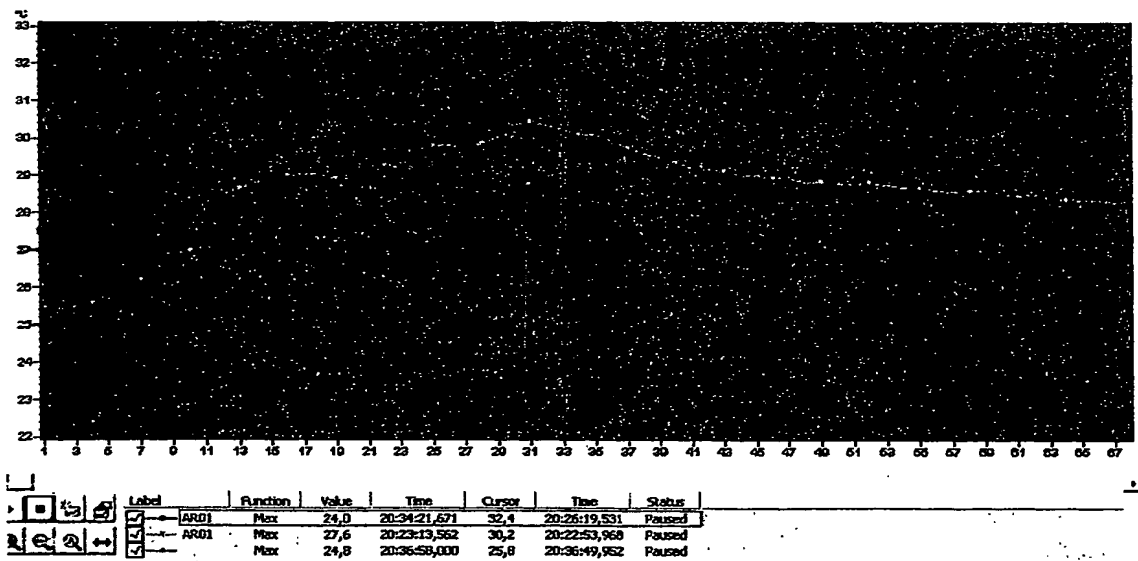Thermal image 3-11 3D presentation of image 3-9 (above) - 15w,CW, no airflow

Thermal image 3-12 3D presentation of image 3-10 (above) - 15w,CW, with airflow


Thermal image 3-13 15w,CW, with 3lpm airflow and 50mmHg vacuum

Graph 1-17 Max. temperature of the surroundings vs. time (sec); 15w, CW

		Label	Function	Value	Time	Cursor	Time	Status
		AR01	Max	28,0	20:26:33,358	32,4	20:26:19,531	Active

		Label	Function	Value	Time	Cursor	Time	Status
		AR01	Max	24,0	20:34:21,671	32,4	20:26:19,531	Paused
		AR01	Max	27,6	20:23:13,562	30,2	20:22:53,968	Paused
			Max	24,8	20:36:58,000	25,8	20:36:49,952	Paused

Graph 3-18 Max. temperature vs. time (secx4); airflow through fiber (red), suction (gray), airflow and suction (blue), none (black); 15w, CW, 7sec; notice differences in start temperatures.
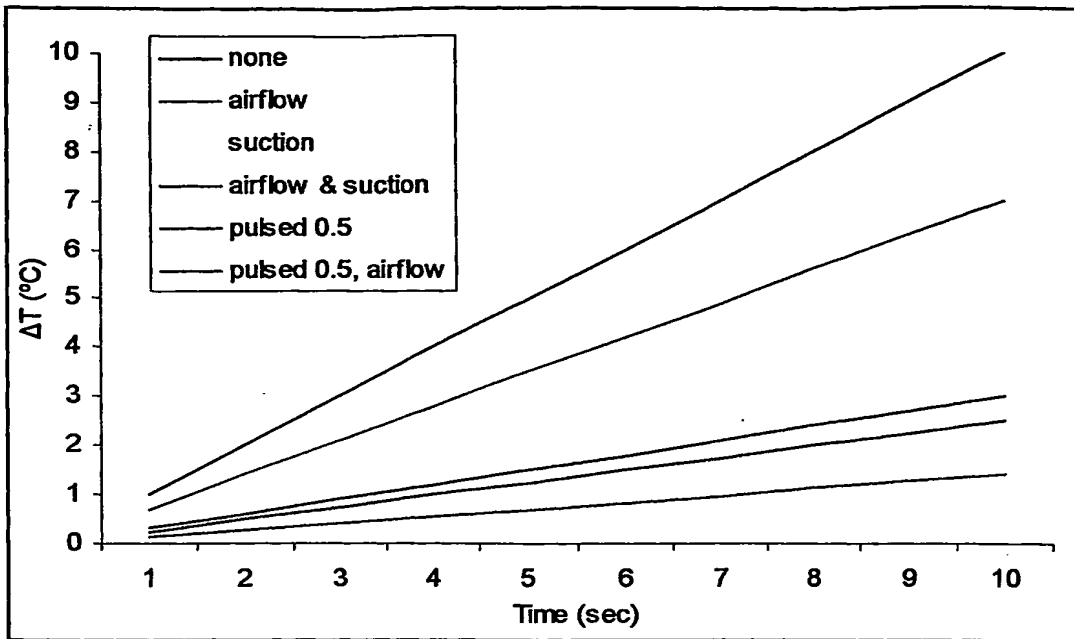
88
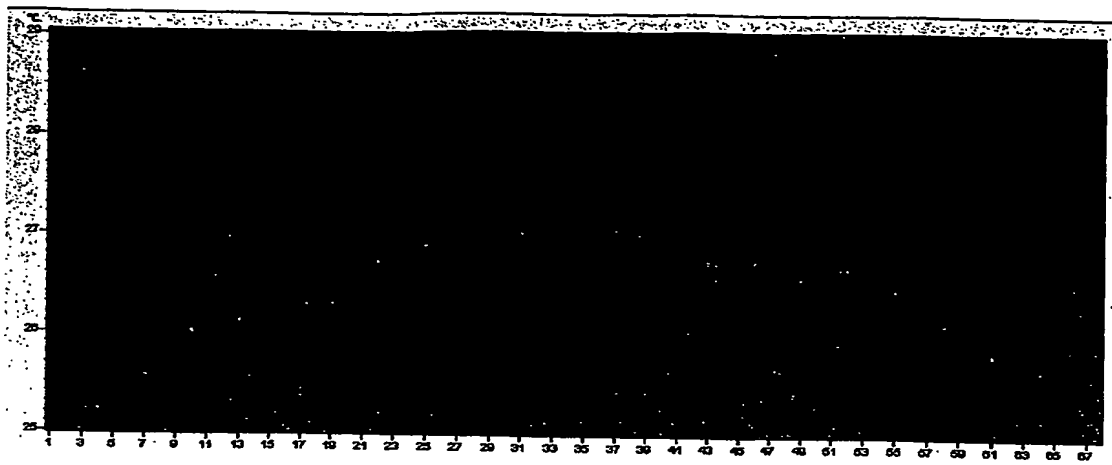
Graph 3-19 Max. temperature vs. time (secx4); 15w; pulse mode: 0.5/0.5; with (red) & w/o (black) airflow through fiber;

Assuming linear slopes during transmission periods of 7 seconds, we calculated the average heating rate (tables 3-5,6). ΔT was defined as the difference between initial temperature (when irradiation starts) and the maximal temperature observed after 7 seconds.

Table 3-5 Average heating rate in the surrounding tissue at different conditions; 15watts, 7 seconds elapsed

| 15watts (750w/cm^2), 7 sec elapsed	Neither air nor suction	Airflow 3lpm	Suction 40mmHg	Airflow & suction	Pulsed, 0.5 on / 0.5 off	Pulsed with Airflow 0.5 on / 0.5 off
ΔT (^{0}C)	7.5	5	2.5	1	2.2	1.8
Av. slope (^{0}C/Sec)	1	0.7	0.35	0.14	0.3	0.25

89

Graph 3-20 Extrapolation via linear regression; 15watts

In these settings, 3lpm airflow reduced the thermal gradient by 33%, 40mmHg vacuum reduced it by 67% and both simultaneously by 80%. The suction dramatic influence will be further investigated in section 3.4.3.3.4.

The pulse mode of 0.5-dutycycle (half the energy) shrank the gradient by 64% with airflow injected and by 70% w/o it. Tissue thermal relaxation between pulses (see sec. 1.3.6) caused greater percentage than the expected 50.

3.4.3.3.2 The effect of various powers

In this section and the one follows, we have solely altered the laser power, to study its effect on the thermal gradients vs. time and place.
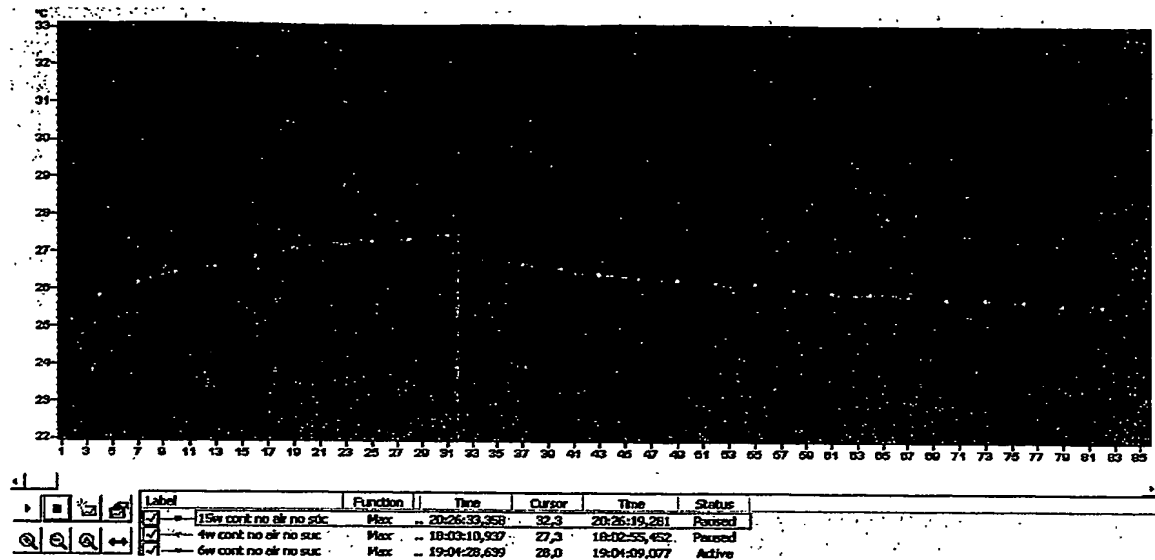
Graph 3-21 Max. temperature vs. time (secx4); 15w (black), 6w (blue), 4w (red); CW, 7sec; notice differences in start temperatures;

Table 3-6 Average heating rate in the surrounding tissue using various powers; 7 seconds

| 7 sec elapsed	15watts (750w/cm²)	6watts (300w/cm²)	4watts (200w/cm²)
ΔT (°C)	7.5	4.5	3
Av. slope (°C/Sec)	1	0.64	0.43
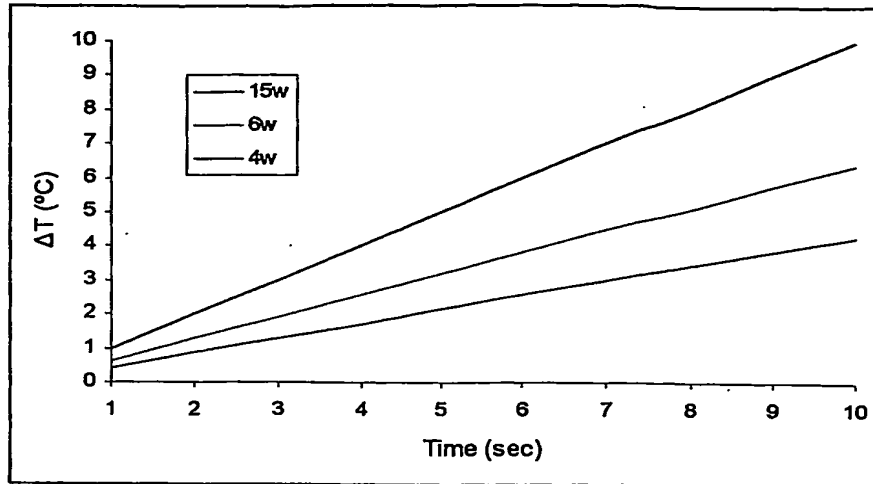
Graph 3-22 Extrapolation via linear regression; various powers; neither air nor suction

3.4.3.3 Longer period of continuous transmission and the thermal gradient along the hotspot
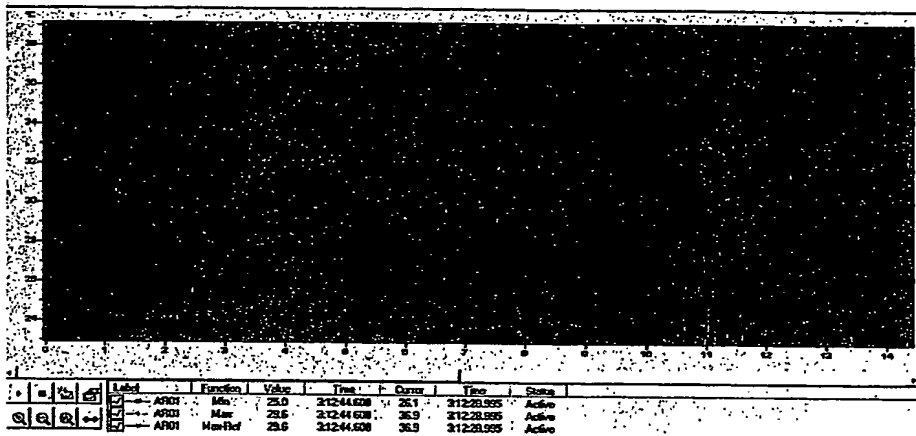
Here we have irradiated tissue for more than 10 seconds to examine the time effect, using different powers. We have also monitored the thermal gradient along the surrounding tissue.
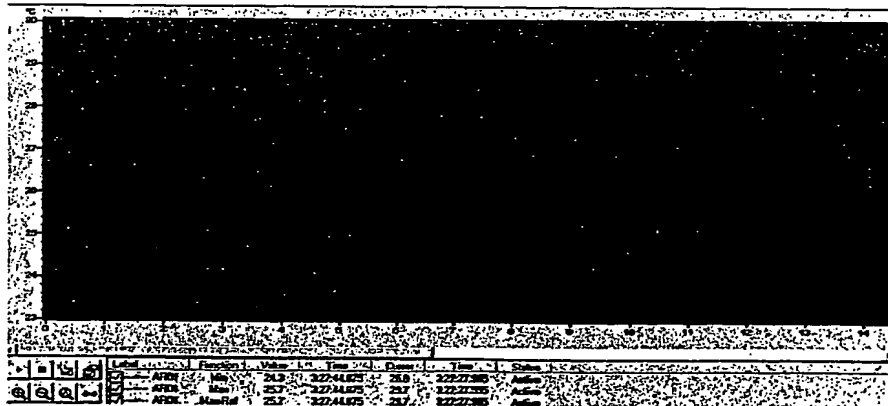
Graph 3-23 6w, CW, no air no suction 1st trial; maxΔT~6°C
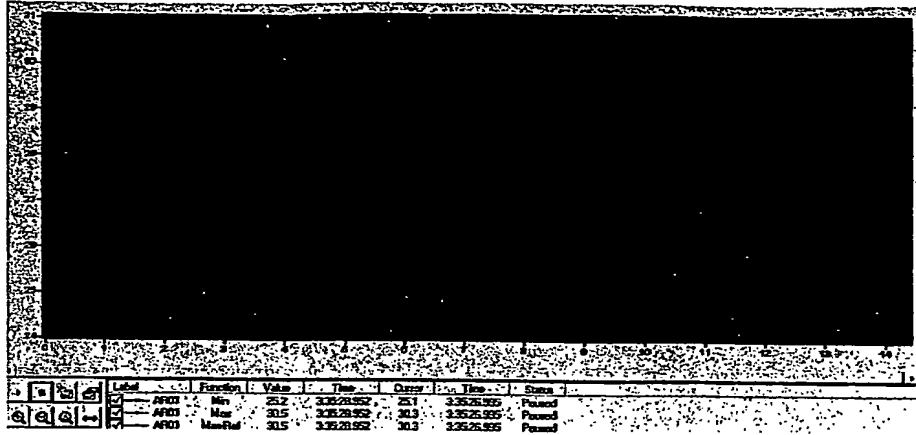
Graph 3-24 6w, CW, no air no suction 2nd trial; maxΔT~5.5°C

Graph 3-25 12w, CW, no air no suction; maxΔT~13°C

Table 3-7 Two types of thermal gradients in surrounding tissue, after 10 seconds; distance between most and least heated points was 1.5cm

10 sec elapsed; neither airflow nor suction	6watts_1st	6watts_2nd	6watts_Av (300w/cm²)	12watts (600w/cm²)
$\Delta T_{1-11sec}$ (°C) Max temp. after 10s	6	5.5	5.75	13
Av. slope (°C/Sec)	0.6	0.55	0.575	1.3
$\Delta T_{1.5cm}$ (°C) (Max temp.) - (min. temp.) in surroundir tissue, after 10sec	4.7	5.2	4.95	10.8

93

The two 6watts-power trials resulted in different gradients (thus were averaged). The average slope of the 12watt-power was unreasonably higher than the one obtained in the 15watt trial (table 3-7) - 1.3 vs. $1^0C/Sec$. Both cases, as well as others, which are not presented here, show poor repeatability of results. This is mainly reasoned by the need to replace or displace tissue sample after every irradiation, so that laser beam hits a fresh mucosa. Yet, another occurrence might have caused the lower gradient during the 15watts test. The likely formation of jet in such a power (see section 3.4.1) could partially shift and blur the demarcated hotspot toward fiber entrance hole. Graph 3-26 demonstrates this trend changing. Up to that point, the relation between ΔT and power is linear.
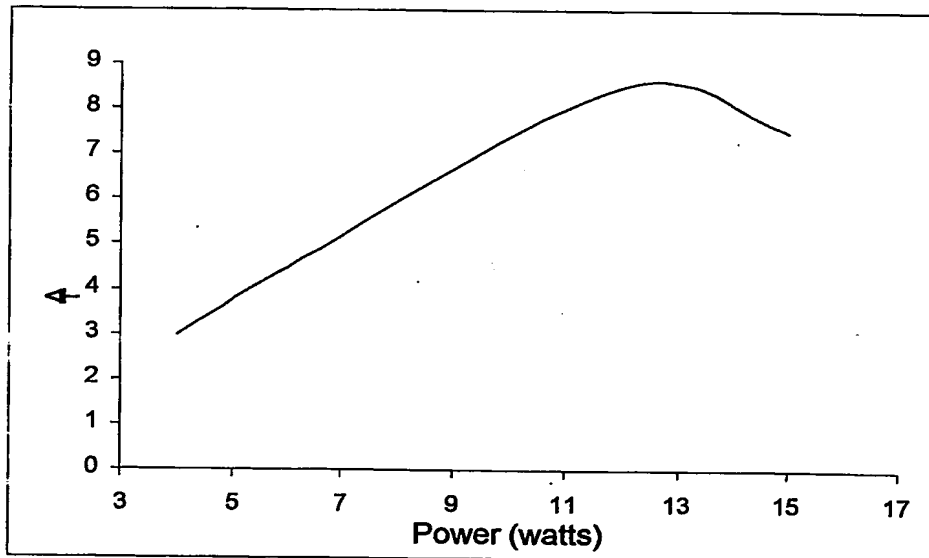
Graph 3-26 Max ΔT vs. power after 7 sec; trend changes around 13 watts

3.4.3.3.4 Interim suction
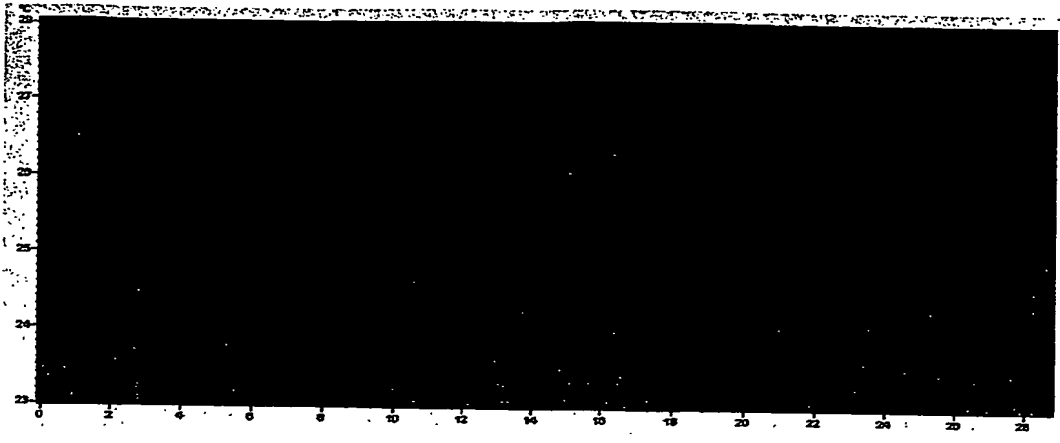
Graph 3-27 Laser transmission 0-10sec; vacuum activation (40mmHg) 2.5 - 6sec; 7w, CW, no air

Max. temperature drops dramatically when suction is activated, and rises again when vacuum gets weakened. Suction efficiently reduces the temperature of the surroundings by eliminating the steam.

3.4.3.3.5 Damage to tissue

Although the maximal temperature of the upper tissue has not exceeded the 46^0C (see sec. 3.4.3.3), along decades of tests, an accumulated, thermal damage has appeared (pic 3-59). Such damages are not likely to appear in practice since the laser-induced target changes constantly.


Picture 3-58 Before: fresh
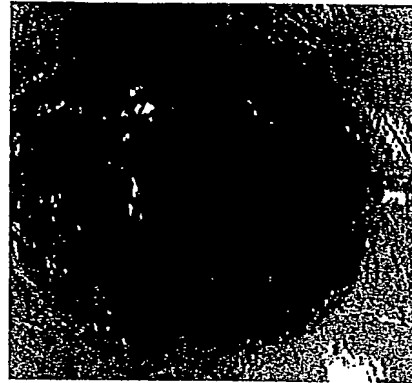

Picture 3-59 After: necrotic

Pictures 3-58,9 Upper (surrounding) tissue sample at the startpoint (left) and by the end of trials (right); the dark stain in the center of pic. 3-59 indicates tissue coagulation.

3.4.4 Activating the software-controlled system

In this section the Labview application controlled all setup components, including the IR camera (refer sec. 3.2 and setup scheme illustrated in fig. 3-20). Pic. 3-60,1,2 demonstrae the cavity-like configuration:
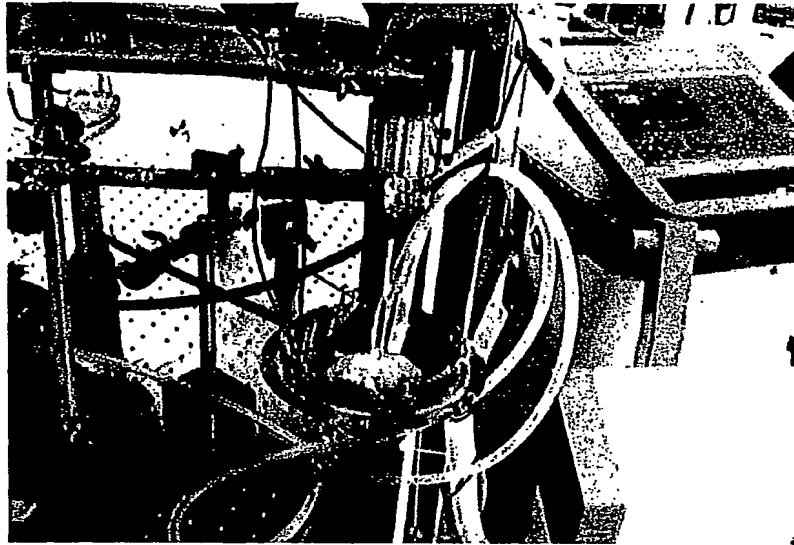
Picture 3-60 The fully software-controlled setup
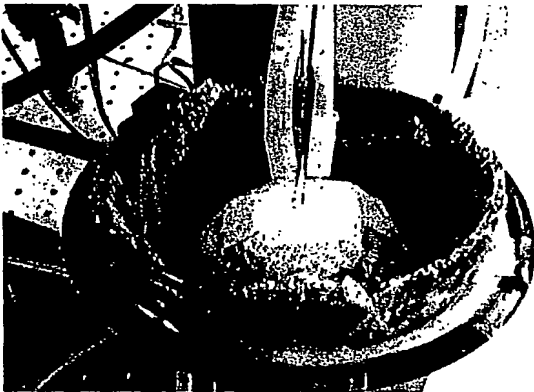
Picture 3-61 Cavity-like phantom - external view

Picture 3-62 Cavity-like phantom - internal view; suction, insufflation and fiber outlets adjacently located, same as in endoscope distal tip

3.4.4.3 Results acquired by the software-controlled system
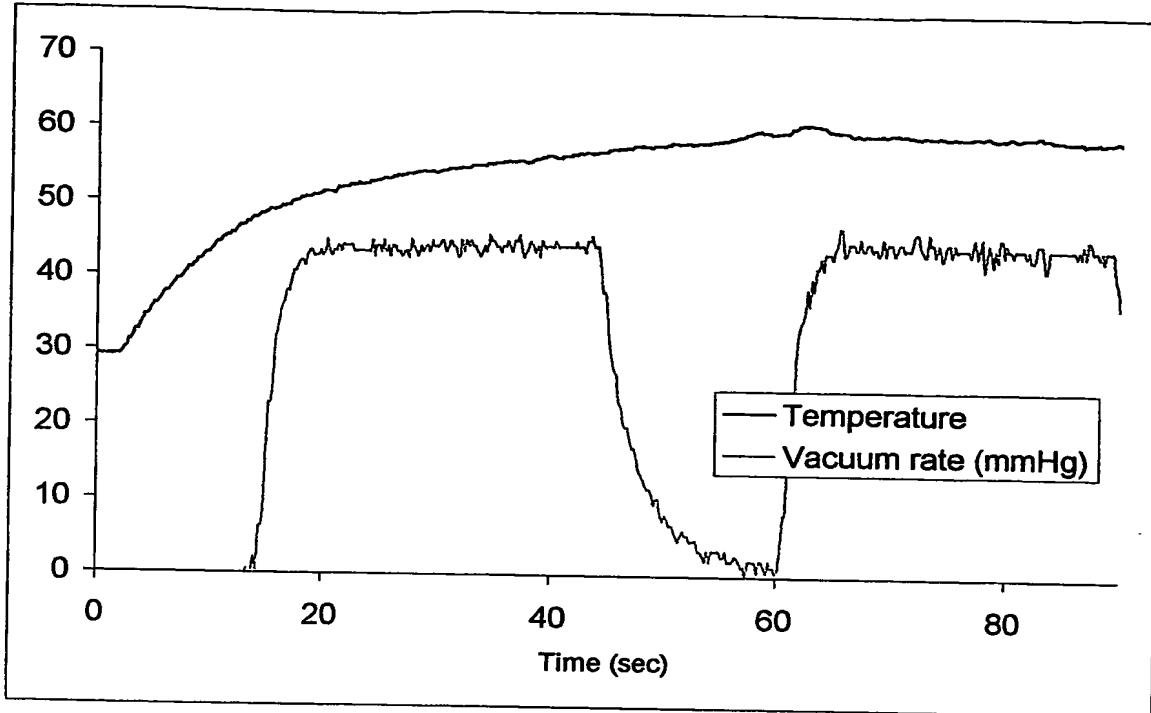
Graph 3-28 Suction test; max vacuum set to 47mmHg, "max temp allowed" set to 46°C (suction is activated when temp. exceeds 46°C); 2w, CW
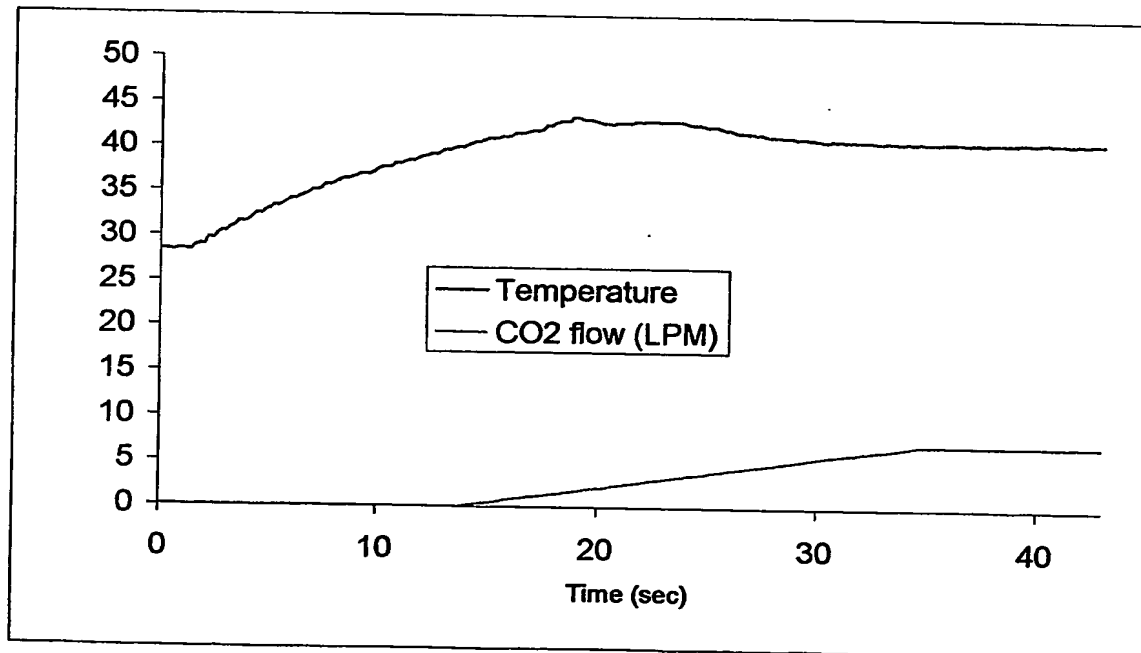
Graph 3-29 CO_2 test; CO_2 flow limit was set to 7lpm and "max temp allowed" to 40°C (flow is activated when temp. exceeds 40°C); Temp. has stabilized around 41°C; 2w, CW
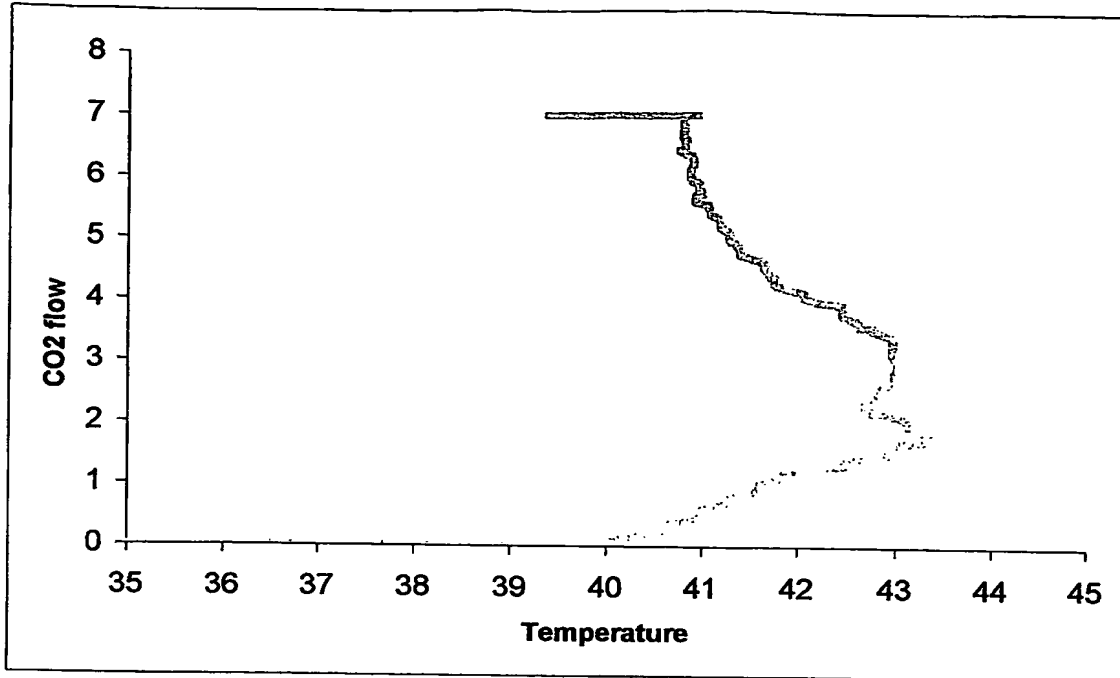
Graph 3-30 CO_2 flow vs. max. temp: XY Relation; CO_2 flow limit set to 7lpm, "max temp allowed" set to 40°C; temp. turns down around 2 lpm and stabilized beyond 6.5 lpm at 41°C; 2w, CW
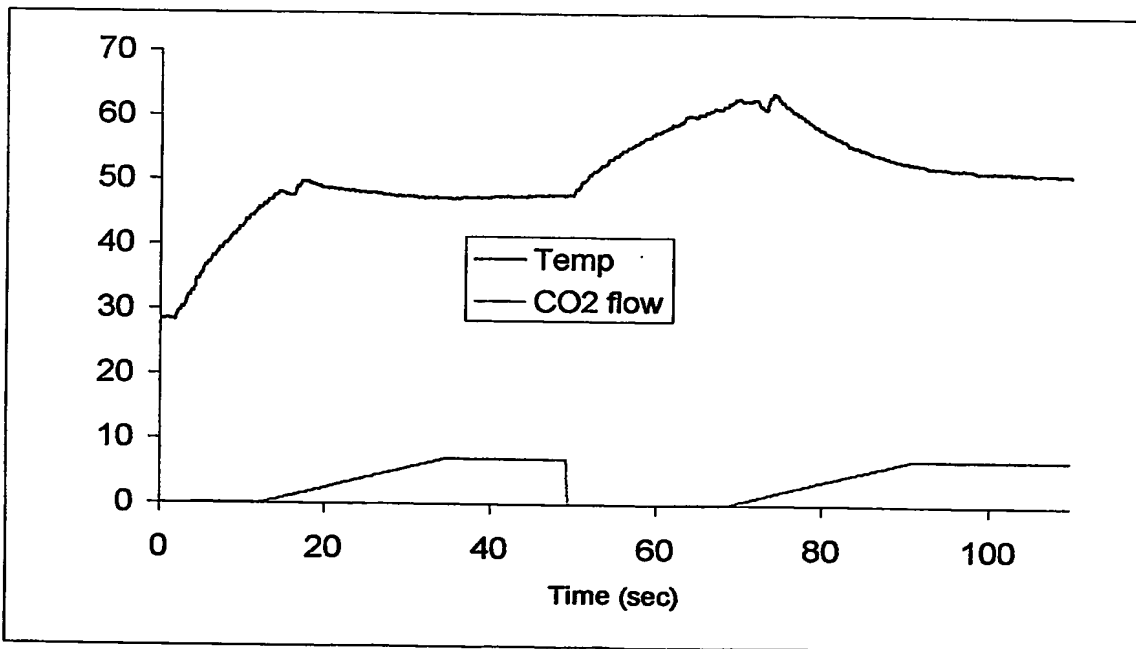
Graph 3-31 CO_2 test; CO_2 flow limit set to 7lpm, "max temp allowed" set to 46°C; flow was manually neutralized and reactivated to observe its effect at very high temperatures; temp has finally stabilized around 53°C; 2w, CW
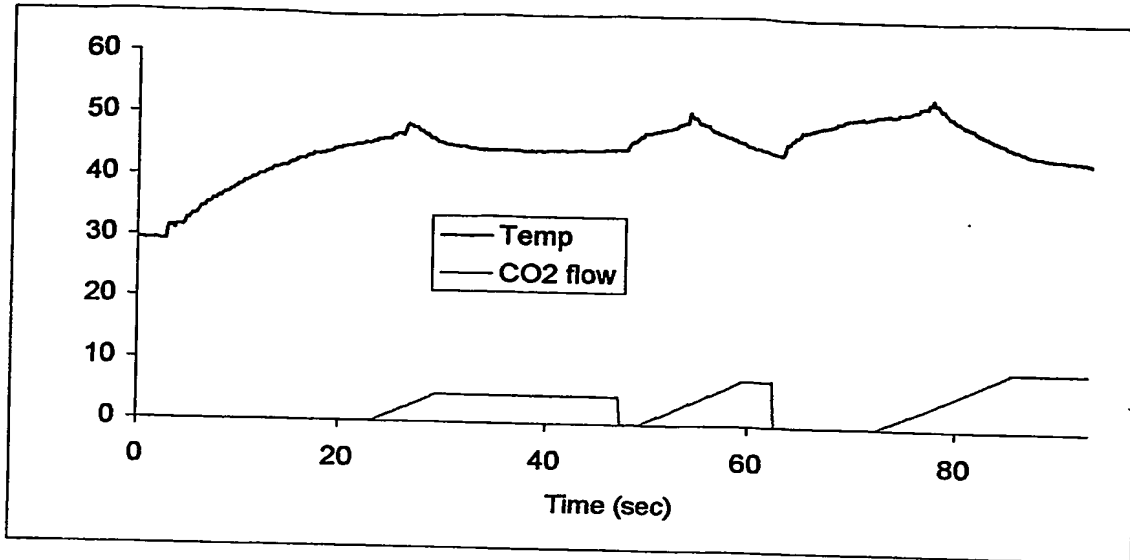
Graph 3-32 2w, CO_2 flow limit set to15lpm, "max temp allowed" set to 46°C; after first two flow automatic activations, flow was manually stopped to enable heat development. Then flow was reactivated and reached its top limit of 15lpm. Temp. had declined back and stabilized on 46°C.

3.4.4.4 Analysis and discussion

Unlike previous experiments, suction had no considerable effect on the temperature (graph 3-28). We assume the following cause: the distance between fiber edge and irradiated tissue was very short (see jet formation in short distance in pic. 3-25), irradiation has lasted 14 sec. (see pic 3-24) and, as explained earlier in this section, air was not injected through fiber. In these conditions, it seems that even the maximal vacuum of 47mmHg is not capable of evacuating the steams and preventing them from penetrating into the fiber. Consequently, fiber gets overheated and heats the surrounding tissue (in practice it might damage the endoscope). We concluded that when fiber edge is very close to tissue and irradiation lasts more few seconds, even when using low powers, airflow injection or higher vacuum must be used.

The CO_2 flow evidences major effect on the temperature (graphs 3-29 - 3-32). When CO_2 flow increases the maximal temperature clearly declines down to a certain value, where it steadies. Higher flow limit enables dealing with higher temperature in shorter time intervals (graph 3-32). There is, however, a major

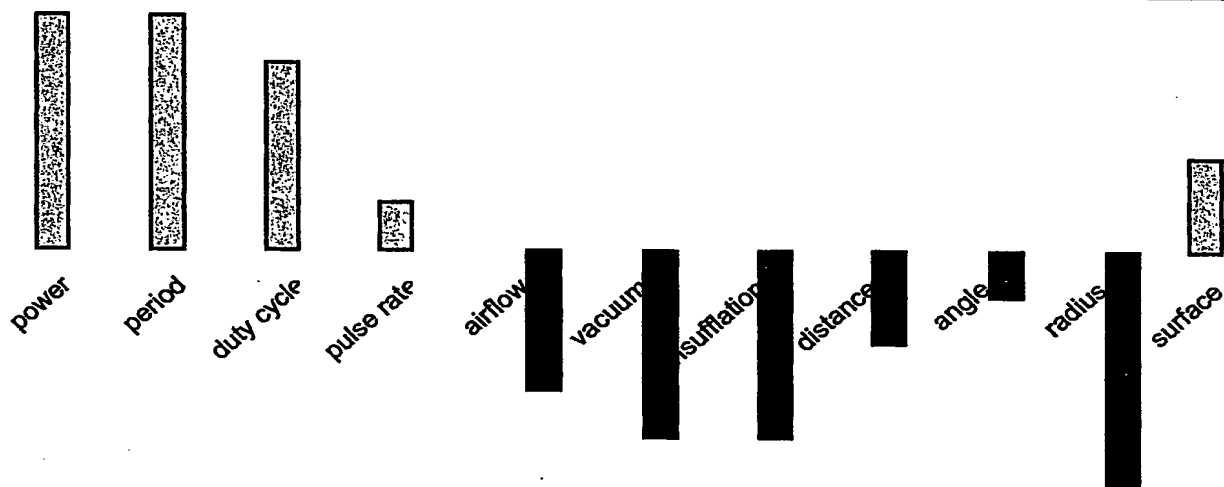| Laser settings					Suction & insufflation		Endoscope tip vs. irradiated tissue		Tissue Charac-teristics	
laser power (watts)	Irradiating period (sec)	duty cycle* (%) — both affect pulse-off duration, during which tissue "relaxes"	pulse frequency* (Hz)	airflow through fiber* (lpm)	vacuum rate (mmHg)	Cold CO_2 flow (lpm)	distance fiber-tissue (mm)	hitting angle (jet direc-ti on) (deg)	cavity radius (cm)	rough-ness of surrou-nding tissue
0-15 tissue; 0-50 Agarose	0-100	0-100	0-3M	0-3	0-50	0-15	2-50	90-45	1.5-4.5	smooth - rough

Figure 4-25 Parameters' fundamental effect on the max. temperature of the surrounding tissue. Red and blue stand for "heaters" and "coolers" respectively. Column length represents the relative effect of each parameter, within the indicated range.

During our observations, the maximal thermal gradient of the surroundings has not exceeded 13°C, even in the considerable severe conditions of 15watts power (750w/cm²), 10seconds continuous exposure, and the absence of airflow, suction and gas insufflating. Moreover, we have used distances of 1.5-2cm between irradiated and surrounding tissues whereas the narrowest diameter in the digestive tract below the esophagus, when constricted, is about 1.5cm (pyloric canal), and the turn-diameter of gastroscope's distal tip is approx 4.5cm.

According to Lumenis [90] these conditions are extremely "worst", comparing to the ones used for superficial ablation, during esophagastric MIS. This means that the highest temperature of the surrounding tissue will *not* cross

5 Prospective research

By conventional order, the subsequent stage of research should be animal study, preferably by using a practical endoscope. To do so, prior to stepping forward we must resolve two major issues:

- Appling the laser energy transendoscopically via flexible fibers
- Obtaining thermal feedback via IR imaging fiber bundle.

We will handle the first by using finest 300μm fiberoptics, custom-built coupler and SMA 905 connectors.

The second issue will be dealt in collaboration with another research group (Katzir et al. [91-93]), which has been developing an IR bundle, transparent to IR wavelengths. The IR signals, exit the bundle, will be optically magnified by a reflecting objective (Cassegrain lens), and then recorded by the thermal camera. Images 5-14,15 demonstrate some preliminary results of thermal images taken through an experimental low grade IR imaging bundle:
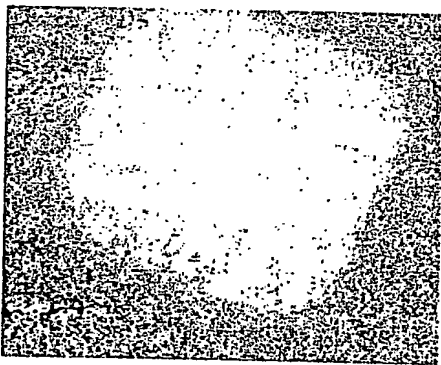
Thermal image 5-14 Centered blowtorch
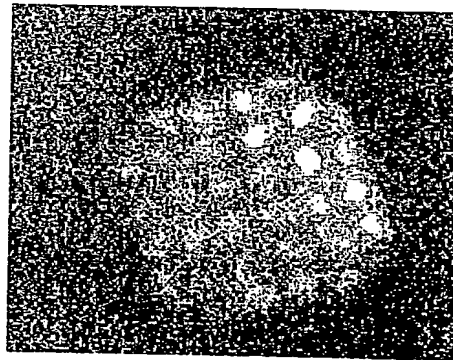
Thermal image 5-15 Marginal hot wire

Thermal images 5-14,15: Acquiring thermal images of two hot objects, by means of flexible optic bundle as the IR waveguide, imaging lens, magnifying lens and IR Camera.

Managing this, we intend to utilize the software-control setup to accomplish optimized results.

6 References

1. Mack, M.J., *Minimally invasive and robotic surgery*. Jama-Journal of the American Medical Association, 2001. **285**(5): p. 568-572.

2. Fuchs, K.H., *Minimally invasive surgery*. Endoscopy, 2002. **34**(2): p. 154-159.

3. *American Society for Gastrointestinal Endoscopy, http://www.asge.org/*.

4. Miller, R.A., *Endoscopic Instrumentation: Evolution, Physical Principles and Clinical Aspects*. British Medical Bulletin, 1986. **42**(3): p. 223-225.

5. Berci, G. and K.A. Forde, *History of endoscopy - What lessons have we learned from the past?* Surgical Endoscopy-Ultrasound and Interventional Techniques, 2000. **14**(1): p. 5-15.

6. Boppart, S.A., T.F. Deutsch, and D.W. Rattner, *Optical imaging technology in minimally invasive surgery - Current status and future directions*. Surgical Endoscopy-Ultrasound and Interventional Techniques, 1999. **13**(7): p. 718-722.

7. Milne, J.S., *Surgical instruments in Greek and Roman times*, ed. A.M. Kelley. 1970, New York.

8. Wallace, D.M., *New lamps for old*. Proc R Soc Med. **66**: p. 455-459.

9. Spaner, S.J. and G.L. Warnock, *A brief history of endoscopy, laparoscopy, and laparoscopic surgery*. Journal of Laparoendoscopic & Advanced Surgical Techniques-Part A, 1997. **7**(6): p. 369-373.

10. Mikulicz, J., *Uber Gastroskopie und Osophagoskopie*. Wien Med Presse, 1881. **45**: p. 1405.

11. Stoerk, P., *Ein neues Osophagoskope*. Wien Med Wochenschr, 1887. **34**: p. 1117.

12. Miller, R.A., ed. *A brief history of endoscopy*. Percutaneous Renal Surgery, ed. M.R. (Eds.). 1983, In Wickham JEA: London. 45-48.

13. Wolf, R., *GMBH 100 years of cystoscopy 1879-1979*, ed. W. Knittlingen. 1979.

14. Hopkins, H.H., *Optical principles of endoscopy*. In: Berci G Endoscopy. 1976, New York: Appleton Century Crofts. 3-63.

15. Heel, A.S., *A new method of transporting optical images without aberrations*. Nature, 1954.

16. Robinson, H.B. and G.B. Smith, *Application for Laparoscopy in General Surgery.* Surg. Gynecol. Obstet, 1976. **143**: p. 829-833.

17. Ravid, A. and A. Katzir, *Theoretical model simulating CO2 laser ablation of biological tissue due to steam pressure generation.* SPIE Progress in biomedical optics, 1997. **3195**: p. 287-295.

18. Bown, S.G., *Laser Endoscopy.* British Medical Bulletin, 1986. **42**(3): p. 307-313.

19. Katzir, A., *Lasers and Optical Fibers in Medicine.* 1993, London: Academic Press.

20. Peters, J.H. and T.R. DeMeester, eds. *Minimally Invasive Surgery of Foregut.* 1994, Quality Medical Publishing Inc.: Missouri.

21. Smith, P.M., *Therapeutic Endoscopy of the Upper Gastrointestinal Tract.* British Medical Bulletin, 1986. **42**(3): p. 249-256.

22. Grendell, J.H., K.R. McQuaid, and S.L. Friedman, eds. *Current diagnosis & treatment in gastroenterology.* 1996, Stamford, Conn. : Appleton & Lange, 1996.

23. Kiefhaber, P., G. Nath, and K. Moritz, *Endoscopical control of massive gastrointestinal heorrhage by irradiation with high-power neodymium YAG laser.* Prog. Surg., 1977. **15**: p. 140-155.

24. Niemz, M.H., *Interaction mechanisms, Medical applications of lasers,* in *Laser-tissue interactions - fundamentals and applications.* 1996, Springer: Heidelberg, Germany. p. 45-236.

25. Reich, H., T.S. Macgregor, and T.G. Vancaillie, *CO2-Laser Used through the Operating Channel of Laser Laparoscopes - Invitro Study of Power and Power-Density Losses.* Obstetrics and Gynecology, 1991. **77**(1): p. 40-47.

26. Fournier, G.R., A.H. Kung, and D. Trost, *High-Powered Co2-Laser Cystoscope for Endoscopic Bladder Surgery.* Lasers in Surgery and Medicine, 1995. **16**(4): p. 390-396.

27. Gannot, I., *Investigation of the flexible waveguide transmitting IR laser radiation and the interaction of the radiation emerging from the waveguide with the tissue,* in *Biomedical Engineering, Faculty of Engineering.* 1994, Tel Aviv: Tel Aviv, Israel.

28. Thibodeau, G.A. and K.T. Patton, *Anatomy & Physiology*. Fourth ed. 1999: Sally Schrefer. 740-785.

29. Mimura, S. and S. Okuda, *Present Status of Photodynamic Therapy (Pdt) for Early Gastric- Cancer*. Internal Medicine, 1992. **31**(12): p. 1436-1436.

30. Hayashi, A.T., et al. *Indocyanine green enhanced diode laser ablation for porcine gastric wall with ablation depth monitoring using scattering light*. in *IEEE Engineering in Medicine and Biology Society*. 1998. Hong Kong, China.

31. Petrakis, I.E., V. Sciacca, and C. Iascone, *Diagnosis and treatment of Barrett's oesophagus. A general survey*. Acta Chirurgica Belgica, 2001. **101**(2): p. 53-58.

32. Plevris, J.N. and R.C. Heading, *Present medical management of Barrett's oesophagus*. Digestive and Liver Disease, 2001. **33**(3): p. 278-283.

33. Wang, K.K. and R.E. Sampliner, *Mucosal ablation therapy of Barrett esophagus*. Mayo Clinic Proceedings, 2001. **76**(4): p. 433-437.

34. Ackroyd, R., et al., *Ablation treatment for Barrett oesophagus: what depth of tissue destruction is needed?* Journal of Clinical Pathology, 1999. **52**(7): p. 509-512.

35. Barham, C.P., et al., *Photothermal laser ablation of Barrett's oesophagus: endoscopic and histological evidence of squamous re-epithelialisation*. Gut, 1997. **41**(3): p. 281-284.

36. Gossner, L., et al., *KTP laser destruction of dysplasia and early cancer in columnar-lined Barrett's esophagus*. Gastrointestinal Endoscopy, 1999. **49**(1): p. 8-12.

37. Gannot, I., et al., *Current status of flexible waveguides for IR laser radiation transmission*. Ieee Journal of Selected Topics in Quantum Electronics, 1996. **2**(4): p. 880-889.

38. Mizaikoff, B. *Recent Trends in Mid-Infrared Sending*. in *SPIE - Optical Fiber and Sensors for Medical Applications*. 2001.

39. Waynant, R.W., I.K. Ilev, and I. Gannot, *Mid-infrared laser applications in medicine and biology*. Philosophical Transactions of the Royal

Society of London Series a-Mathematical Physical and Engineering Sciences, 2001. **359**(1780): p. 635-644.

40. Webster, J.G., ed. *Encyclopedia of medical devices and instrumentation.* 1988, Wiley-Interscience: USA.

41. Montgomery, e.a., *Comparative gross and histologic study of the effects of scalpel, electric knife and CO2 laser on skin and uterine horn incisions in dogs.* Lasers in Surgery and Medicine, 1983. **3**: p. 9-22.

42. *Tutorials.* Therapeutic Applications of Advanced Laser Products. Vol. 1. 1993, JGM Associates Inc.

43. Welch, A.J., J.C. Martin, and V. Gemert, eds. *Opticla-thermal response of laser-irradiated tissue.* Lasers, Photonics, and Electro-Optics, ed. H. Kogelnik. 1995, Plenum Press: NY. 367-902.

44. Jacques, S.L., *Laser-tissue interactions: photochemical, photothermal and photomechanical.* Surg. Clin. North Am., 1992. **72**: p. 531-558.

45. Vangemert, M.J.C. and A.J. Welch, *Time Constants in Thermal Laser Medicine.* Lasers in Surgery and Medicine, 1989. **9**(4): p. 405-421.

46. Gannot, I. and M. Ben-David, *Optical Fibers and Waveguides for Medical Aplications*, in *Biomedical Photonics handbook*, T. Vo-Dinh, Editor. to be publishied in 2003, CRC Press.

47. Gannot, I., et al., *Beam shape analysis of waveguide delivered infrared lasers.* Optical Engineering, 2002. **41**(1): p. 244-250.

48. Gannot, I., et al., *Flexible Wave-Guides for Er-Yag Laser-Radiation Delivery.* Ieee Transactions on Biomedical Engineering, 1995. **42**(10): p. 967-972.

49. Gannot, I., et al. *Flexible Plastic Waveguides Suitable For Large Interval of The Infrared Radiation Spectrum.* in *Proc. SPIE.* 1994.

50. Inberg, A., et al. *Hollow Silica, Metal and Plastic Waveguides for Hard Tissue Medical Applications.* in *Proc. SPIE.* 1997.

51. Inberg, A., et al., *Hollow waveguide for mid and thermal infrared radiation.* Journal of Clinical Laser Medicine & Surgery, 1998. **16**(2): p. 127-133.

52. Ben-David, M., et al., *The effect of scattering on the transmission of infrared radiation through hollow waveguides.* Journal of Optoelectronics and Advanced Materials, 1999. **1**(3): p. 23-30.

53. Shi, Y.W., et al., *Cyclic olefin polymer-coated silver hollow glass waveguides for the infrared.* Applied Optics, 1998. **37**(33): p. 7758-7762.

54. Harrington, J.A., C. Rabii, and D. Gibson, *Transmission properties of hollow class waveguides for the delivery of CO2 surgical laser power.* Ieee Journal of Selected Topics in Quantum Electronics, 1999. **5**(4): p. 948-953.

55. Nubling, R.K. and J.A. Harrington, *Hollow-waveguide delivery systems for high-power, industrial CO2 lasers.* Applied Optics, 1996. **35**(3): p. 372-380.

56. Harrington, J.A., *A review of IR transmitting, hollow waveguides.* Fiber and Integrated Optics, 2000. **19**(3): p. 211-227.

57. Miyagi, M. and S. Karasawa, *Wave-Guide Losses in Sharply Bent Circular Hollow Wave-Guides.* Applied Optics, 1990. **29**(3): p. 367-370.

58. Daoning, S. and e. al. *Thermal loading in launching and butt connection with hollow waveguides for CO2 laser beam delivery.* in *SPIE Proc. of biomedical fiber optics.* 1996.

59. Duck, F.A., *Thermal properties of tissue; Tissue composition,* in *Physical properties of tissue - a comprehensive reference book.* 1990, Academic Press: Bath, England. p. 9-37, 318-328.

60. Dai, J.W. and J.A. Harrington, *High-peak-power, pulsed CO2 laser light delivery by hollow glass waveguides.* Applied Optics, 1997. **36**(21): p. 5072-5077.

61. Vogel, A., W. Lauterborn, and R. Timm, *Optical and Acoustic Investigations of the Dynamics of Laser- Produced Cavitation Bubbles near a Solid Boundary.* Journal of Fluid Mechanics, 1989. **206**: p. 299-338.

62. McKenzie, A.L., *Physics of Thermal-Processes in Laser Tissue Interaction.* Physics in Medicine and Biology, 1990. **35**(9): p. 1175-1209.

63. Loze, M.K. and C.D. Wright, *Temperature distributions in semi-infinite and finite-thickness media as a result of absorption of laser light (vol 36, pg 494, 1997).* Applied Optics, 1997. **36**(20): p. 4890-4890.

64. Eichler, J., et al., *Temperature distribution for combined laser hyperthermia- photodynamic therapy in the esophagus*. Medical Engineering & Physics, 2000. **22**(4): p. 307-312.

65. Lecarpentier, G.L., et al., *Continuous-Wave Laser Ablation of Tissue - Analysis of Thermal and Mechanical Events*. Ieee Transactions on Biomedical Engineering, 1993. **40**(2): p. 188-200.

66. Iizuka, M.N., M.D. Sherar, and I.A. Vitkin, *Optical phantom materials for near infrared laser photocoagulation studies*. Lasers in Surgery and Medicine, 1999. **25**(2): p. 159-169.

67. *Biochemicals and organic compounds catalog*. 1994, Sigma Chemical Company.

68. *Sigma Material Safety Data Sheet*, Sigma Chemical Company.

69. Surowiec, A., et al., *Utilization of a Multilayer Polyacrylamide Phantom for Evaluation of Hyperthermia Applicators*. International Journal of Hyperthermia, 1992. **8**(6): p. 795-807.

70. *Development of a tissue phantom for experimental studies on laser interstitial thermotherapy of breast cancer*. in *Proceedings of SPIE - the International Society for Optical Engineering*. 2000. Miami Univ., FL, USA: Bascom Palmer Eye Inst.

71. Yonemura, Y., et al., *Multimodal therapy using hyperthermia for gastric cancer with special reference to histological studies*, in *Japanese Journal of Cancer & Chemotherapy*. 1987, Dept. of Surgery II, School of Medicine, Kanazawa University. p. 2890-4.

72. Wagnieres, G., et al., *An optical phantom with tissue-like properties in the visible for use in PDT and fluorescence spectroscopy*. Physics in Medicine and Biology, 1997. **42**(7): p. 1415-1426.

73. Vulcan, T.G., et al., *Comparison between isotropic and nonisotropic dosimetry systems during intraperitoneal photodynamic therapy*. Lasers in Surgery and Medicine, 2000. **26**(3): p. 292-301.

74. Whelan, W.M., et al., *Laser thermal therapy: utility of interstitial fluence monitoring for locating optical sensors*. Physics in Medicine and Biology, 2001. **46**(4): p. N91-N96.

75. *Optical and Thermal Performance Characteristics of Sidefiring Optical Fibers*. 1996, FDA, Office of Science and Technology.

76. Jones, B.F., *A reappraisal of the use of infrared thermal image analysis in medicine.* Ieee Transactions on Medical Imaging, 1998. **17**(6): p. 1019-1027.

77. Cadeddu, J.A., S.V. Jackman, and P.G. Schulam, *Laparoscopic infrared imaging.* Journal of Endourology, 2001. **15**(1): p. 111-116.

78. *Thermovision manuals.* 2001, FLIR Systems: Danderyd, Sweden.

79. Klocek, P., ed. *Handbook of Infrared Optical Materials.* Optical Engineering, ed. T. B.J. 1991, Marcel Dekker Inc: Dallas, Texas.

80. Sade, S. and A. Katzir, *Fiber optic infrared thermometer for accurate measurement of the core temperature of the human body.* Optical Engineering, 2001. **40**(6): p. 1141-1143.

81. Bramson, K.A., ed. *Infrared Radiation, A Handbook for Applications.* Plenum press: NY.

82. Wolfe, I.L. and G.J. Zissis, *The Infrared Handbook*, Washington DC: Office of Naval Research, Department of Navy.

83. Mading, R.P., *Thermographic Instruments and systems*, University of Wisconsin - Extension, Department of Engineering and Applied Science: Madison, Wisconsin.

84. Wolfe, I.L., *Handbook of Military Infrared Technology*, Washington, DC: Office of Naval Research, Department of Navy.

85. Vicek, J., *Determination of emissivity with imaging radiometers and some emissivities.* Photogrammetric Engineering and Remote Sensing.

86. Ohman, C., *Emittansmatningar med AGEMA E-Box.* 1999, AGEMA.

87. Torres, J.H., et al., *Experimental Evaluation of Mathematical-Models for Predicting the Thermal Response of Tissue to Laser Irradiation.* Applied Optics, 1993. **32**(4): p. 597-606.

88. Khosrofian, J.M. and B.A. Garetz, *Measurement of Gaussian laser beam diameter through direct inversion of knife-edge data.* Applied Optics, 1983. **22**(21): p. 3406-3410.

89. Turek, S., S. Kilian, and M. Altieri, *Smoke Rings*, IANUS.

90. *Surg Dept, Lumenis Ltd.* 2002.

91. Rave, E., L. Nagli, and A. Katzir, *Ordered bundles of infrared-transmitting AgClBr fibers: optical characterization of individual fibers.* Optics Letters, 2000. **25**(17): p. 1237-1239.

92. Rave, E., D. Shemesh, and A. Katzir, *Thermal imaging through ordered bundles of infrared- transmitting silver-halide fibers.* Applied Physics Letters, 2000. **76**(14): p. 1795-1797.

93. Rave, E. and A. Katzir, *Ordered bundles of infrared transmitting silver halide fibers: attenuation, resolution and crosstalk in long and flexible bundles.* Optical Engineering, 2002. **41**(7): p. 1467-1468.

94. *Present status of photodynamic therapy for cancer of upper gastrointestinal tract.* Review of Laser Engineering, 1992. **20**(7): p. 461-74.

95. Bouchard, L.S. and M.J. Bronskill, *Magnetic resonance imaging of thermal coagulation effects in a phantom for calibrating thermal therapy devices.* Medical Physics, 2000. **27**(5): p. 1141-1145.

96. Crezee, J. and J.J.W. Lagendijk, *Experimental-Verification of Bioheat Transfer Theories - Measurement of Temperature Profiles around Large Artificial Vessels in Perfused Tissue.* Physics in Medicine and Biology, 1990. **35**(7): p. 905-923.

97. Dobson, S.J. and H.H. Hopkins, *A New Rod-Lens Relay System Offering Improved Image Quality.* Journal of Physics E-Scientific Instruments, 1989. **22**(7): p. 450-455.

98. Eisendrath, P., J.L. Van Laethem, and J. Deviere, *Follow-up of Barrett's epithelium after ablation by endoscopic argon plasma coagulation.* Gastrointestinal Endoscopy, 2001. **54**(1): p. 137-137.

99. Greve, B., S. Hammes, and C. Raulin, *The effect of cold air cooling on 585 nm pulsed dye laser treatment of port-wine stains.* Dermatologic Surgery, 2001. **27**(7): p. 633-636.

100. Haubrich, W.S., *The centennial year: The development of important ideas during the last 100 years - The advent and evolution of endoscopy.* Gastroenterology, 1997. **112**(2): p. 591-593.

101. Hess, R., et al., *A new setup for the determination of emissivity by a dynamic method.* High Temperatures-High Pressures, 1999. **31**(3): p. 307-320.

102. Hilton, A.R. *Infrared Imaging Bundles with Good Image Resolution.* in *SPIE - Optical Fiber and Sensors for Medical Applications.* 2001.

103. Hooper, B.A., et al., *Precise, controlled laser delivery with evanescent optical waves.* Applied Optics, 1999. **38**(25): p. 5511-5517.

104. Iizuka, H., et al., *Mechanical properties of woodceramics: A porous carbon material.* Journal of Porous Materials, 1999. **6**(3): p. 175-184.

105. Karamzadeh, A.M., et al., *Laser-mediated cartilage reshaping with feedback-controlled cryogen spray cooling: Biophysical properties and viability.* Lasers in Surgery and Medicine, 2001. **28**(1): p. 1-10.

106. Kern, ed. *Evaluation of infrared emission of clouds and ground as measured by weather satellites.* Defence Documentation Center.

107. Linder, T.E., D. Simmen, and S.E. Stool, *Revolutionary inventions in the 20th century - The history of endoscopy.* Archives of Otolaryngology-Head & Neck Surgery, 1997. **123**(11): p. 1161-1163.

108. Loza, P., D. Kouznetsov, and R. Ortega, *Temperature Distribution in a Uniform Medium Heated by Linear Absorption of a Gaussian Light-Beam.* Applied Optics, 1994. **33**(18): p. 3831-3836.

109. Marcatili, E.A.J. and R.A. Schmeltzer, *Hollow metallic and dielectric waveguides for long distance optical transmission and lasers.* Bell Syst. Tech. J., 1964. **43**: p. 1783-1809.

110. McNally, K.M., et al., *Dynamic optical-thermal modeling of laser tissue soldering with a scanning source.* Ieee Journal of Selected Topics in Quantum Electronics, 1999. **5**(4): p. 1072-1082.

111. Middleton, W.G., D.A. Tees, and M. Ostrowski, *Comparative Gross and Histological Effects of the Co2-Laser, Nd-Yag Laser, Scalpel, Shaw Scalpel and Cutting Cautery on Skin in Rats.* Journal of Otolaryngology, 1993. **22**(3): p. 167-170.

112. Milne, P.J., et al., *Development of stereotactically guided laser interstitial thermotherapy of breast cancer: In situ measurement and analysis of the temperature field in ex vivo and in vivo adipose tissue.* Lasers in Surgery and Medicine, 2000. **26**(1): p. 67-75.

113. Muller, J.M., et al., *Endoscopic surgery: Fit for malignancy?* World Journal of Surgery, 1999. **23**(8): p. 808-815.

114. Nelson, J.S. and S. Kimel, *Safety of cryogen spray cooling during pulsed laser treatment of selected dermatoses.* Lasers in Surgery and Medicine, 2000. **26**(1): p. 2-3.

115. Nelson, J.S., et al., *Dynamic Epidermal Cooling During Pulsed-Laser Treatment of Port-Wine Stain - a New Methodology with Preliminary Clinical- Evaluation.* Archives of Dermatology, 1995. **131**(6): p. 695-700.

116. Oraevsky, A.A., et al., *Pulsed laser ablation of soft tissues, gels, and aqueous solutions at temperatures below 100 degrees C.* Lasers in Surgery and Medicine, 1996. **18**(3): p. 231-240.

117. Ortner, M.A., et al., *Is topical delta-aminolevulinic acid adequate for photodynamic therapy in Barrett's esophagus? A pilot study.* Endoscopy, 2002. **34**(8): p. 611-616.

118. Overholt, B.F., *Acid suppression and reepithelialization after ablation of Barrett's esophagus.* Digestive Diseases, 2000. **18**(4): p. 232-239.

119. Pennes, H.H., *Analysis of tissue and arterial blood temperatures in the resting human forearm (Reprinted from Journal of Applied Physiology, vol 1, pg 93-122, 1948).* Journal of Applied Physiology, 1998. **85**(1): p. 5-34.

120. Raulin, C., B. Greve, and S. Hammes, *Cold air in laser therapy: First experiences with a new cooling system.* Lasers in Surgery and Medicine, 2000. **27**(5): p. 404-410.

121. Roberts, W.W., et al., *Laparoscopic infrared imaging.* Surgical Endoscopy-Ultrasound and Interventional Techniques, 1997. **11**(12): p. 1221-1223.

122. Ross, E.V., Y. Domankevitz, and R.R. Anderson, *Effects of heterogeneous absorption of laser radiation in biotissue ablation: Characterization of ablation of fat with a pulsed CO2 laser.* Lasers in Surgery and Medicine, 1997. **21**(1): p. 59-64.

123. Schirmer, B., *Special problems in minimally invasive surgery of the foregut: Part I.* Journal of Gastrointestinal Surgery, 2001. **5**(2): p. 214-215.

124. Stal, P., et al., *Gastroesophageal reflux in healthy subjects - Significance of endoscopic findings, histology, age, and sex.* Scandinavian Journal of Gastroenterology, 1999. **34**(2): p. 121-128.

125. Steiner, R., et al., *Optimization of laser epilation by simulation of the thermal laser effect.* Laser Physics, 2001. **11**(1): p. 146-153.

126. Stolte, M., et al., *Prognosis of Carcinoid-Tumors of the Stomach.* Leber Magen Darm, 1988. **18**(5): p. 246-&.

127. Sumanac, K., et al., *Minimizing postcolonoscopy abdominal pain by using CO_2 insufflation: a prospective, randomized, double blind, controlled trial evaluating a new commercially available CO_2 delivery system.* Gastrointestinal Endoscopy, 2002. **56**(2): p. 190-194.

128. Tunnell, J.W., et al., *Epidermal protection with cryogen spray cooling during high fluence pulsed dye laser irradiation: An ex vivo study.* Lasers in Surgery and Medicine, 2000. **27**(4): p. 373-383.

129. van den Boogert, J., et al., *Endoscopic ablation therapy for Barrett's esophagus with high- grade dysplasia: A review.* American Journal of Gastroenterology, 1999. **94**(5): p. 1153-1160.

130. Vitkin, I.A., et al., *Magnetic resonance imaging of temperature changes during interstitial microwave heating: A phantom study.* Medical Physics, 1997. **24**(2): p. 269-277.

131. Vogel, A., S. Busch, and U. Parlitz, *Shock wave emission and cavitation bubble generation by picosecond and nanosecond optical breakdown in water.* Journal of the Acoustical Society of America, 1996. **100**(1): p. 148-165.

132. Walsh, J.T., et al., *Pulsed Co2-Laser Tissue Ablation - Effect of Tissue-Type and Pulse Duration on Thermal-Damage.* Lasers in Surgery and Medicine, 1988. **8**(2): p. 108-118.

133. Wesleysmith, J., et al., *Cryopreservation of Desiccation-Sensitive Axes of Camellia- Sinensis in Relation to Dehydration, Freezing Rate and the Thermal-Properties of Tissue Water.* Journal of Plant Physiology, 1992. **140**(5): p. 596-604.

134. Zuccaro, G., et al., *Optical coherence tomography of the esophagus and proximal stomach in health and disease.* American Journal of Gastroenterology, 2001. **96**(9): p. 2633-2639.

Note: references # 94-134 have backgrounded this study though are not cited specifically throughout its sections [94-134].

Appendix A

Samples of Labview panels (user interfaces) and diagrams (codes)
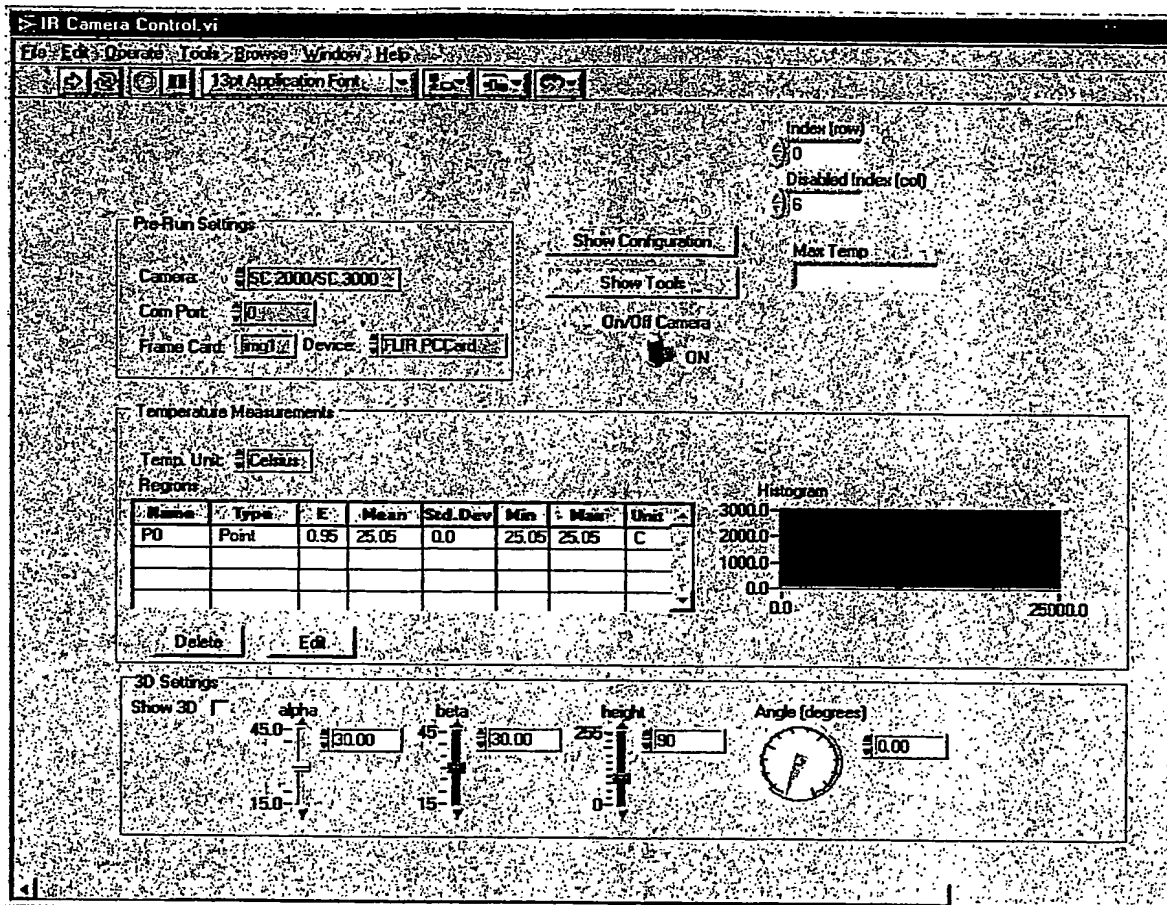
IR camera control panel
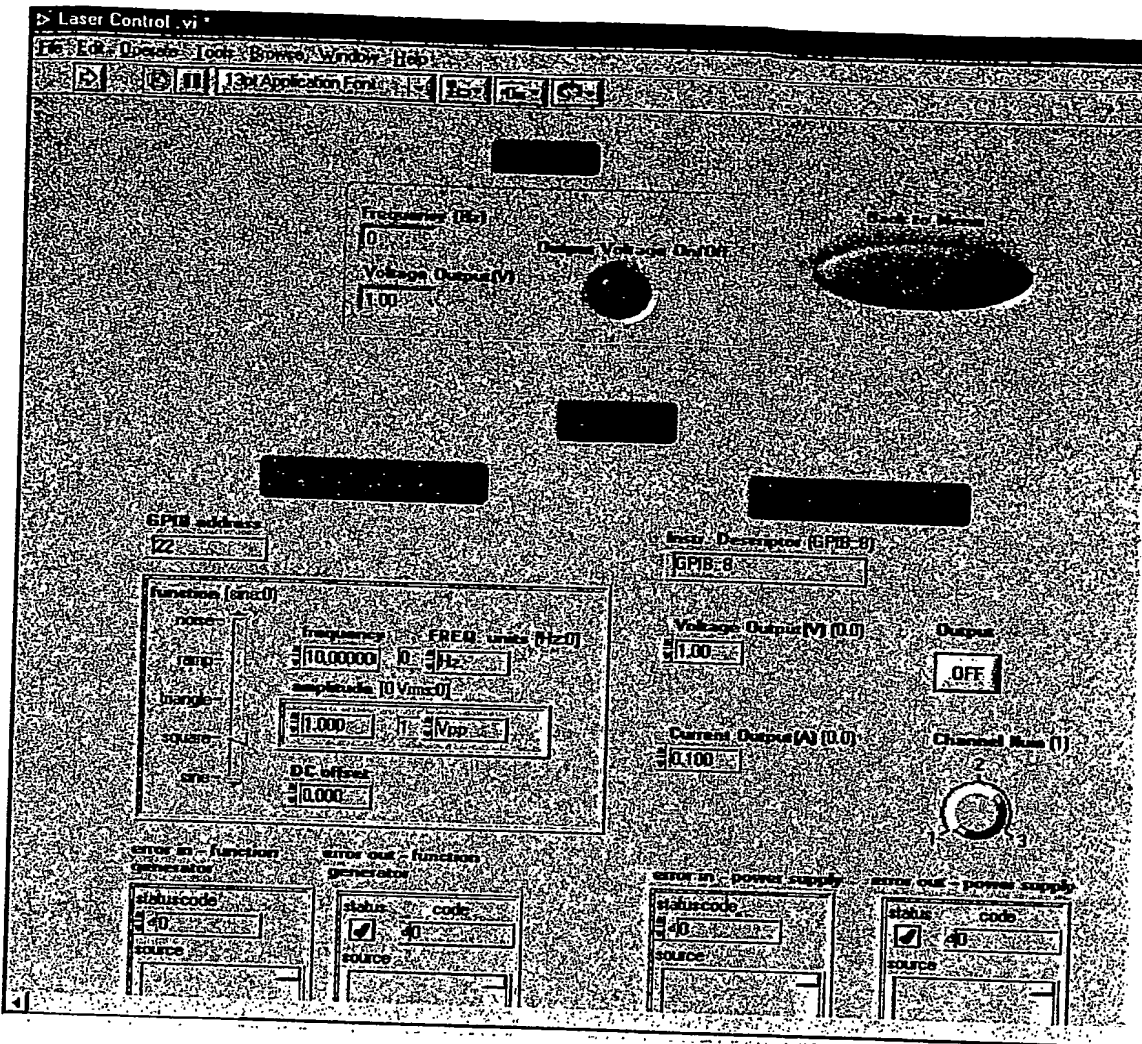
Laser power and pulse control panel (GPIB application)
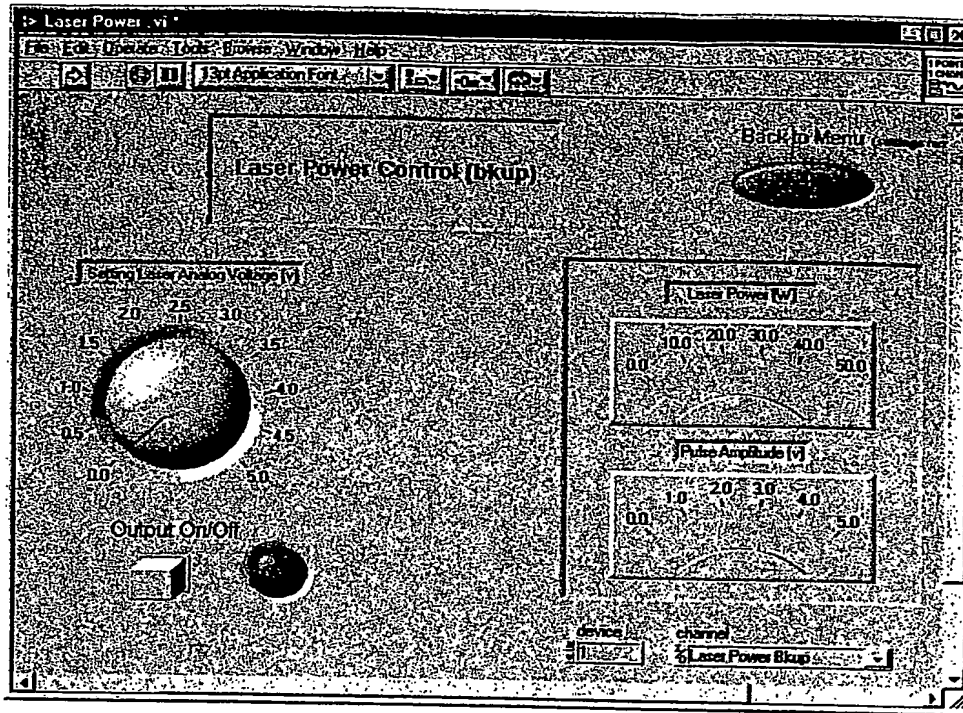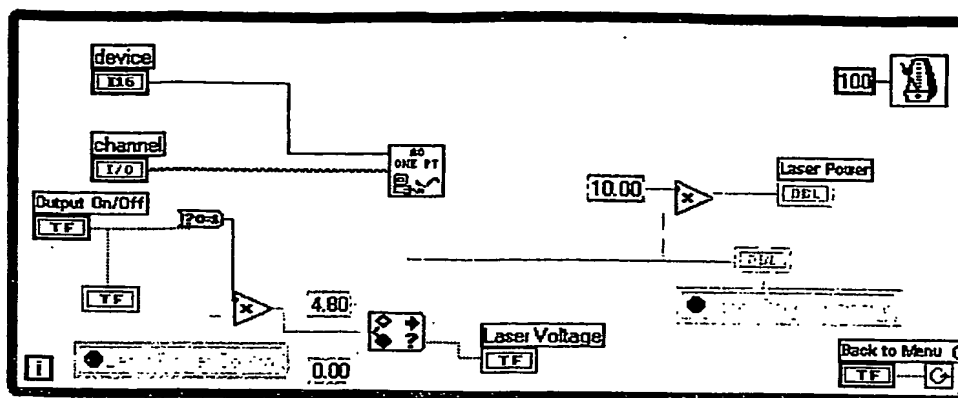
Laser power control panel (DAQ application)
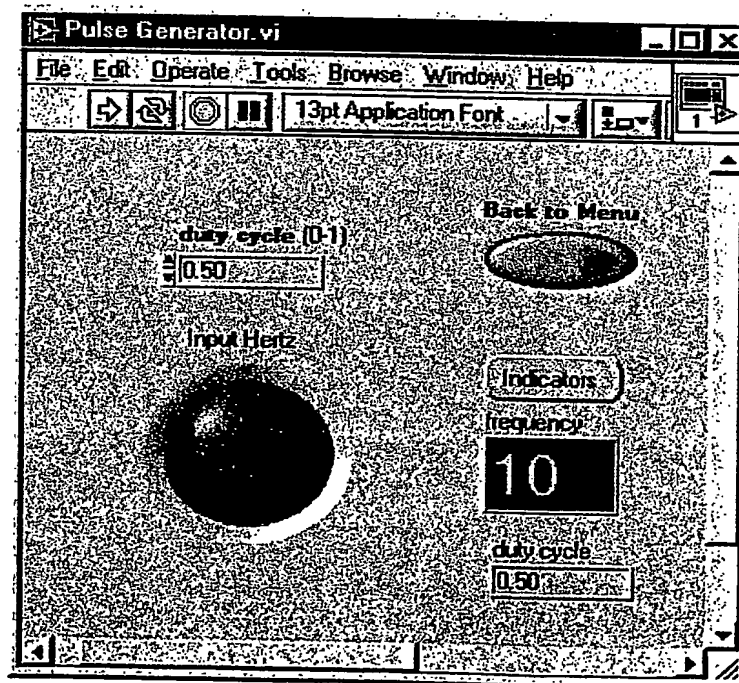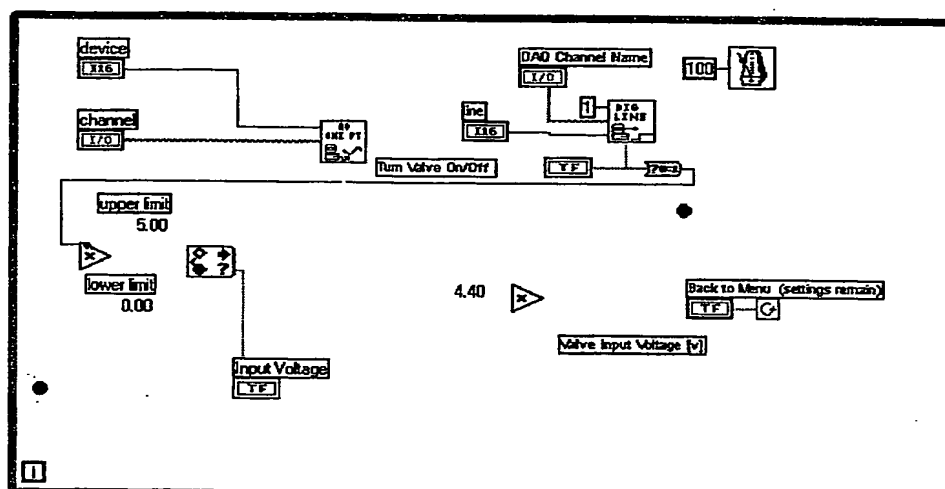
Laser pulse control panel (DAQ application)
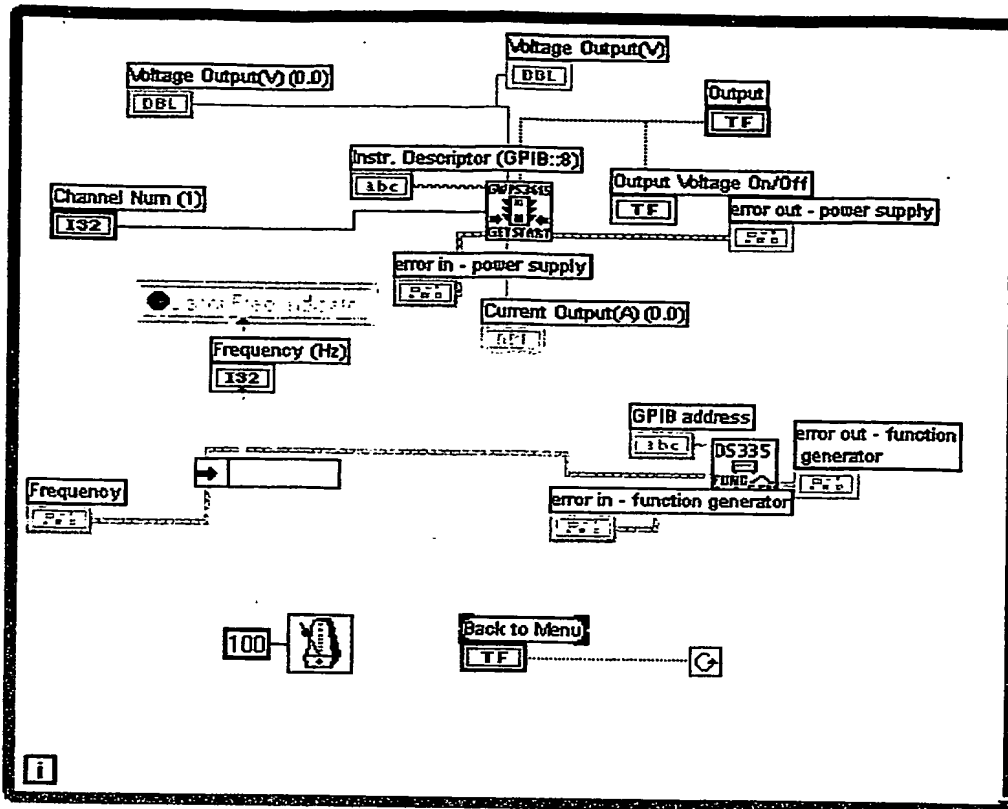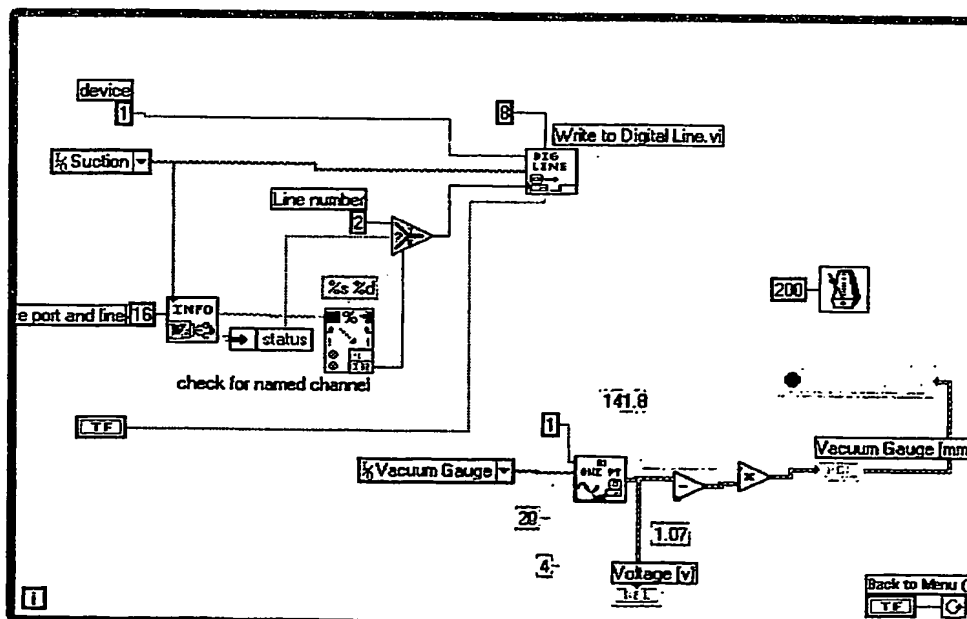
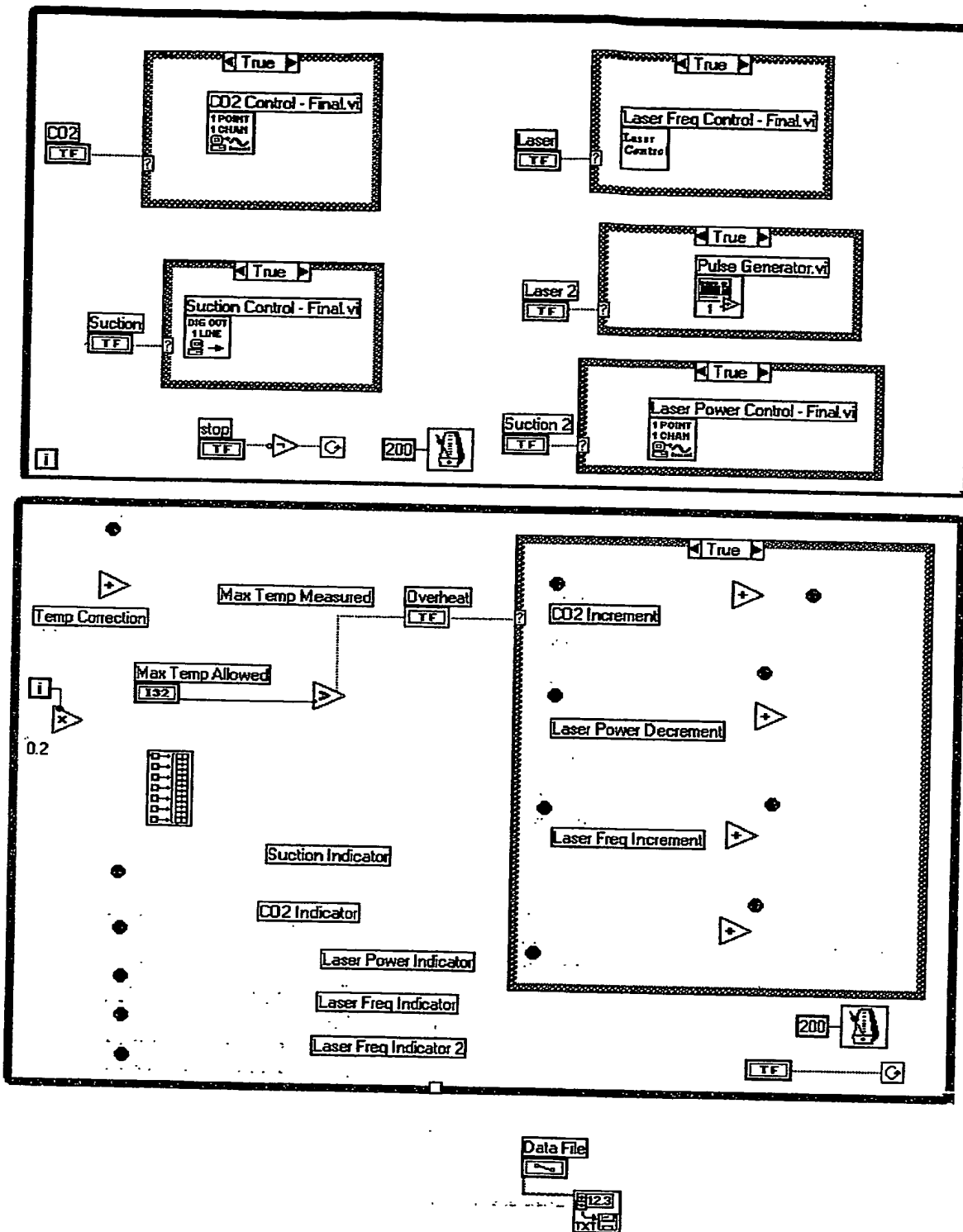Laser power and pulse diagram (GPIB)
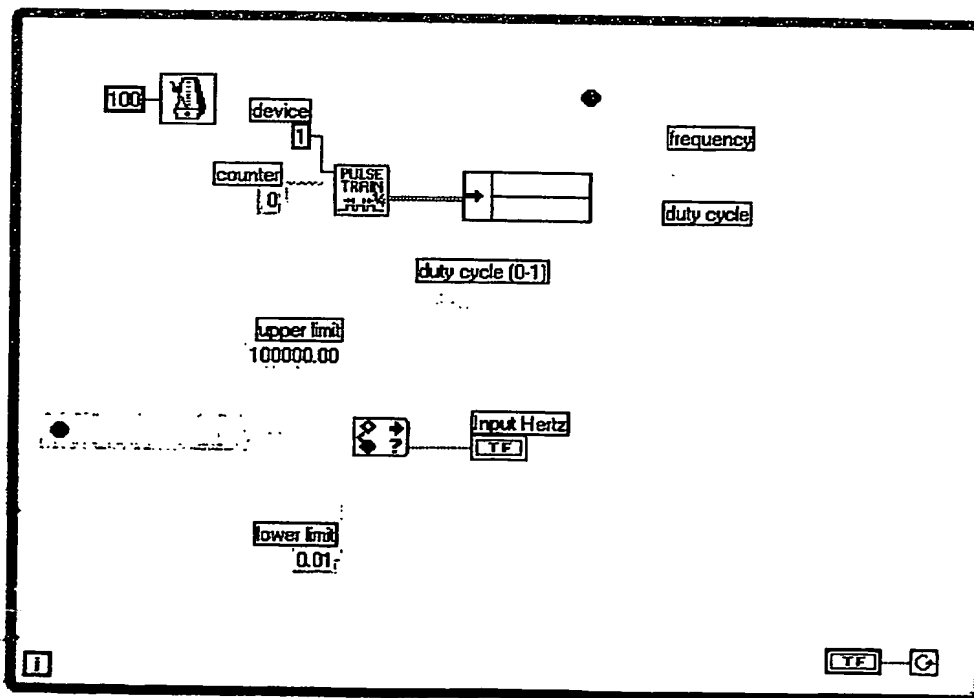
Laser pulse diagram (DAQ)

Laser power diagram (DAQ)

CO_2 insufflation diagram
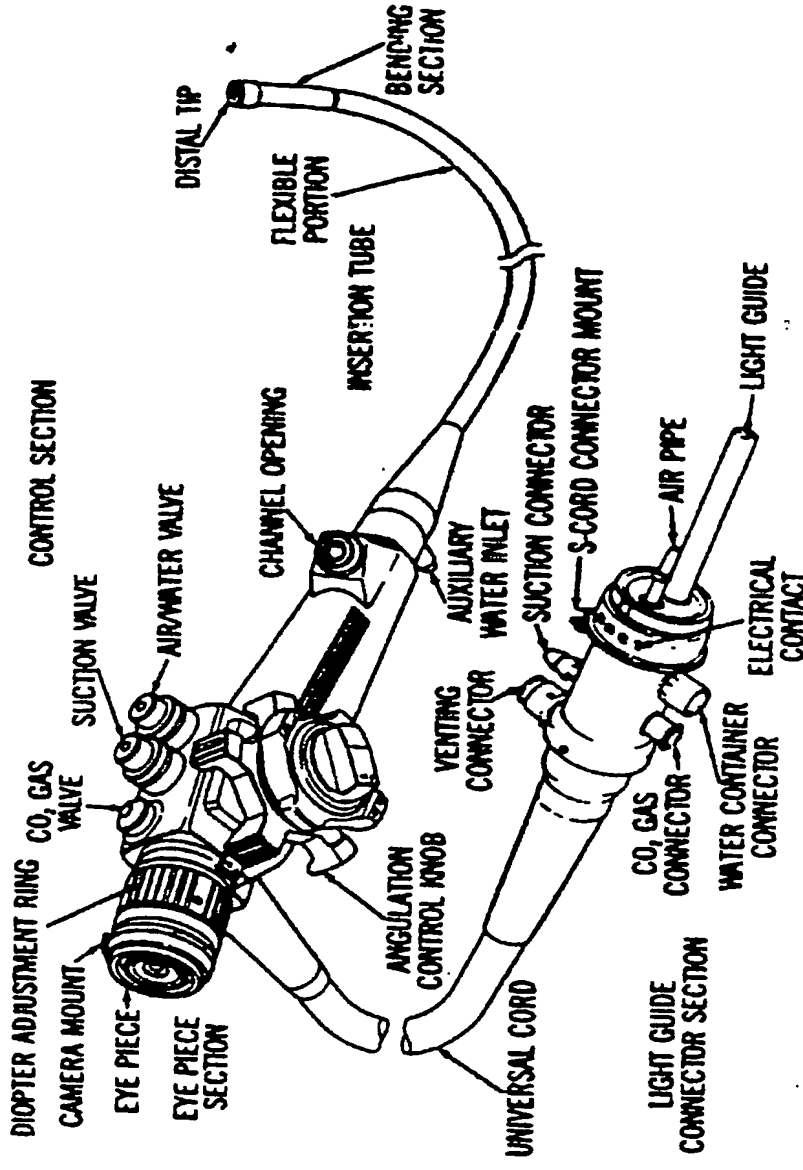

Suction diagram

Main control diagram

Main control panel is exhibited in sec. 3.2.2 (fig. 3-23).

123

Claims:

1.   Laser power injection system for enclosed cavity substantially as hereinbefore described with reference to the accompanying drawings.

2.   Laser power injection system for minimally invasive surgery, substantially as hereinbefore described with reference to the accompanying drawings.

3.   Laser power injection method for enclosed cavity substantially as hereinbefore described with reference to the accompanying drawings.

4.   Laser power injection method for minimally invasive surgery, substantially as hereinbefore described with reference to the accompanying drawings.

5.   Simulation system for effects of laser power in enclosed body cavity, substantially as hereinbefore described with reference to the accompanying drawings.

6.   Simulation method for effects of laser power in enclosed body cavity, substantially as hereinbefore described with reference to the accompanying drawings.

DR. GAL EHRLICH
28 BEZALEL STREET
52521 RAMAT GAN

Minimally Invasive Surgery (MIS)

Modern Gastroscope

Labels: CONTROL SECTION, AIR/WATER VALVE, SUCTION VALVE, CO₂ GAS VALVE, DIOPTER ADJUSTMENT RING, CAMERA MOUNT, EYE PIECE, EYE PIECE SECTION, CHANNEL OPENING, ANGULATION CONTROL KNOB, BENDING SECTION, DISTAL TIP, FLEXIBLE PORTION, INSERTION TUBE, AUXILIARY WATER INLET, VENTING CONNECTOR, SUCTION CONNECTOR, S-CORD CONNECTOR MOUNT, LIGHT GUIDE, AIR PIPE, ELECTRICAL CONTACT, WATER CONTAINER CONNECTOR, CO₂ GAS CONNECTOR, LIGHT GUIDE CONNECTOR SECTION, UNIVERSAL CORD

Source: Katzir, A., Lasers and Optical Fibers in Medicine. 1993, London: Academic Press

Gastroscopy, 1881

Source: Surgical Endoscopy- Ultrasound and Interventional Techniques, 2000

5

Practical Gastroscope
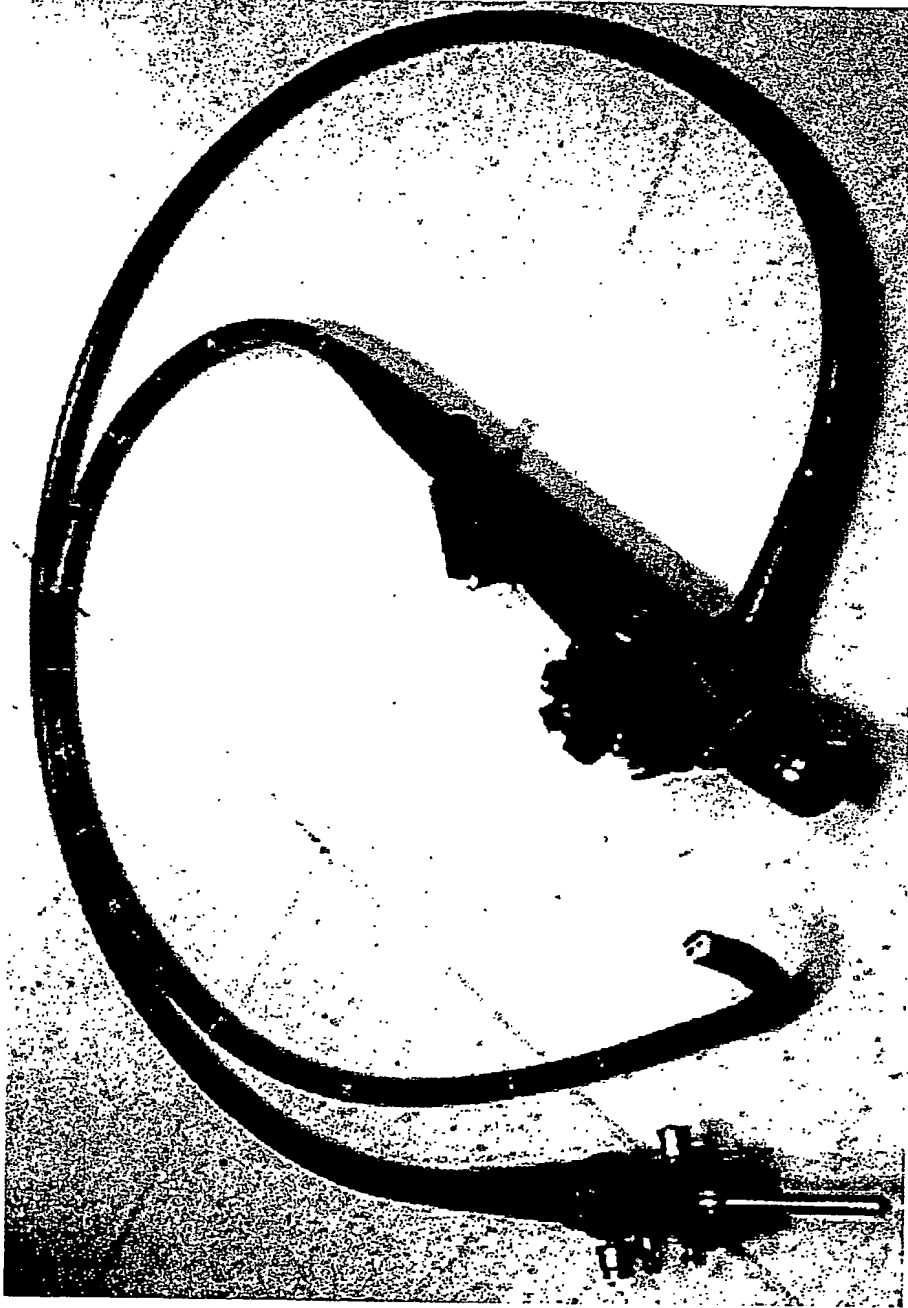
Surgical Procedures Performed by a Minimally Invasive Approach, 1999

Procedure	No. of Proc.	% MIS
General Surgery	2,882,308	47
Gynecology	1,157,036	37
Urology	248,007	55
Thoracic Surgery (Lung)	160,000	60
Cardiothoracic Surgery	436,000	17

5

The Clinical Need

Ablating neoplastic superficial tissues within body cavities

Cases along the digestive tract:

- Barrett Esophagus
- Mucosal gastric cancer

Accessing the stomach endoscopically

Stomach Anatomy

Fundus

Body

Serosa

Longitudinal muscle layer

Circular muscle layer

Oblique muscle layer

Mucosa

Submucosa

Esophagus

Gastroesophageal opening

Lower esophageal sphincter

Pylorus

Lesser curvature

Greater curvature

Pyloric sphincter

Rugae

Duodenal bulb

Duodenum
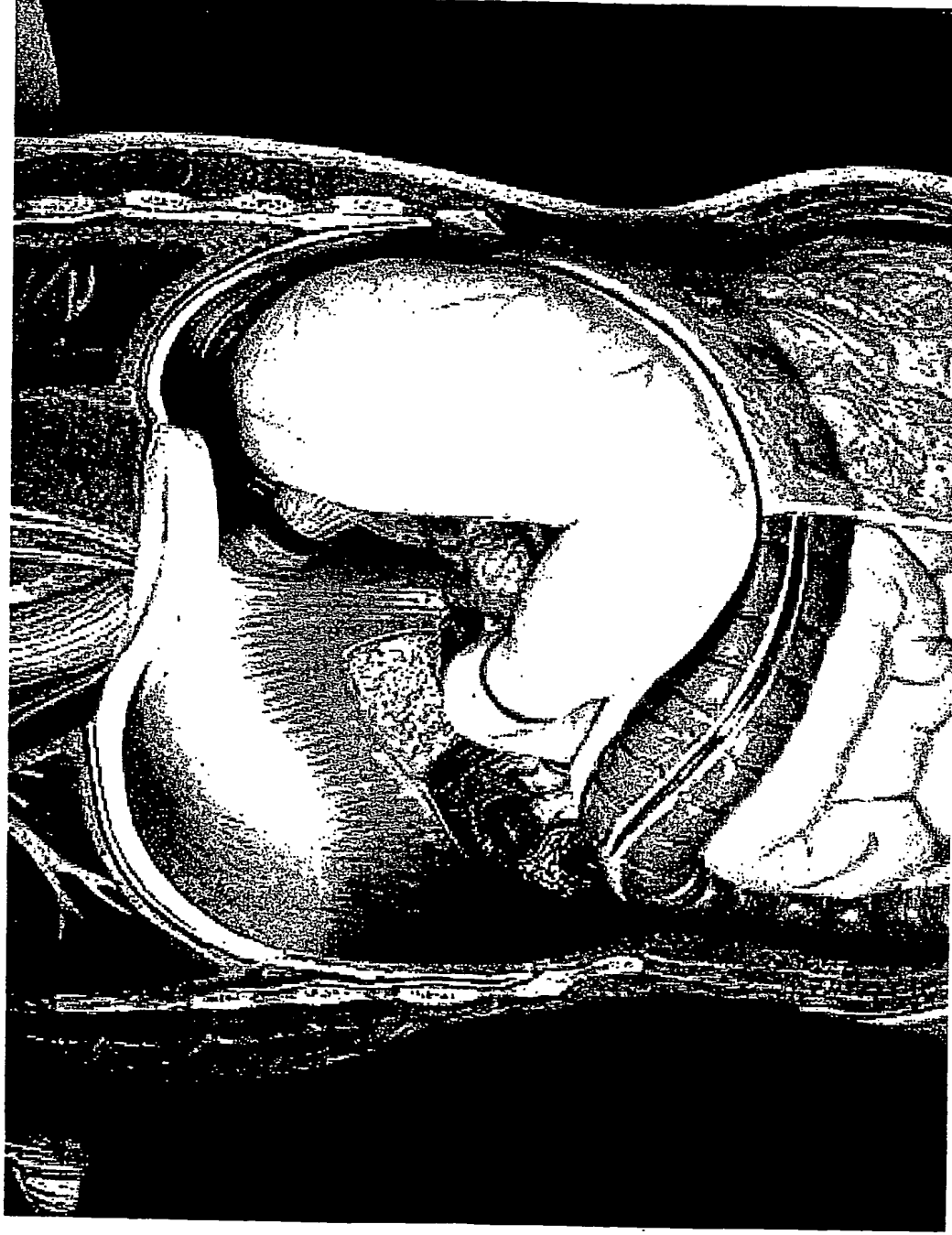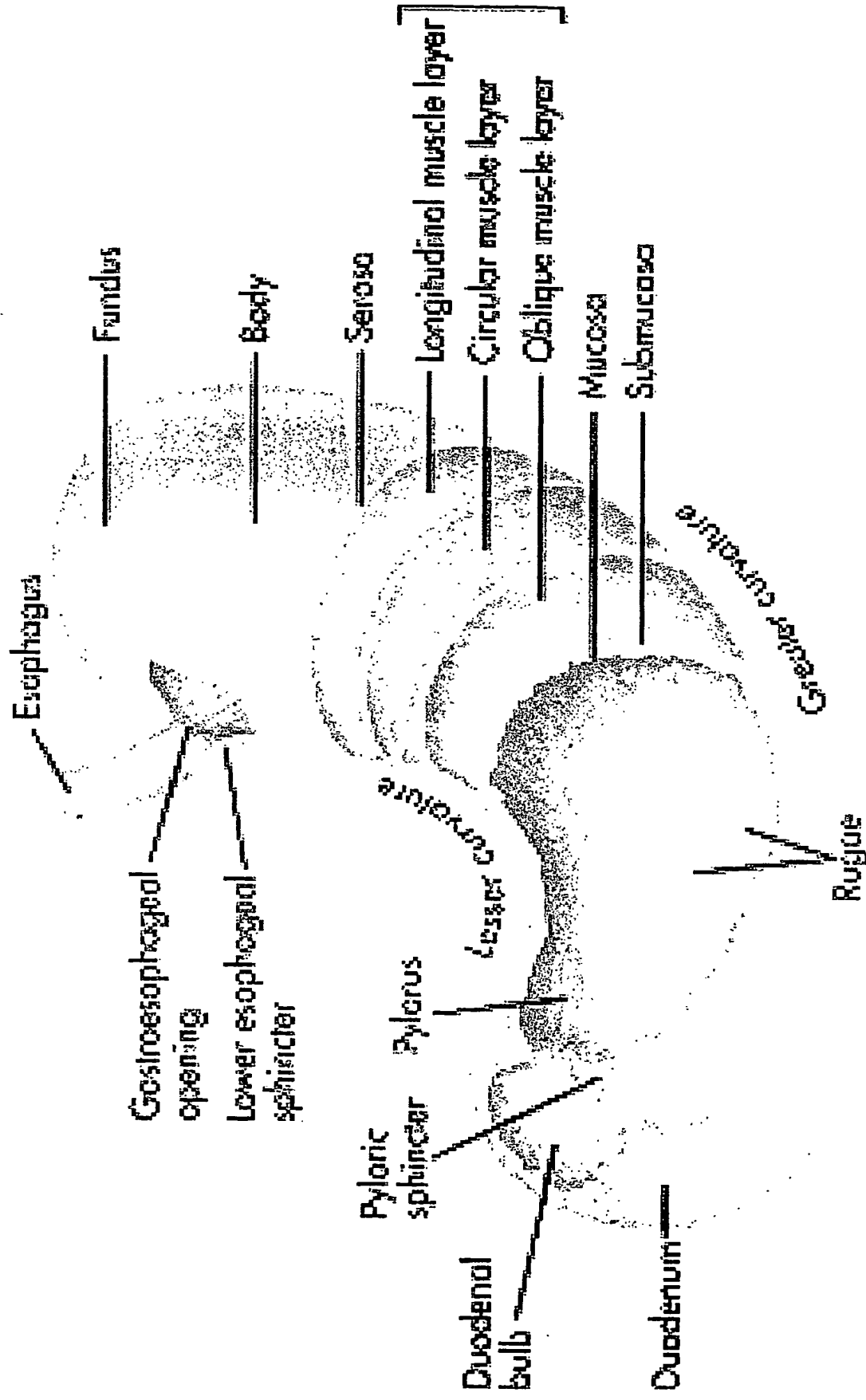
Source: Thibodeau, G.A. and K.T. Patton, Anatomy & Physiology. 4th ed. 1999

6

Absorption coefficient and penetration depth vs. IR wavelength in water

Wieliczka, Weng & Querry
(Appl. Opt. 28, 1714–1719, 1989)
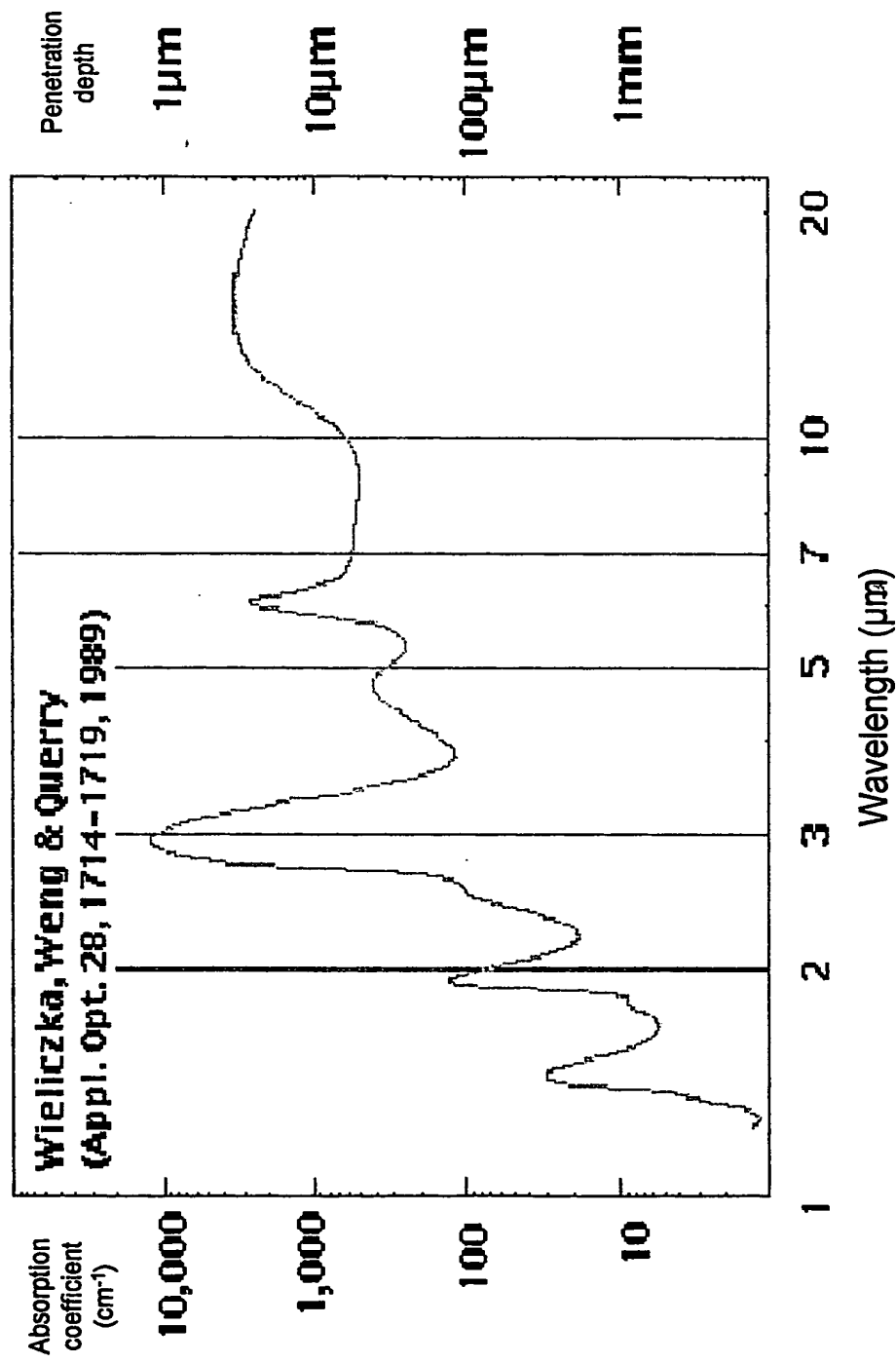
The Technological Drive:

Flexible Waveguides for the MID-IR

Metal layer
Air core
Dielectric layer
Hollow tube
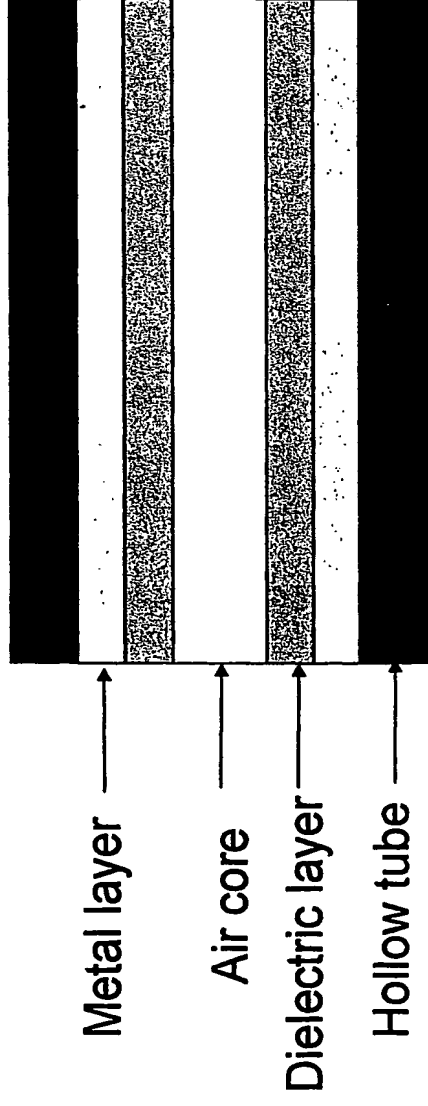
Source: Gannot, I. and M. Ben-David,
Biomedical Photonics handbook,
T.B.P. in 2003

8
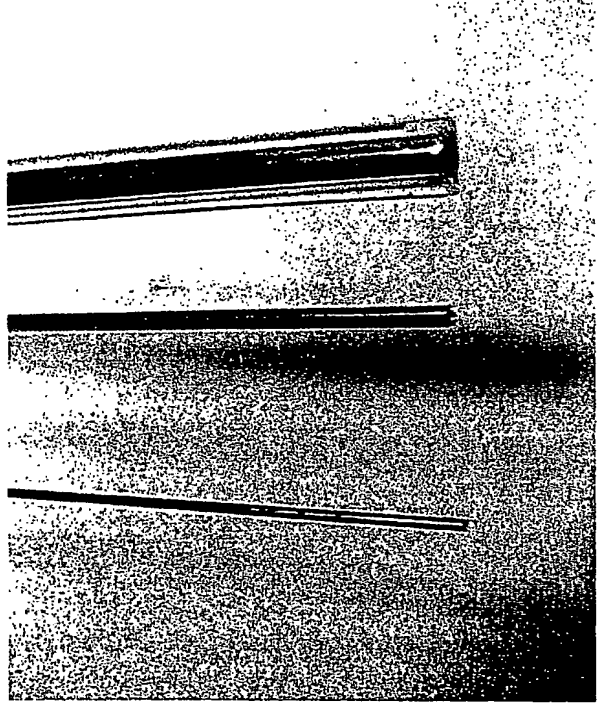
The problem of Thermal Side Effects
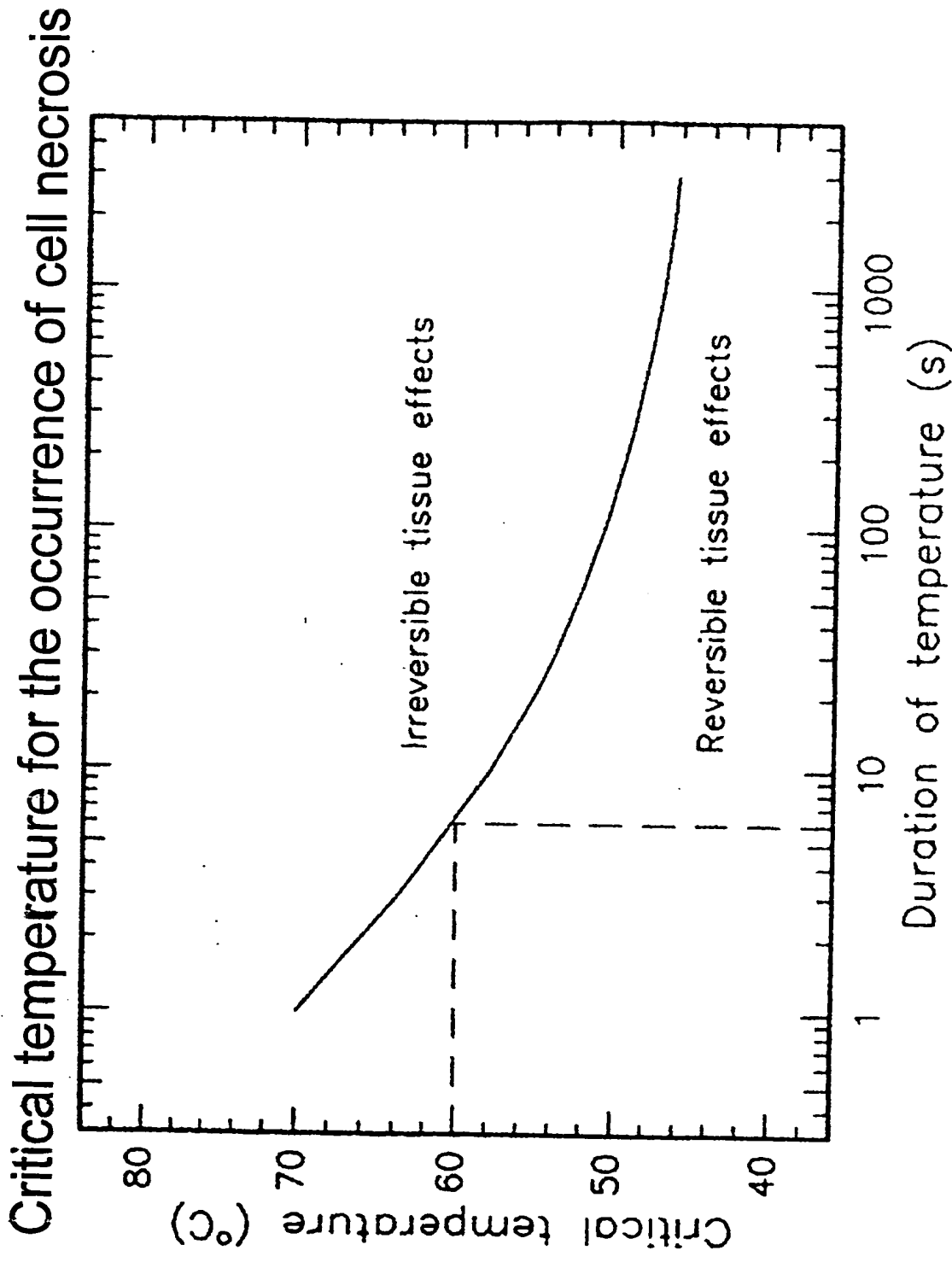
Critical temperature for the occurrence of cell necrosis

Thermography Basics

The electromagnetic spectrum

Source: FLIR Systems AB, 2001

Thermal Imaging utilizes array of IR detectors

10

Thermography Basics (cont.)

Stefan-Boltzmann law

$$W = \varepsilon \sigma T^4 \ (\text{Watt/m}^2)$$

W - spectral radiant emittance

σ - Stefan-Boltzmann constant

$(5.7 \times 10^{-8} \text{ Watt/m}^2)$

$\varepsilon_\lambda = W_{\lambda o} / W_{\lambda b}$

Planckian curves

SPECTRAL RADIANT EMITTANCE (Watts/cm² (µm))

WAVELENGTH (µm)

1000 K 900 800 700 600 500 400 300 200 100

Study Goals

- Experimental investigation of the thermal side effects in a closed body cavity, during endoscopical, CO_2 laser-based surgery
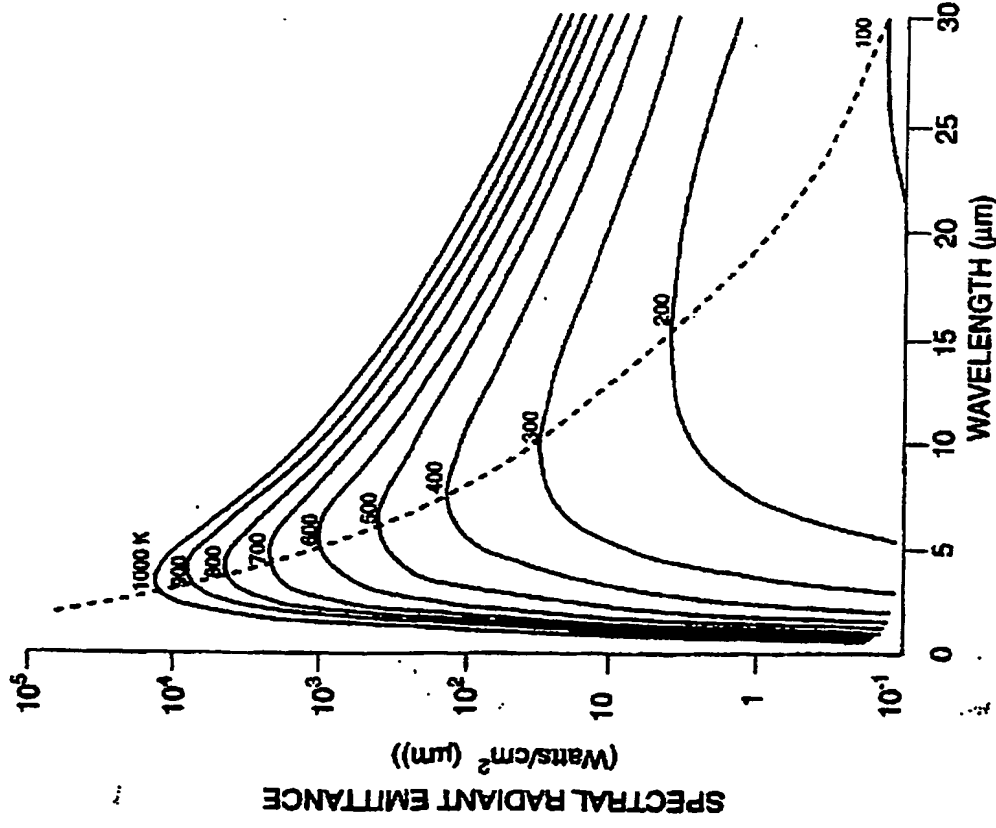
- Optimizing the procedure, thermally, via a software-controlled setup that simulates practical conditions

1. Experimental investigation of the thermal side effects in a closed body cavity, during endoscopical, CO_2 laser-based surgery

2. Optimizing the procedure, thermally, via a software-controlled setup that simulates practical conditions

12

Preliminary investigation with Agarose phantoms
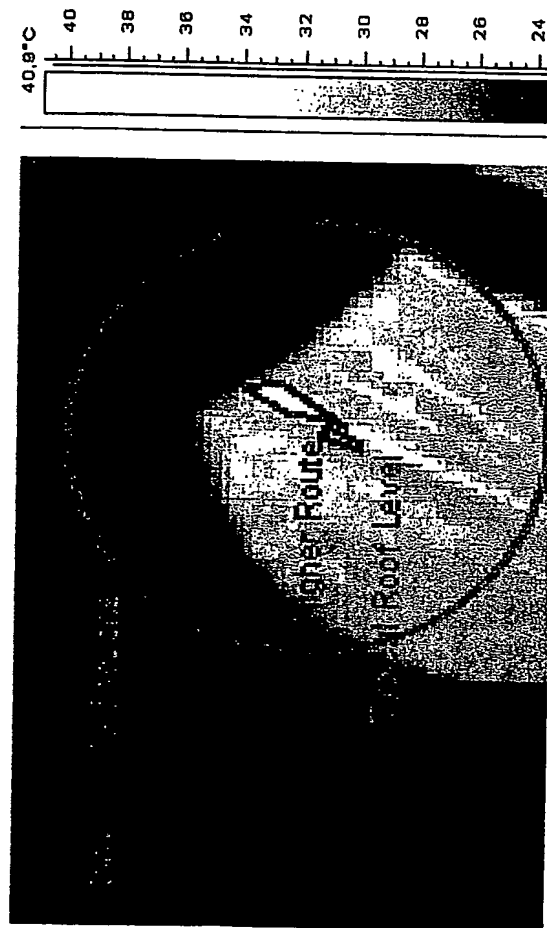
Cavity-like phantoms (porcine samples)
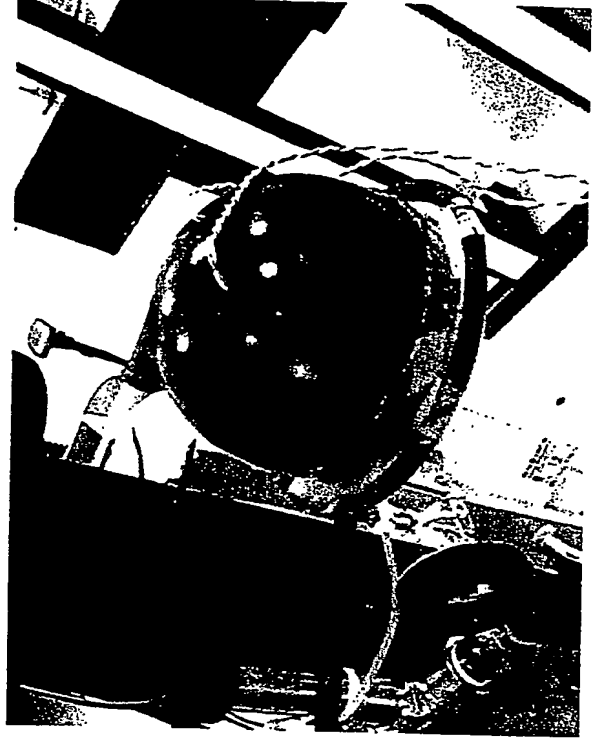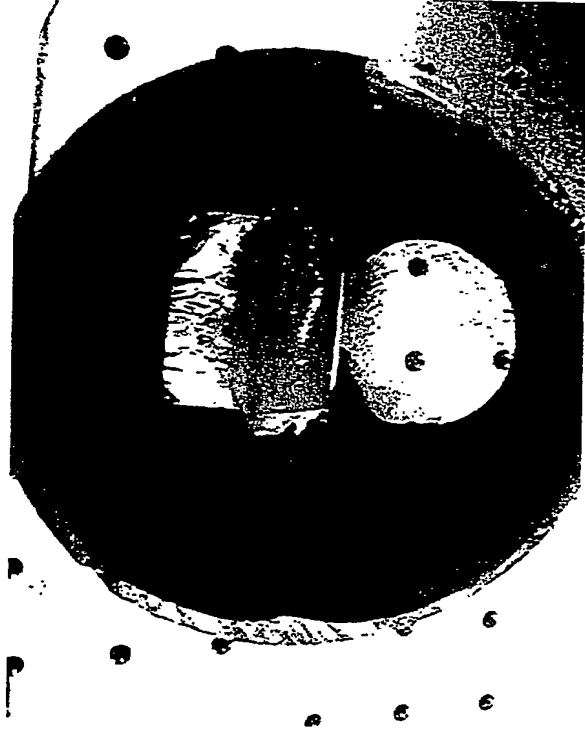
The jet effect
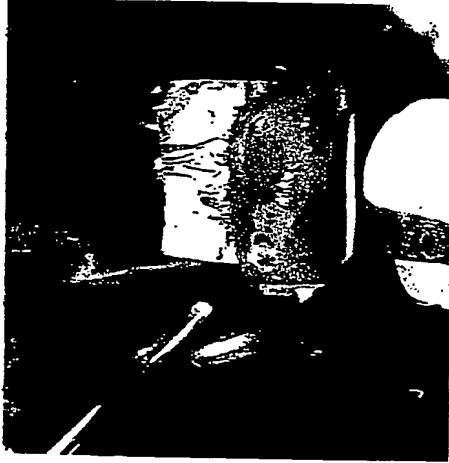
24w, jet

6w, plume

6w (300w/cm²),
plume

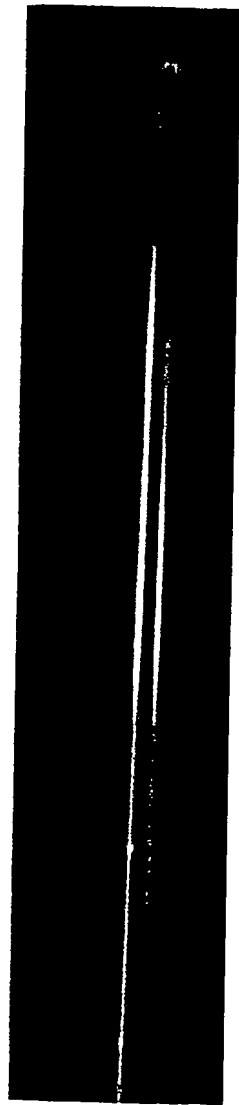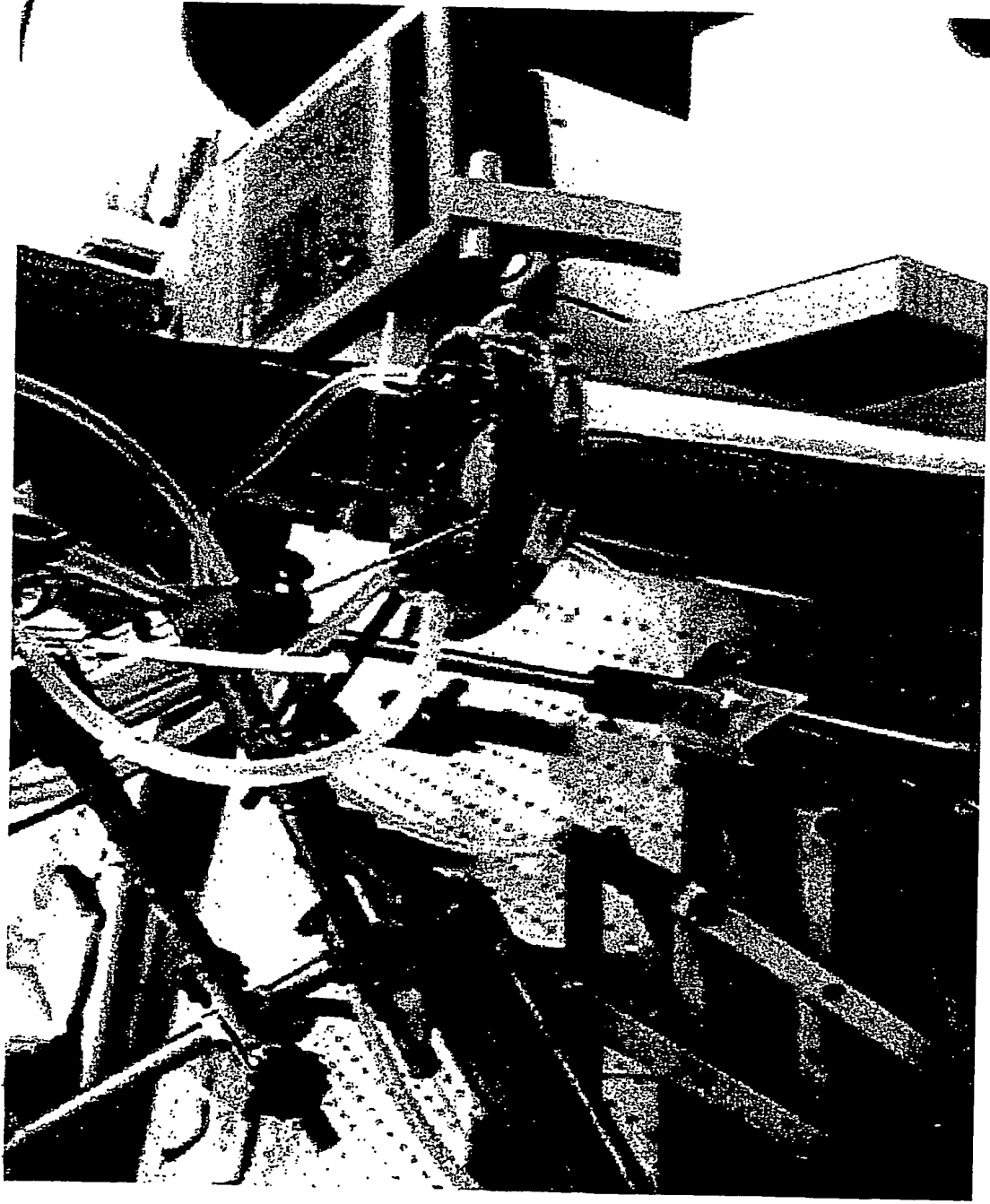# Visualization of smoke distribution within a closed space
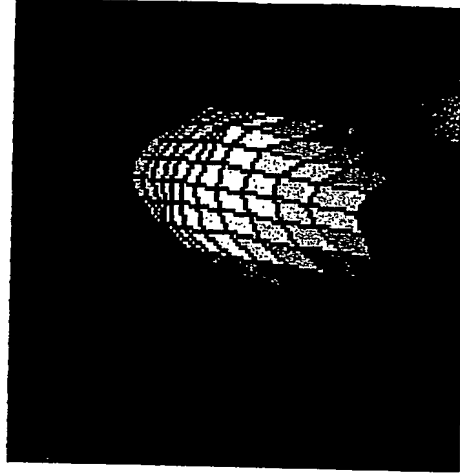
Setup - Phase I
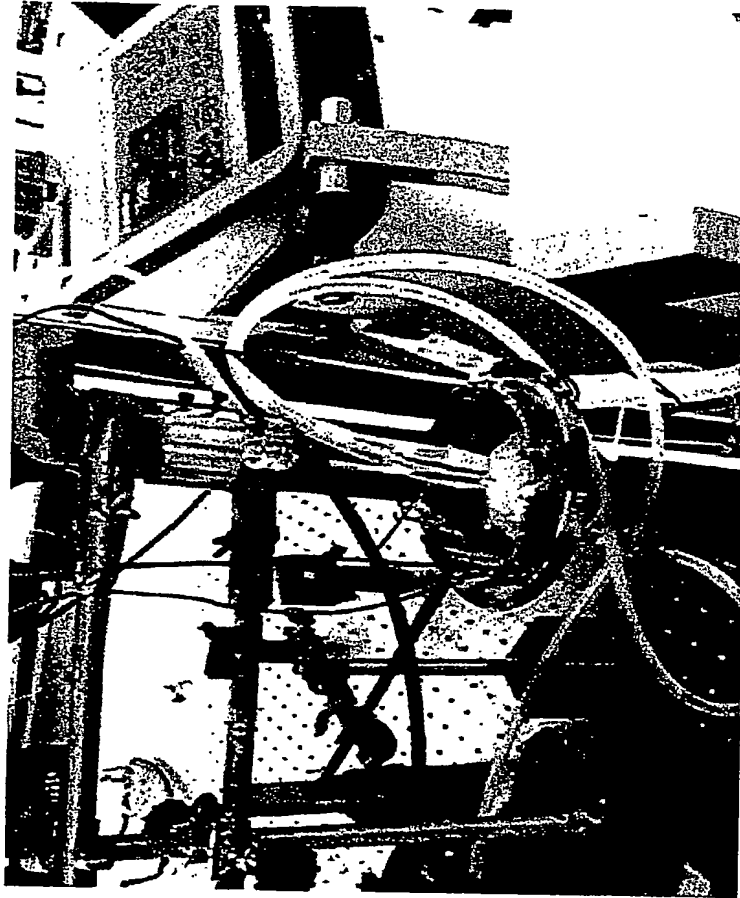
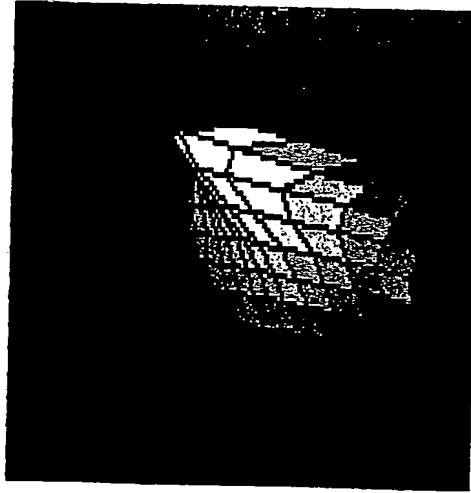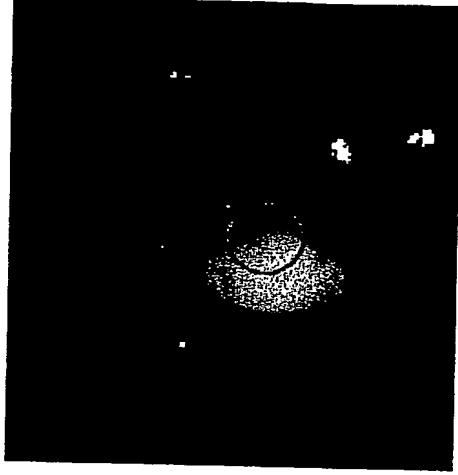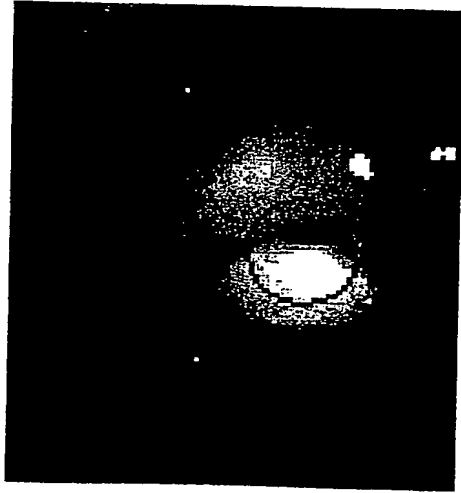Setup - Phase I (cont.)
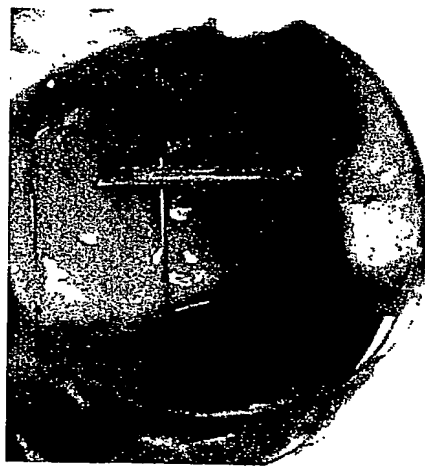
The problem of fiber heating
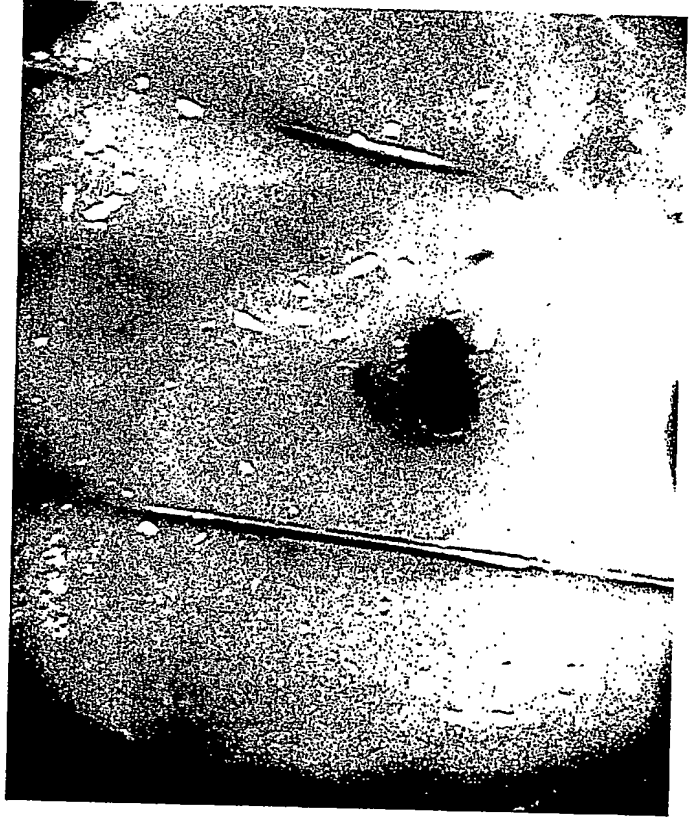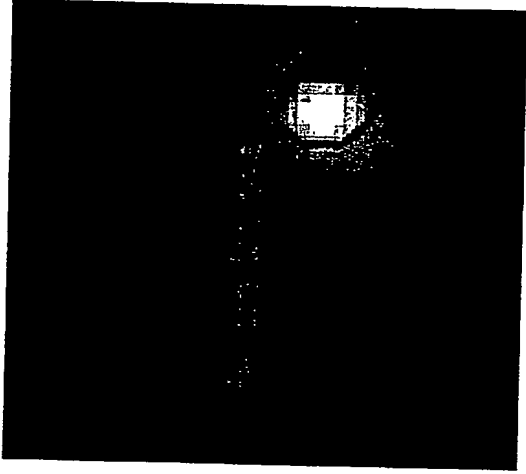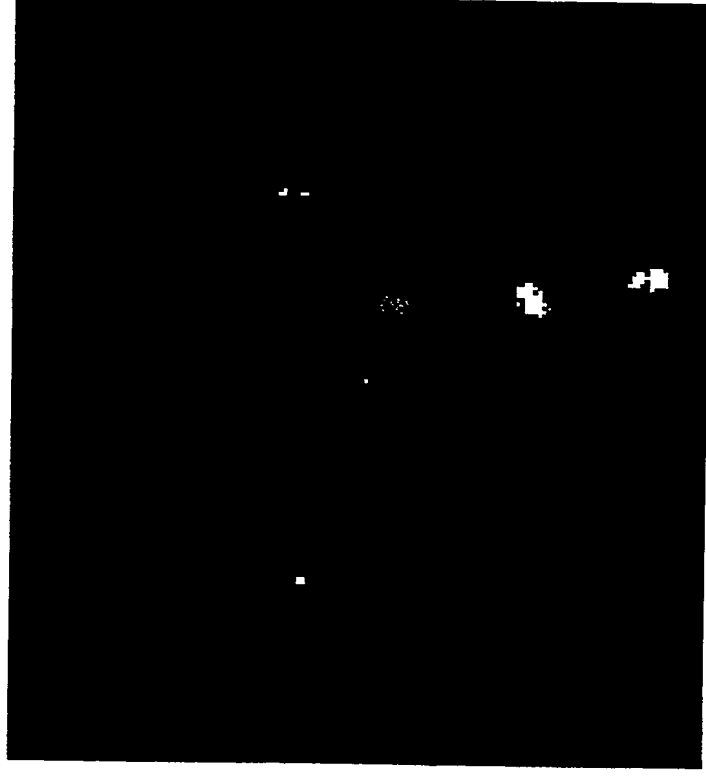
Fiber diffusivity
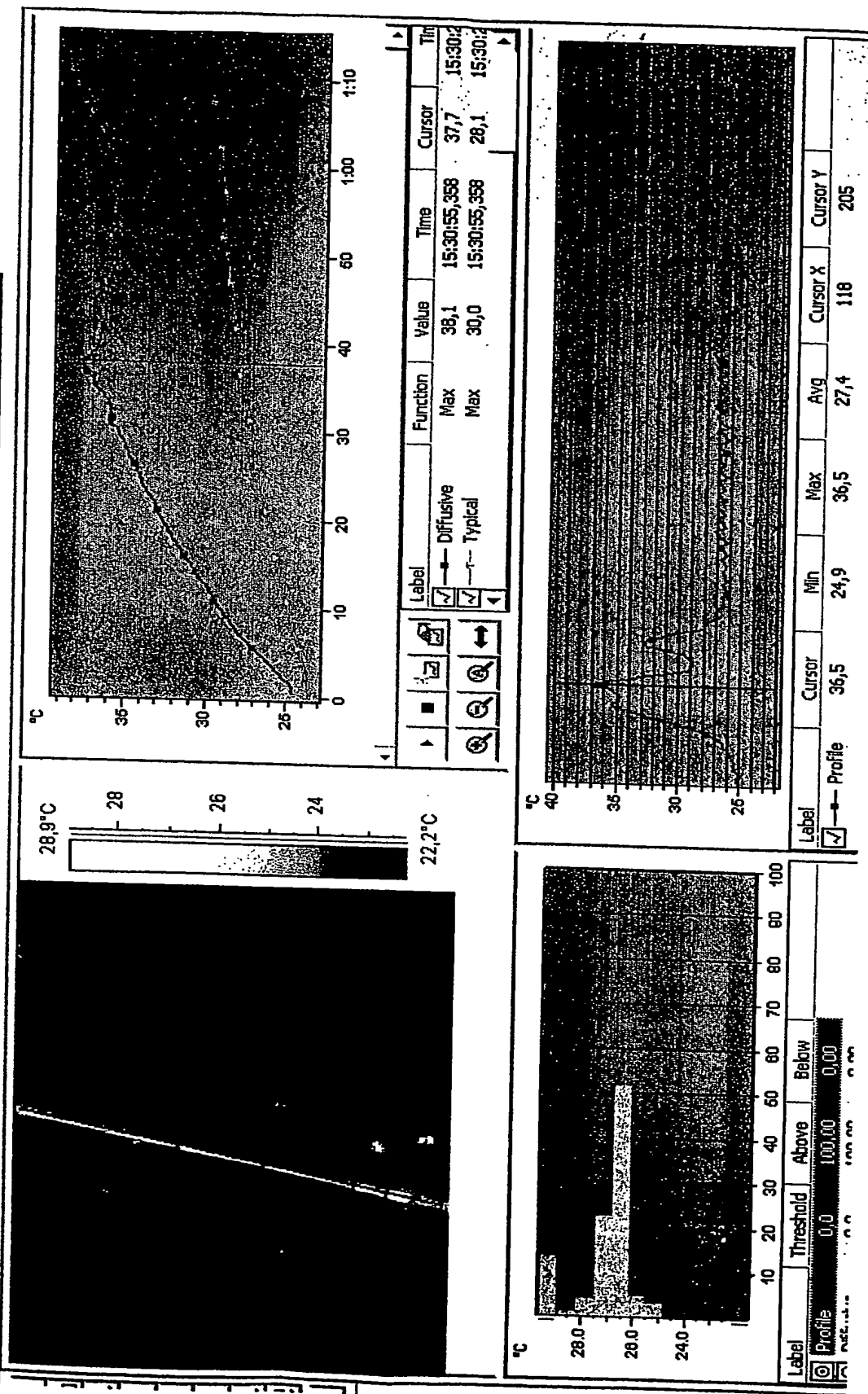
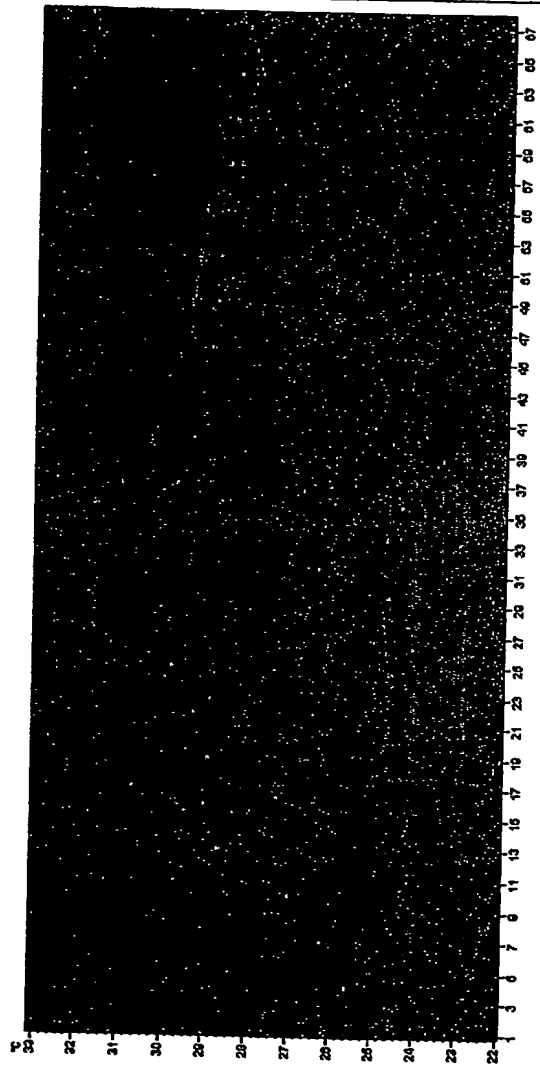# Setup - Phase II

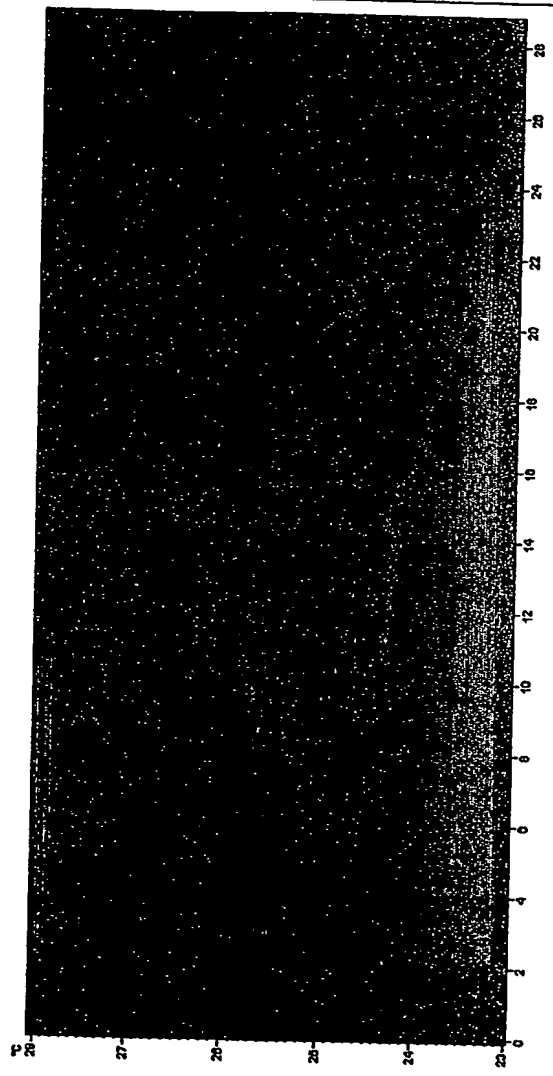# Airflow thermal effect

3lpm, 15w, CW

22

Thermal images of heat build-up along the surrounding tissue

Thermal analysis at varying conditions

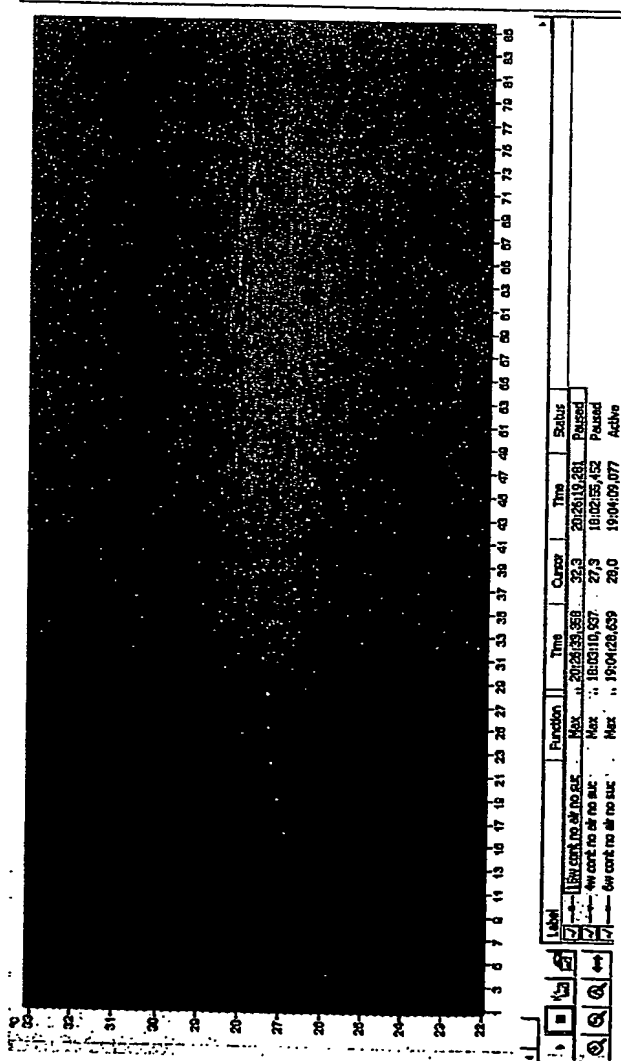Max. temperature: airflow (red), suction (gray), airflow & suction (blue), none (black); 15w, CW, 7sec
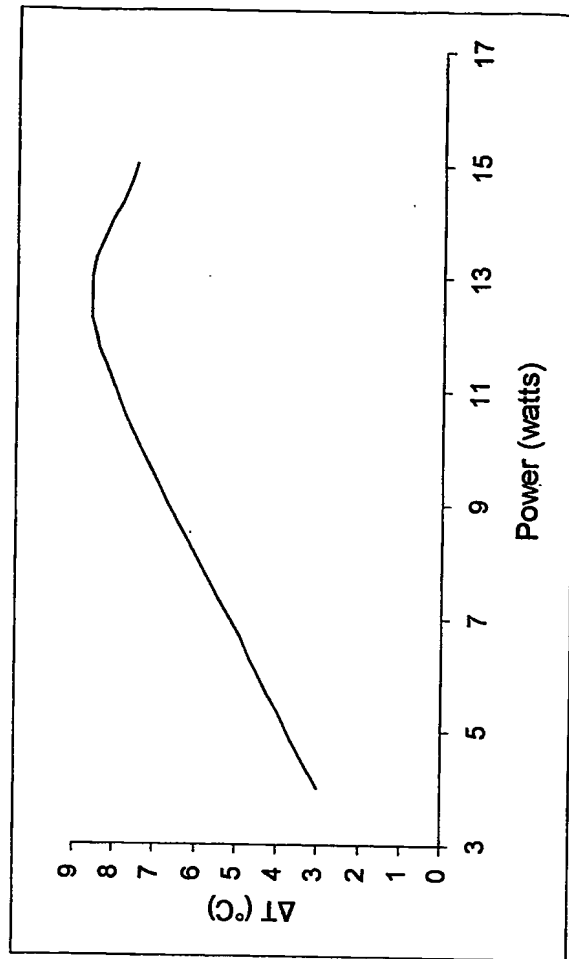

Instant suction effect

24

Thermal analysis (cont.)

Max. temperature:15w (black), 6w (blue), 4w (red); CW, 7sec

ΔT (°C) vs. Power (watts)

Predicted vs. Measured Results

Maximal temperature (C)

12w

Time (seconds)
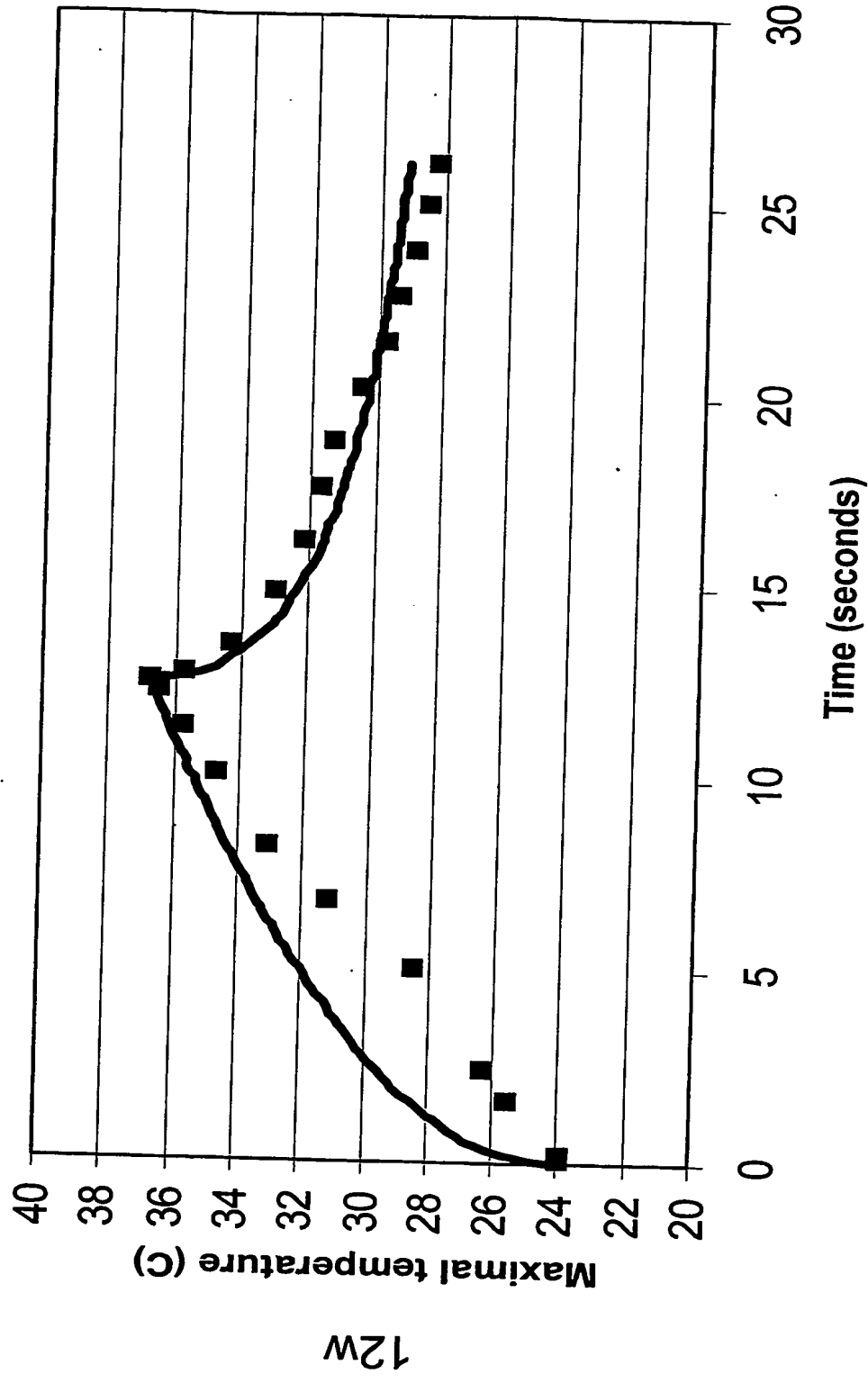
The theoretical part was carried out with Dr. Avi Dayan

The software-controlled setup scheme

ThermaCAM Researcher

Temp. mapping

IR Camera

Temp. analysis

DAQ DO
(On/Off)

Surgical
Suction

Labview
application

Cavity-like
Phantom

DAQ AO

Vacuum
Control
& Meter

DAQ AO
& DO

Pressure &
Flow Meters

Gastroscope

Valve
Controller

GPIB interface

GPIB interface

Proportional
Valve

Hollow
waveguide

CO2
Cylinder

Function
Generator

Optic
Coupler

Power
Supplier

Pulse freq. rate (Laser DI)

Pulse voltage rate (Laser AI)

CO2 Laser

Control line

Feedback line

DO - Digital Output; AI - Analog Input

2B

Main Control Panel
(User Interface)
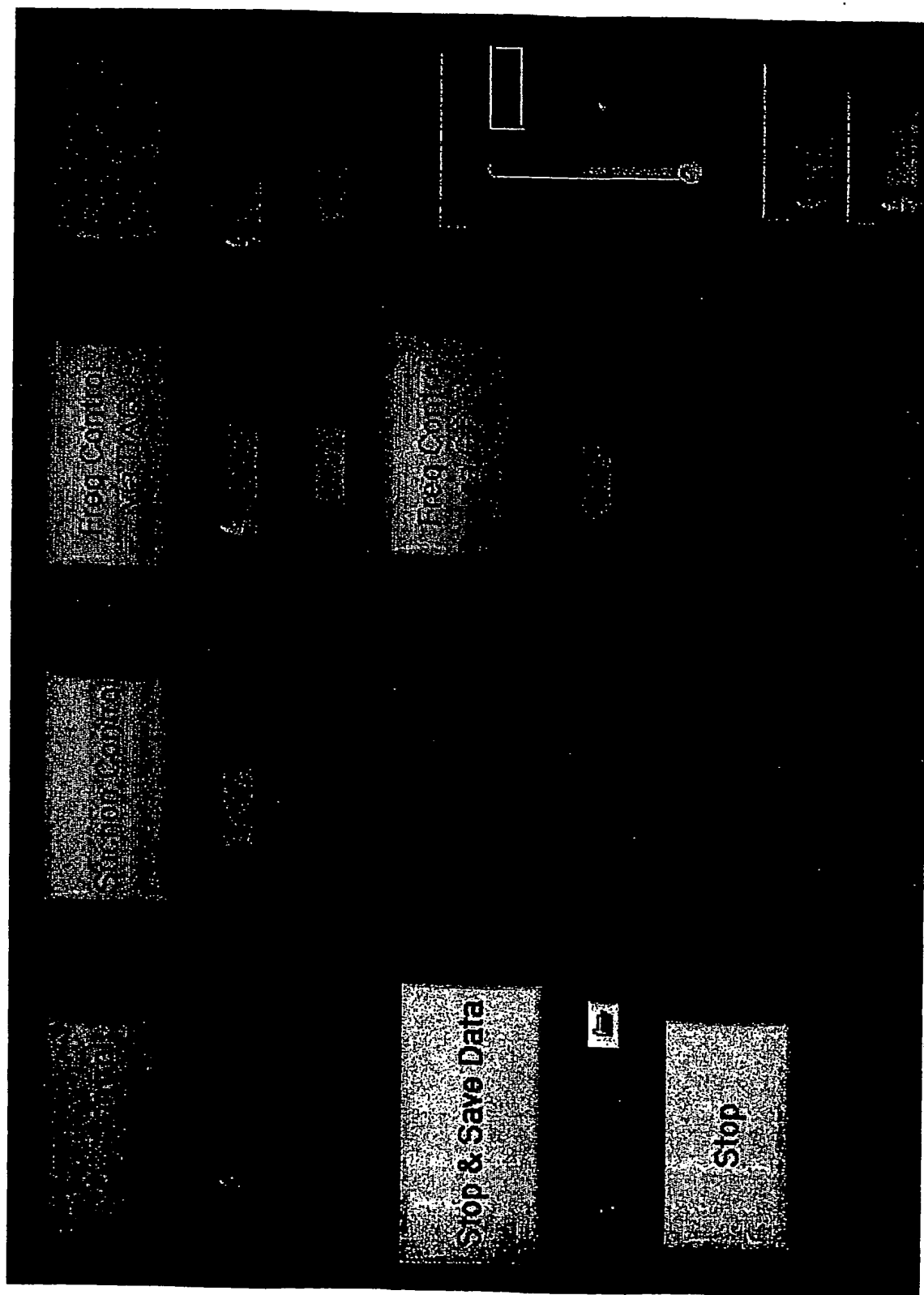
Laser & IR Camera Control Panels

Controlling thermal gradient via CO$_2$ auto-regulation
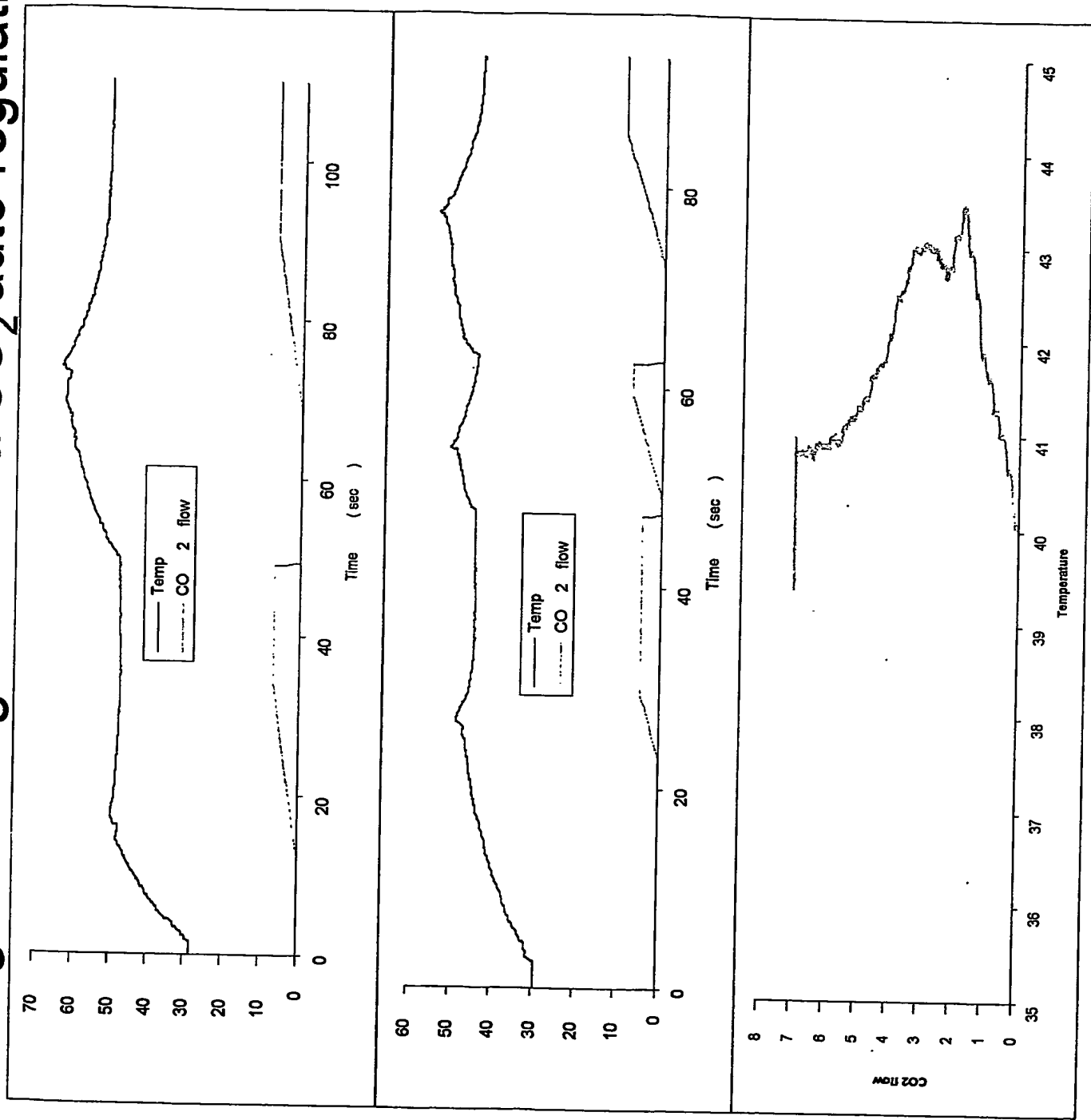
Relative Contribution of the Controllable Parameters on the Max. Temperature of the surrounding Tissue

surface

radius

angle

distance

insufflation

vacuum

airflow

pulse rate

duty cycle

period

power

32
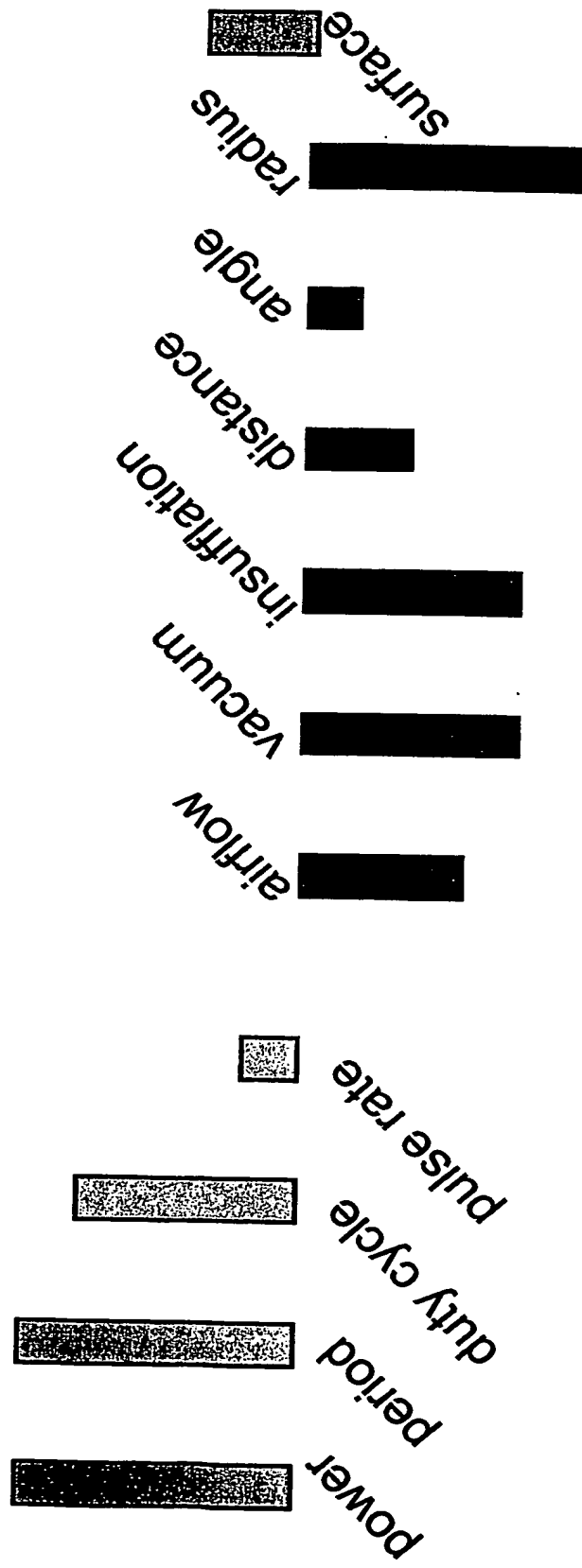
Findings

1. Modes of heat distribution within biological cavity (jet)

2. Hotspots along the surrounding tissue

3. The heating problem of hollow fiberoptic and ways to overcome it

Findings (cont.)

- 4. The relative contribution of user-controlled parameters to the thermal side effect

- 5. Mismanagement of a manual control of the multivariable procedure

Summary

- Experimental proof of the analytical model

- Discovery of fiberoptics capabilities & limitations

- Demonstration of a multi-parameter, closed-loop control system, by which MIS can be thermally optimized

Subsequent Research

Obtaining thermal feedback via IR imaging fiber bundle

Appling the laser energy transendoscopically via flexible fibers

Animal study

Preliminary trials with the IR Bundle
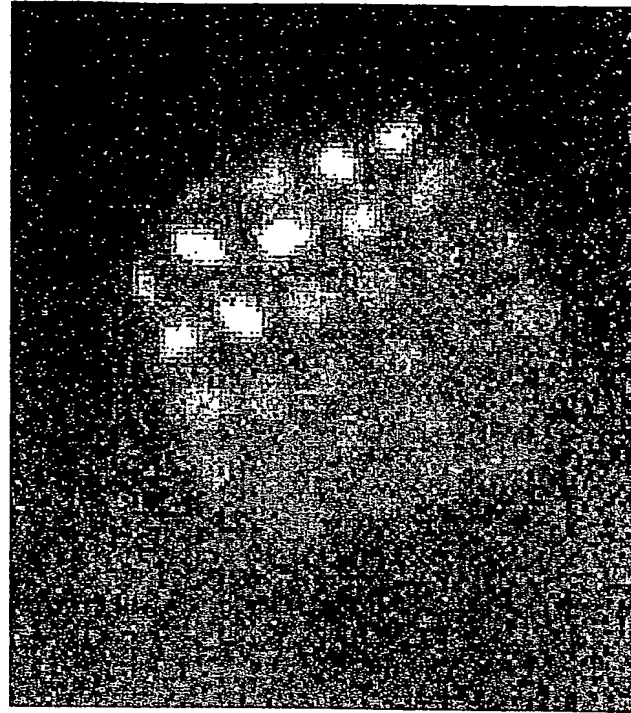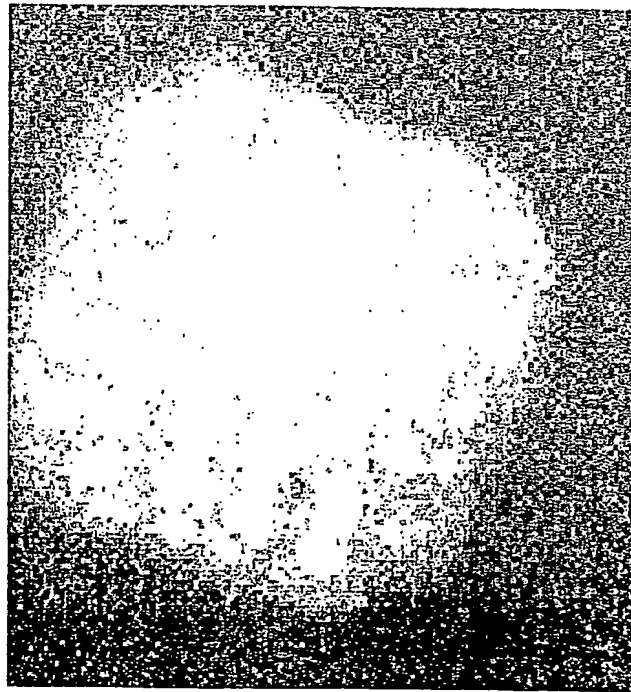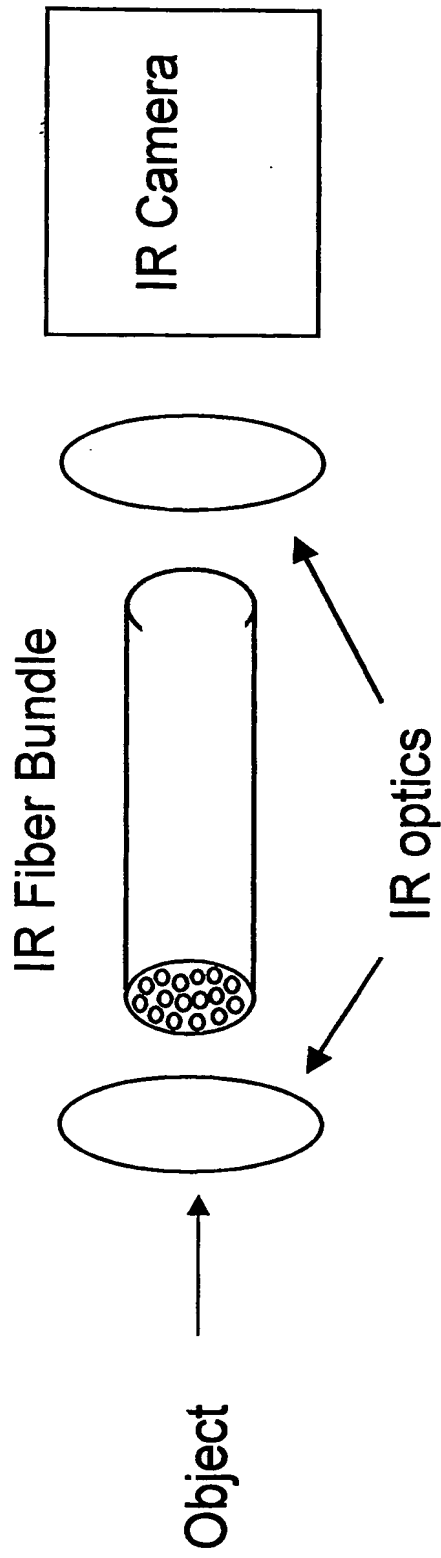
Acknowledgment

Prof. Avraham Katzir

Mr. Eran Rave

Dr. Avi Dayan

Prof. Nathan Croitoru

Dr. Alexandra Inberg

Dr. Ronit Argaman

Lumenis ltd., Surgical Division

38

END

Appendixes

Dilemmas & Obstacles

1. Fiber: heat (thermal isolators), attenuation (rigid-flexible), diffusion (coating), coupling

2. IR Camera: filtering laser reflection, synchronization

3. Biological phantoms: poor repeatability

42

Laser settings					Suction & insufflation			Endoscope tip vs. irradiated tissue		Tissue Characteristics	
laser power (watts)	Irradiating period (sec)	duty cycle* (%)	pulse frequency* (Hz)		airflow through fiber* (lpm)	vacuum rate (mmHg)	Cold CO_2 flow (lpm)	distance fiber-tissue (mm)	hitting angle (jet direction) (deg)	cavity radius (cm)	roughness of surrounding tissue
0-15 Tissue ; 0-50 Agarose	0-100	0-100	0-3M	both affect pulse-off duration, during which tissue "relaxes"	0-3	0-50	0-15	2-50	90-45	1.5-4.5	smooth -rough

power period duty cycle pulse rate airflow vacuum insufflation distance angle radius surface

42

Thermal Effects in Tissue

1. 37-42°C: local warming only – no biological alternations

2. 42-50°C: *hyperthermia*: structural changes of molecules, accompanied by bond destruction and membrane alterations of the cells; edema is observed; for long exposure time necrosis may start.

3. 50-60°C: reduction in enzyme activity, cellular energy transfer and repair mechanisms (i.e. repair of mistakes in DNA producing); inflammation may occur.

4. 60°C: permanent denaturation of proteins and collagen leads to tissue coagulation and shrinkage (generally in blood vessels)

5. 80-100°C: permeabilization of the membrane is drastically increased, destroying the chemical concentration equilibrium

6. 100°C: water molecules, contained in most tissues, start to vaporize; cavitation bubbles cause ruptures and thermal decomposition of tissue fragments, whereby adjacent tissue is preserved.

7. 150°C: carbonization; observable by the blackening of tissue and smoke escape.

8. 3000°C and up: melting

Geometry of reflection, absorption, and scattering

Incident beam

Scattering

Absorption

Reflection

Transmitted beam
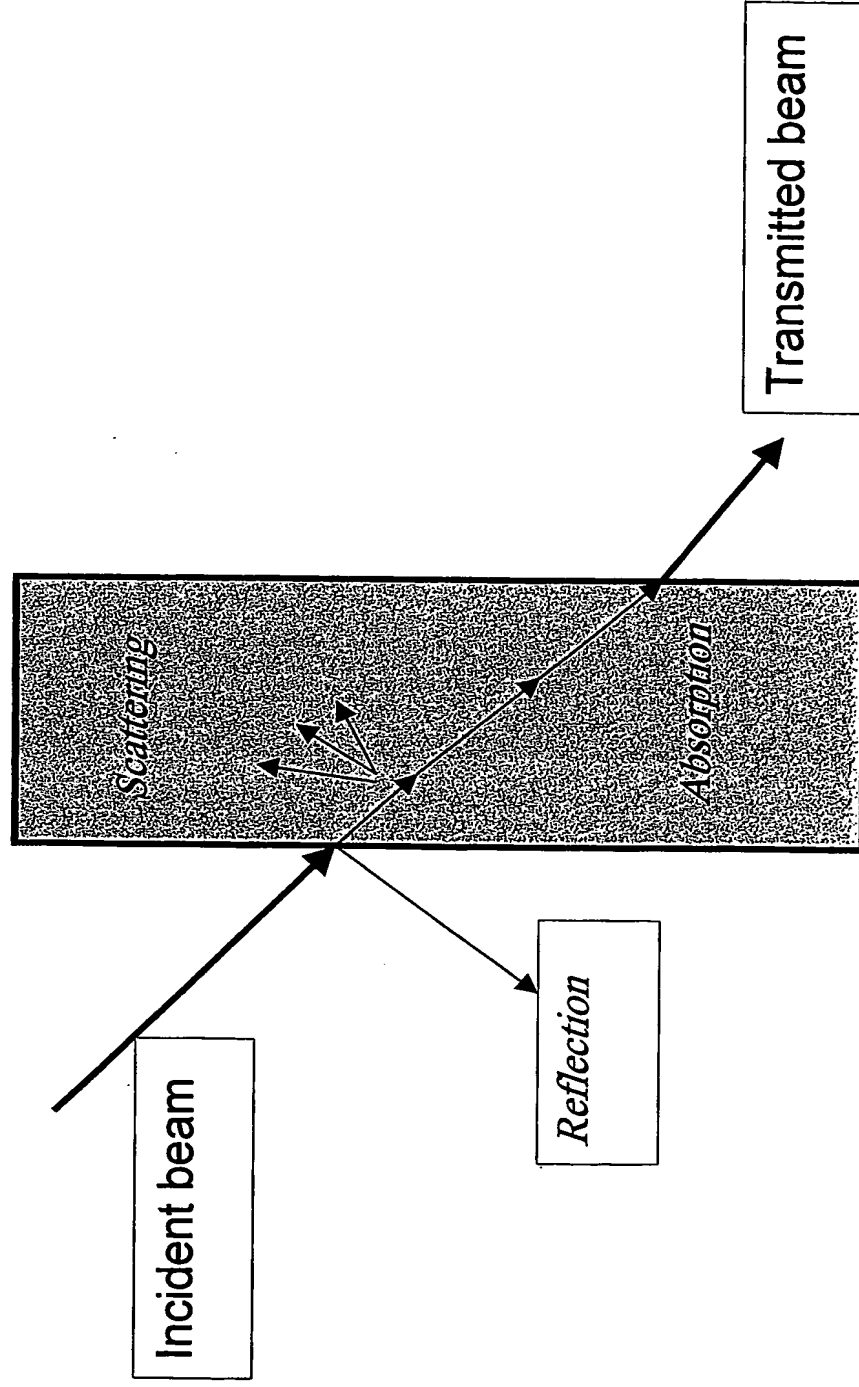
Optical penetration depth - the depth within which scattering and absorption processes, in a biological tissue, attenuates an incident laser beam.

Within this depth the beam energy can induce significant biological effects. If one processes, however, substantially more dominant it will determine the penetration depth, namely it will be either absorption depth or a scattering depth (this depends on the type of biological effects discussed).

Absorption depth - the physical process by which atoms and molecules that comprise tissue convert light energy (laser energy) into other forms of energy, such as heat.

Assuming that the cross-sectional area of the beam is constant, at certain depth, the power in the forward-directed laser beam is diminished and eventually cannot produce a significant biological effect.

From the optical penetration depth can be referred the *absorption coefficient* α as 1/D

D - optical penetration depth.

The absorption coefficient strongly depends on the wavelength of the incident laser radiation.

Thermal penetration depth - the distance in which the temperature has decreased to 1/e of its peak value:

$$Z_{thermal}(t) = \sqrt{4\alpha_1 t_p}$$

t_p - pulse duration; α_1 - thermal diffusivity for water ($\alpha_1 = 0.0015$ cm²/sec).

For example, if supposed pulse duration of 200μsec : $Z_{thermal}$ 0.011 mm

45

Lasers in widespread use for their photothermal effects

● CO2 and Er: Yag (Erbium Yttrium Aluminum Garnet) in the mid IR, Nd (Neodymium) YAG (1064nm) in the near IR and Argon ion, which has 2 main lines (488 and 514 nm) in the blue and green regions of the visible spectrum.

● Nd: YAG and Argon wavelengths are absorbed more in pigmented cells.

In soft tissue, such as bladder, applying sufficient energy, to vaporize solely the surface cells, only causes lesser damage to a depth of 0.1mm with the CO_2 laser. When the same surface effect is produced with the Argon laser, damage extends for 1mm and with the Nd: YAG, it extends for 5mm.

46

Surgical Procedures Performed by a Minimally Invasive Approach, 1999

	No. of Procedures	Minimally Invasive, %†
General surgery		
Gallbladder	1 084 882	85
Nissen fundoplication	47 087	95
Adhesiolysis	215 760	72
Appendectomy	334 388	22
Colon resection	380 000	7
Hernia repair	820 191	14
Total	2 882 308	47
Gynecology		
Hysterectomy	582 000	15
Myomectomy	64 977	70
Pelvic floor reconstruction	160 000	40
Removal of adnexal structures	350 059	65
Total	1 157 036	37
Urology		
Nephrectomy	44 863	75
Cystocele/rectocele	158 144	45
Pediatric urology (orchiopexy, vesicoreflux)	25 000	80
Adrenalectomy	20 000	60
Total	248 007	55
Plastic surgery		
Breast reconstruction	182 000	15
Face and forehead lifts	80 000	25
Total	262 000	18
Thoracic surgery		
Lung biopsy	90 000	75
Lung resection	47 124	60
Total	160 000	60
Cardiothoracic surgery		
Coronary artery bypass surgery	330 000	17
Heart valve replacement	81 000	15
Congenital defect surgery	25 000	20
Total	436 000	17
Vascular interventional surgery		
Saphenous vein harvest	220 000	35
Peripheral vascular bypass	80 000	2
Aortoiliofemoral bypass	75 000	1
Abdominal aortic aneurysm	51 000	10
Total	428 000	20

Source: Mack, M.J., *Minimally invasive and robotic surgery.* Journal of the American Medical Association, 2001.

Blackbody Emission

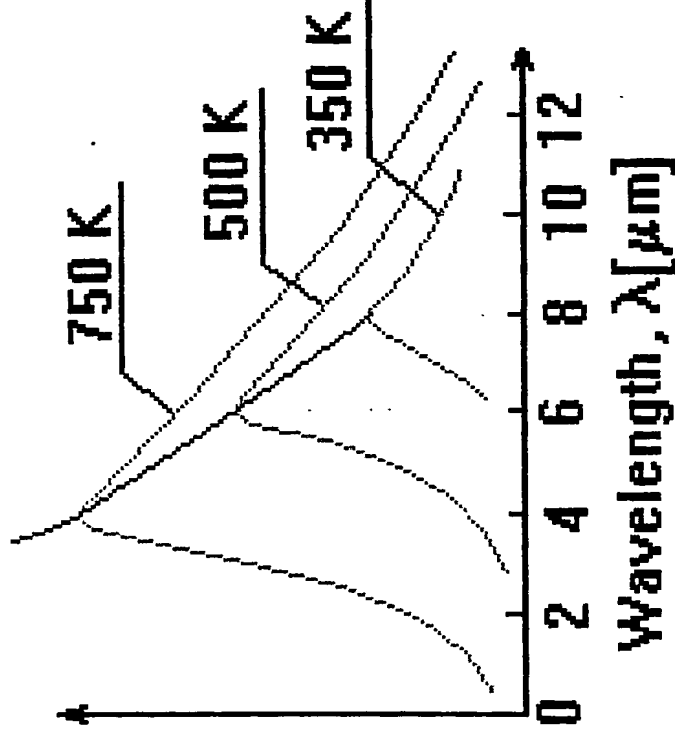- An object that absorbs all radiation impinges on it, w/o reflection.

- Kirchoff's law: Absorptivity and emissivity of a body are equal at any given temperature

- This means that a good absorber is also a good emitter.

48

Wien's Law

The wavelength, λmax, for maximum emissive power from a black body is a function of temperature:

$$\lambda max = 2898/T$$

Distribution of emissive power from a black body